ISTANBUL TECHNICAL UNIVERSITY ★ GRADUATE SCHOOL

INVESTIGATION OF THE MECHANISMS OF hERG1 BLOCKER TOXINS AS ANTI-CANCER AGENT WITH MOLECULAR MODELING TECHNIQUES

Ph.D. THESIS

Beril ÇOLAK GÜNAY

Department of Chemistry

Chemistry Programme

FEBRUARY 2024

ISTANBUL TECHNICAL UNIVERSITY ★ GRADUATE SCHOOL

INVESTIGATION OF THE MECHANISMS OF hERG1 BLOCKER TOXINS AS ANTI-CANCER AGENT WITH MOLECULAR MODELING TECHNIQUES

Ph.D. THESIS

Beril ÇOLAK GÜNAY
(509092222)

Department of Chemistry

Chemistry Programme

Thesis Advisor: Prof. Dr. Mine YURTSEVER
Thesis Co-Advisor: Prof. Dr. Serdar DURDAĞI

FEBRUARY 2024

ISTANBUL TEKNİK ÜNİVERSİTESİ ★ LİSANSÜSTÜ EĞİTİM ENSTİTÜSÜ

ANTİ KANSER AJAN OLARAK hERG1 BLOKER TOKSİNLERİN ETKİME MEKANİZMALARININ MOLEKÜLER MODELLEME TEKNİKLERİ İLE İNCELENMESİ

DOKTORA TEZİ

Beril ÇOLAK GÜNAY
(509092222)

Kimya Anabilim Dalı

Kimya Programı

Tez Danışmanı: Prof. Dr. Mine YURTSEVER
Eş Danışman: Prof. Dr. Serdar DURDAĞI

ŞUBAT 2024

Beril ÇOLAK GÜNAY, a Ph.D. student of İTU Graduate School student ID 509092222, successfully defended the thesis/dissertation entitled "INVESTIGATION OF THE MECHANISMS OF hERG1 BLOCKER TOXINS AS ANTI-CANCER AGENT WITH MOLECULAR MODELING TECHNIQUES", which she prepared after fulfilling the requirements specified in the associated legislations, before the jury whose signatures are below.

Thesis Advisor :	**Prof. Dr. Mine YURTSEVER** İstanbul Technical University	.....
Co-advisor :	**Prof. Dr. Serdar DURDAĞI** Bahçeşehir University	.....
Jury Members :	**Assoc. Prof. Dr. Ayşe Özge KÜRKÇÜOĞLU LEVİTAS** Istanbul Technical University	.....
	Assist. Prof. Dr. Bülent BALTA Istanbul Technical University	.....
	Prof. Dr. Nurcan TÜZÜN Istanbul Technical University	.....
	Assoc. Prof. Dr. Özge ŞENSOY Istanbul Medipol University	.....
	Assoc. Prof. Dr. Abdulilah ECE Biruni University	.....

Date of Submission : 4 January 2024
Date of Defense : 20 February 2024

To Ufuk and Eda Defne,

FOREWORD

This thesis has been carried out under the supervision of Prof. Dr. Mine YURTSEVER and Prof. Dr. Serdar DURDAĞI.

First of all, I would like to thank to my advisor, Prof. Dr. Mine YURTSEVER and co-advisor Prof. Dr. Serdar DURDAĞI for their scientific support, kind guidance and inspiring comments throughout this thesis.

This thesis was supported by Istanbul Technical University (ITU), Scientific Research Fund (Grant number: 39258). The numerical calculations reported in this thesis were performed at TUBITAK ULAKBIM, High Performance and Grid Computing Center (TRUBA Resources). I would like to thank them for providing me computational resources and technical help for this thesis.

Finally, I would like to thank my family. I am very grateful for their infinite support and love.

January 2024

Beril ÇOLAK GÜNAY
(Chemist)

TABLE OF CONTENTS

Page

ABBREVIATIONS

FDA	**:** U.S Food And Drug Administration
hERG	**:** Human ether-à-go-go-related gene
LINCS	**:** Linear Constraint Method
LQTS	**:** Long QT Syndrome
MD	**:** Molecular Dynamics
MM-GBSA	**:** Molecular Mechanics Generalized Born Solvation Area
MM-PBSA	**:** Molecular Mechanics Poisson-Boltzmann Solvation Area
NPT	**:** Isothermal-Isobaric Ensemble
NVT	**:** Isochoric-Isothermal Ensemble
PME	**:** Particle Mesh Ewald
RMSD	**:** Root mean square deviation
RMSF	**:** Root mean square fluctuation
SD	**:** Steepest Descent

SYMBOLS

Å	**:** Angstrom
Cmax	**:** Maximum Concentration
fs	**:** femto second
IC50	**:** Inhibitor concentration-half maximum
MW	**:** Molecular Weight
nm	**:** nanometer
ns	**:** nano second
µM	**:** micro molar
µs	**:** micro second
ps	**:** pico second
K	**:** Kelvin
T	**:** Temperature

LIST OF TABLES

Page

LIST OF FIGURES

Page

INVESTIGATION OF THE MECHANISMS OF hERG1 BLOCKER TOXINS AS ANTI-CANCER AGENT WITH MOLECULAR MODELING TECHNIQUES

SUMMARY

Ion channels are membrane-inserted proteins which regulate the movement of ions through cell membrane. Potassium (K^+) ion channels ubiquitously exist in almost all species and locate in cell membranes. Members of this channel family play important roles in cellular signaling, including various processes. It is well-known that K^+ ion channels involved in signaling pathways lead to cell proliferation or apoptosis. Because of their location on cell surface and their well-known pharmacology, they can be used as potential targets in anticancer therapies.

The human ether-a-go-go related gene 1 (hERG1) K^+ channels play crucial role in the heart, different regions of brain, endocrine cells, smooth muscle cells, and numerous tumor cells. It is known that the inherited mutations of hERG1 gene may lead to the disorder of cardiac repolarization (i.e., long QT syndrome (LQTS)), which may result in sudden cardiac death. It is known that K^+ ion channels involved in signaling pathways lead to cell proliferation or apoptosis and some specific toxins were investigated for diverse therapeutic applications on targeting the hERG1 K^+ channel. Thus, investigation of channel/toxin interactions mechanisms in atomic level is an important topic for the development of toxin-based therapeutics.

Thus, in the first part of this thesis, the interaction mechanisms of two toxins named as BeKm-1 and BmTx3b with the closed-state hERG1 channel have been studied by using different molecular modeling techniques including protein-protein docking and molecular dynamics (MD) simulations. The crucial residues of toxins in channel interactions have been elucidated. It is found that R1, K6, K18, R20, K23 and R27 residues in BeKm-1 and F1, K7, K19, K20 and K28 in BmTx3b are the important residues involved in the strong interactions with the closed-state hERG1 K^+ channel.

The results of this study can be used by medicinal chemists in the designing of diverse therapeutic applications of natural or synthetic peptides targeting the closed state hERG1 K^+ channels.

In the second part of the thesis, the information that obtained from hERG-BeKm-1 and hERG-BmTx3b interactions, was used to design *de novo* peptides. The designed *de novo* peptides were investigated on open-state hERG. In addition to *de novo* peptides, peptidomimetics and FDA-approved molecules were included in the study to increase the number of molecules studied.

It is believed that the data obtained in the thesis study will provide guidance for hERG inhibition for therapeutic purposes. In this way, it is expected to be able to eliminate various types of disease without causing sudden cardiac death.

ANTİ KANSER AJAN OLARAK hERG1 BLOKER TOKSİNLERİN ETKİME MEKANİZMALARININ MOLEKÜLER MODELLEME TEKNİKLERİ İLE İNCELENMESİ

ÖZET

İyon kanalları, hücre zarından iyonların hareketini düzenleyen, zarın içine yerleştirilmiş proteinlerdir. Gözenek oluşturan proteinler olan iyon kanalları, plazma zarları ve hücre içi organellerin zarları dahil olmak üzere, zarlar boyunca iyonların geçişini kolaylaştırır. Sodyum (Na^+), potasyum (K^+), kalsiyum (Ca^{2+}) ve belirli klor (Cl^-) iyonları için olanlar gibi çok sayıda iyon kanalı, voltaj değişiklikleriyle kontrol edilir. İyon kanalları genel olarak dört ana tipe ayrılabilir: Voltaj kapılı iyon kanalları, mekanosensitif iyon kanalları, ligand kapılı iyon kanalları, ikinci haberci kapılı iyon kanalları ve sızıntı kanalları. Voltaj kapılı iyon kanalları, zar potansiyelindeki değişikliklere yanıt olarak açılmalarını veya kapanmalarını düzenler. Ligand kapılı iyon kanalları, belirli moleküllerin, ligandlar olarak adlandırılan, kanal proteinine bağlanmasına yanıt olarak açılmalarını veya kapanmalarını modüle eder. Mekanosensitif iyon kanalları, hücre zarının gerilmesi gibi mekanik basınçlara yanıt verir. İkinci haberci kapılı iyon kanalları, ikinci haberci olarak adlandırılan hücre içi sinyal molekülleri tarafından etkilenir. Sızıntı kanalları sürekli olarak açık kalır ve zar boyunca sürekli pasif iyon hareketine izin verir.

Potasyum (K^+) iyon kanalları hemen hemen tüm türlerde hücre zarlarında bulunur. Bu kanal ailesinin üyeleri, çeşitli süreçler de dahil olmak üzere hücresel sinyalleşmede önemli roller oynarlar. Sinyal yollarında yer alan K^+ iyon kanallarının hücre çoğalmasına veya apoptoza yol açtığı iyi bilinmektedir. Hücre yüzeyindeki konumları ve iyi bilinen farmakolojileri nedeniyle antikanser tedavilerinde potansiyel hedefler olarak kullanılabilirler.

İnsandaki eter-a-go-go gen 1 (hERG1 (KCNH2)), voltaj kapılı K^+ kanallarının eter-a-go-go ailesinin bir alt ailesine (Kv11.x) aittir. Ailede Kv11.1 (hERG1), Kv11.2 (hERG2) ve Kv11.3 (hERG3) olmak üzere üç üye bulunmaktadır.

Her hERG proteini (veya bir alt birimi) kendi hücre içi amino ve karboksil uçlarıyla birlikte altı transmembran alanına (S1–S6) sahiptir. S1–S4 alanları, transmembran voltaj değişikliklerine yanıt veren voltaj sensör alanını (VSD) oluşturur; S5 ve S6 helisleri ise gözenek ve seçicilik filtresini oluşturur. Dört alt birim, ortasında bir gözenek oluşturan birim ve çevresinde dört VSD bulunan bir iyon kanalı oluşturmak üzere tetramerize olur.

hERG kanalı, diğer voltaj kapılı K^+ kanalları gibi kapalı, açık ve açık-inaktif durumları olmak üzere üç tip düşük enerji yapısına sahiptir. hERG1 kanal yapısının açık durumu yakın zamanda kriyo-elektron mikroskobu tekniği kullanılarak çözülmüştür. hERG1 kanalının kapalı ve açık-inaktif durumları için henüz çözülmüş yapılar bulunmamasına rağmen, bu farklı konformasyonlar için şu ana kadar birçok *in silico* modeli rapor edilmiştir.

İnsandaki eter-a-go-go gen 1 (hERG1) K^+ kanalları, kalpte, beynin farklı bölgelerinde, endokrin hücrelerinde, düz kas hücrelerinde ve çok sayıda tümör hücresinde çok önemli bir rol oynar. hERG1 genindeki kalıtsal mutasyonların, ani kardiyak ölümle sonuçlanabilecek kardiyak repolarizasyon bozukluğuna (uzun QT sendromu (LQTS)) yol açabileceği bilinmektedir. Sinyal yollarında yer alan K^+ iyon kanallarının hücre çoğalmasına veya apoptoza yol açtığı bilinmektedir ve hERG1 K^+ kanalını hedeflemeye yönelik çeşitli terapötik uygulamalar için bazı spesifik toksinler araştırılmıştır. Atomik düzeyde kanal/toksin etkileşim mekanizmalarının araştırılması, toksin bazlı tedavilerin geliştirilmesi için önemli bir konudur.

Ligandlar, hERG1 kanalının farklı bölgelerinden etkileşime girebilirler. Küçük moleküllerin çoğu kanalın merkezi bağlanma boşluğundan etkileşime girerken, daha önce bazı toksinlerin (örneğin, peptidlerin) kanalın dış vestibülüne (S5-por bağlayıcı bölgesi) bağlanma eğiliminde olduğu gösterilmiştir. Toksinler; yılanlar, akrepler, deniz anemonları, kabuklular, koni salyangozları ve örümcekler gibi hayvan zehirlerinden elde edilen küçük proteinlerdir ve bunlar cilt enfeksiyonu, tip 2 diyabet, hepatit C ve kanser gibi farklı tedavi uygulamalarında kullanılabilirler.

Literatürde toksin/hERG kanal etkileşimleri hakkında birkaç çalışma olmasına rağmen, tezin ilk bölümünde kapsamlı bir yaklaşım uygulanmıştır. Diğer çalışmalarda genellikle sadece PD bölgesi yani kanalın kısmi bölümleri kullanılırken burada, hERG1 kanalının tüm S1-S6 bölgeleri (hem PD hem de VSD kısımlarını) kullanılmıştır.

Tezin ilk bölümünde BeKm-1 ve BmTx3b olarak adlandırılan iki toksinin kapalı durum hERG1 kanalı ile etkileşim mekanizmaları, protein-protein kenetlenmesi ve moleküler dinamik (MD) simülasyonlar dahil olmak üzere farklı moleküler modelleme teknikleri kullanılarak incelenmiştir. Kanal etkileşimlerindeki önemli toksinlerin kalıntıları aydınlatılmıştır. BeKm-1'deki R1, K6, K18, R20, K23 ve R27 kalıntılarının ve BmTx3b'deki F1, K7, K19, K20 ve K28'in kapalı durum hERG1 K^+ kanalı ile güçlü etkileşimlerde yer alan önemli kalıntılar olduğu bulunmuştur. Çalışılan toksinlerin ve hedef proteinin önemli kalıntıları ile aralarındaki bağlanmayan kimyasal etkileşimler detaylandırılıp vurgulandığı için, bu bilgiler toksinleri taklit eden daha iyi terapötiklerin tasarımında kullanılabilir.

Bununla birlikte, bu çalışmanın sonuçları tıbbi kimyagerler tarafından kapalı durumdaki hERG1 K^+ kanallarını hedef alan doğal veya sentetik peptitlerin çeşitli terapötik uygulamalarının tasarlanmasında kullanılabilir.

Tezin ikinci bölümünde hERG-BeKm-1 ve hERG-BmTx3b etkileşimlerinden elde edilen bilgiler *de novo* peptitlerin tasarımında kullanılmıştır. Tasarlanan *de novo* peptitler açık durumdaki hERG'de araştırılmıştır. İncelenen molekül sayısını artırmak amacıyla *de novo* peptitlerin yanı sıra peptit benzeri moleküller (peptidomimetikler) ve FDA onaylı moleküller de çalışmaya dahil edilmiştir.

Bu çalışmada, açık durumdaki hERG'in küçük moleküllerle kısmi inhibisyonu atomik simülasyonlar kullanılarak incelenmiş ve terapötik hERG inhibisyonu hedefleme çalışmaları için bir iş akışı önerilmiştir. Bu iş akışı, moleküllerin hERG'in iç boşluğuna yerleştirilmesini, bu bölgedeki yüksek afiniteye sahip olanların elenmesini ve seçilen moleküllerin seçicilik filtresinin üst bölgesine yerleştirilerek kısmi hERG inhibisyonu sağlayan moleküllerin belirlenmesini içerir. Ardından, MD simülasyonları ile elde edilen bu moleküllerin yerleşim pozisyonları rafine edilecektir. Böylece, atomik düzeyde kısmi hERG inhibisyonu açıklanabilecektir.

Son olarak, bu kısmi inhibisyonun doğru ve detaylı bir şekilde anlaşılması, demans, glioblastoma ve bazı diğer kanserlerde kardiyotoksisite riski olmadan tedavi seçeneği sunan küçük moleküllü terapötik uygulamaların yolunu açacaktır.

Bu tez çalışmasında elde edilen verilerin terapötik amaçlı hERG inhibisyonuna yol göstereceğine inanılmaktadır. Bu sayede ani kalp ölümüne yol açmadan çeşitli hastalık türlerinin ortadan kaldırılabilmesi beklenmektedir.

1. INTRODUCTION

Ion channels are membrane-inserted proteins which regulate the movement of ions through cell membrane [1]. Ion channels, which are pore-forming proteins, facilitate the passage of ions across membranes, including plasma membranes and those of intracellular organelles. A significant number of ion channels, such as those for sodium (Na^+), potassium (K^+), calcium (Ca^{2+}), and certain chloride (Cl^-) ions, are controlled by changes in voltage. Ion channels can be broadly categorized into four main types: Voltage-gated ion channels, mechanosensitive ion channels, ligand-gated ion channels, second messenger-gated ion channels, and leak channels. Voltage-gated ion channels regulate their opening or closing in response to changes in membrane potential. Ligand-gated ion channels modulate their opening or closing in response to the binding of certain molecules, called ligands, to the channel protein. Mechanosensitive ion channels respond to mechanical pressures, such as tension or stretching of the cell membrane. Second messenger-gated ion channels are influenced by intracellular signaling molecules called second messengers. Leak channels remain permanently open, allowing continuous passive movement of ions across the membrane.

Potassium (K^+) ion channels ubiquitously exist in almost all species and locate in cell membranes [2]. Members of this channel family play important roles in cellular signaling, including various processes [3]. It is well-known that K^+ ion channels involved in signaling pathways lead to cell proliferation or apoptosis [4]. Because of their location on cell surface and their well-known pharmacology, they can be used as potential targets in anticancer therapies [5].

The human ether-a-go-go related gene 1 (hERG1 (aka KCNH2)) belongs to a subfamily (Kv11.x) of the ether-a-go-go family of voltage gated K^+ channels. There are three members in the family, Kv11.1 (hERG1), Kv11.2 (hERG2) and Kv11.3 (hERG3) [6].

Each hERG protein (or a subunit) has six transmembrane domains (S1–S6) with their respective intracellular amino and carboxyl termini [7, 8] (Figure 1.1). The S1–S4 domains form the voltage sensor domain (VSD), which responds to transmembrane voltage changes; whereas the S5 and S6 helices form the pore and the selectivity filter. Figure 1.1 also shows an ion channel tetramer (B). Four subunits tetramerize to form an ion channel with a central poreforming unit surrounded by four VSDs.

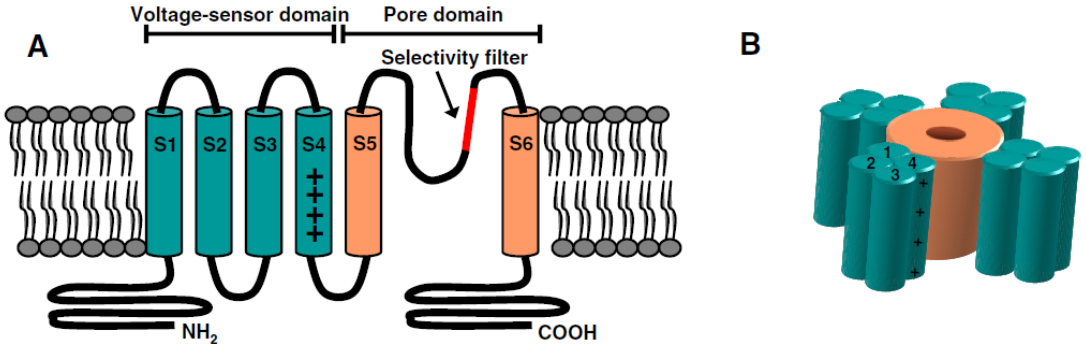

Figure 1.1 : General architecture of a voltage-gated ion channel [7].

Like other voltage gated K^+ channels, it has three types of low energy conformations which are closed, open and open-inactivated states [9] (Figure 1.2).

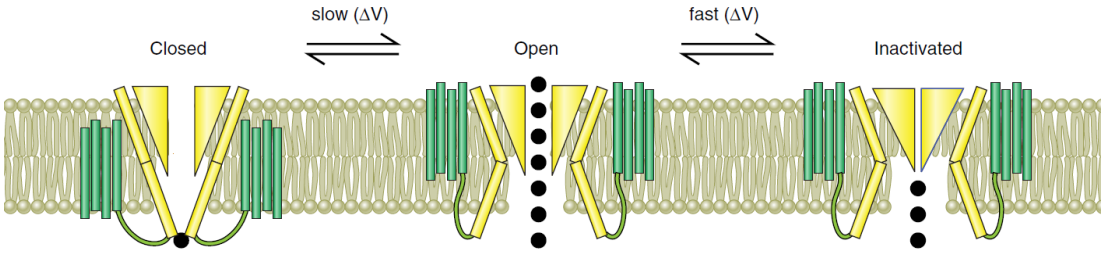

Figure 1.2 : Closed, open and inactivated conformations of hERG1 channel [6].

Wang and MacKinnon solved the open-state of hERG1 channel structure recently by using cryo-electron microscopy technique [10]. Although there are no availabe solved structures yet for the closed and open-inactivated states of hERG1 channel, several *in silico* models have been reported so far for those distinct conformations [1, 11-17].

hERG1 K^+ channels play crucial role in the heart, different regions of brain, endocrine cells, smooth muscle cells, and numerous tumor cells [6]. It is well-known in the literature that the inherited mutations of hERG1 gene may lead to the disorder of cardiac repolarization (i.e., long QT syndrome (LQTS)), which may result in sudden cardiac death [9]. Since hERG1 K^+ channel has a large binding pocket space at the

pore domain (PD) region, it can host chemically diverse small compounds including approved drugs [18]. Thus, LQTS can be occurred by blockage of hERG1 channel with regularly used medications such as antipsychotics, antihistaminics and antibiotics [9, 19]. Due to their effect on the function of the hERG1 channel, some Food and Drug Administration (FDA) approved drugs (i.e., cisapride, terfenadine, astemizole and grepafloxin, etc.) have been removed from the market and usage of others (i.e., haloperidol, thioridazine, sertindole, and pimozide) have been restricted. Hence, FDA and the European Medicines Agency (EMEA) have mandatory assays on drug screening for their hERG1 blockage [18].

Each drug has different channel blocking properties depending on the drug's conformation, structure and binding affinities. Drug binding in the pore cavity of Kv11.1 channels is shown in Figure 1.3. Residues involved in drug binding include Thr623, Ser624, and Val625 close to the intracellular entrance to the selectivity filter as well as two aromatic residues Tyr652 and Phe656. Channels have to open before drugs can enter the pore cavity. Once open, drugs can enter the pore cavity and interact with one or more drug binding residues. Channel inactivation involves reorientation of drug binding residues such that drugs may bind in different orientations in the open and inactivated states [6].

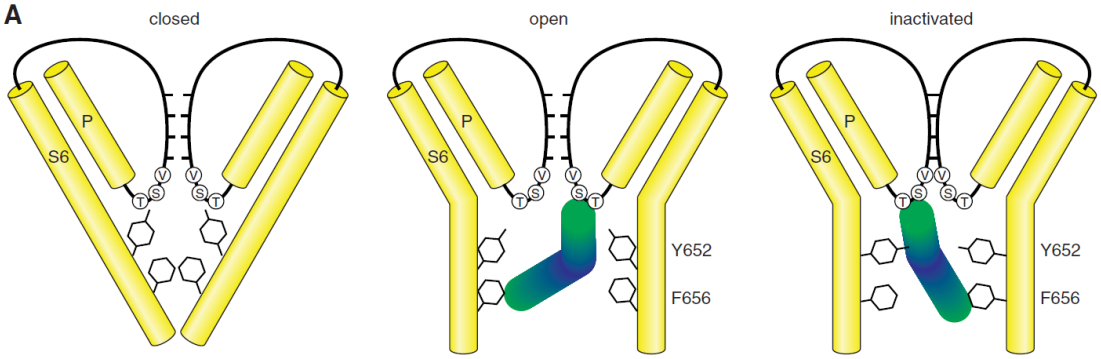

Figure 1.3 : Drug binding in the pore cavity of Kv11.1 channels.

Ligands may interact from different regions of hERG1 channel. While majority of small molecules interacts from central binding pocket of the channel, it has been shown previously that some toxins (i.e., peptides) tend to bind to the outer vestibule (S5-pore linker region) of the channel [6, 20].

Two step model for a scorpion toxin binding to Kv11.1 channels is shown in Figure 1.4. Toxin binds to the channel, interacting with the S5P helix. Block of ion

conduction, however, requires a second step, which is hypothesized to be conformational rearrangements of the external mouth of the channel. Note the toxin can unbind from the nonblocked conformation, and this can explain the incomplete block of conductance even at high concentrations of toxin [6].

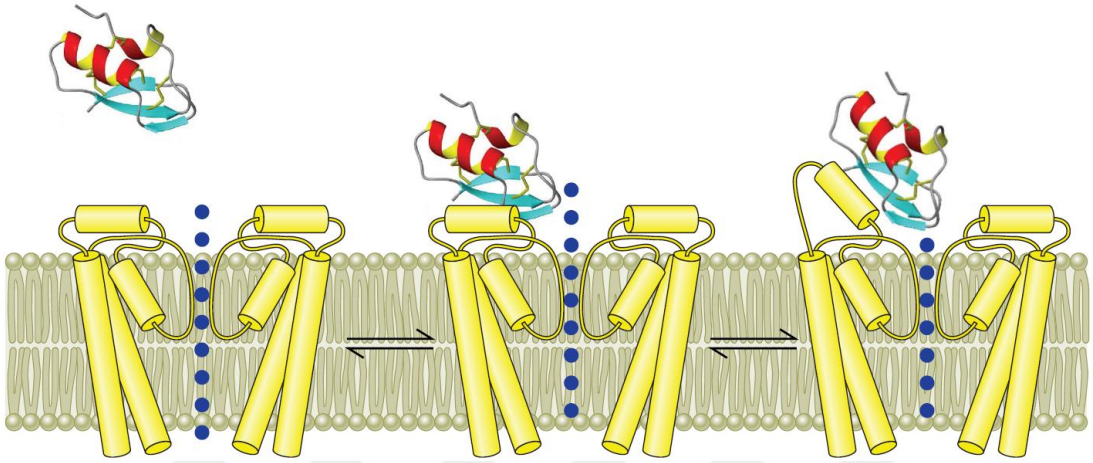

Figure 1.4 : Two step model for a scorpion toxin binding to Kv11.1 channels.

Toxins are small proteins, obtained from animal venoms such as snakes, scorpions, sea anemons, shellfishes, cone snails and spiders [22-24] and they can be used in different therapeutic applications such as skin infection, type 2 diabetes, hepatitis C, and cancer [21]. Calmette et al. [25] is known as the first reporter of venom usage in cancer on laboratory animals. K^+ channel-specific peptides are generally isolated from scorpion venoms and known as potassium toxins (KTx) [26]. For instance, margatoxin (MgTX), which is isolated from scorpion, is the first *in vivo* tested peptide and it is known as the potent blocker of voltage gated K^+ channels [27]. According to literature ErgTx [20], BeKm-1 [28], BmTx3 [29] and APETx-1 [30] toxins have been subjected *in vitro* or *vivo* studies with hERG1 channel and they show therepautic activities.

Because of the limited *in silico* studies [1, 31-32] have been done on hERG1 K^+ channel-toxin interactions, remained unclear. In this thesis, the mechanistic investigation of hERG1 K^+ channel/BeKm-1 and hERG1 K^+ channel/BmTx3b interactions have been studied using integrated *in silico* techniques such as protein-protein docking, molecular dynamics (MD) simulations, and free energy calculations. Since BeKm-1 toxin binds selectively to the closed state of hERG1 target [16], here the hERG1 K^+/toxin interactions were studied on the closed state of hERG1 model, previously developed by our group [1].

In addition to hERG interactions with toxins, the interactions of small molecules (usually drugs or drug-like compounds) and the determinants of these interactions have been extensively studied in the literature. The objective of these studies was to elucidate the mechanism of hERG blockade and to elucidate the molecular interactions necessary for this mechanism. To this end, the molecular docking method was employed extensively, with the aim of predicting the hERG blocking capacity of newly synthesized or synthesized molecules. One example of these studies is the 2011 study by Durdagi et al., which revealed the amino acids important in hERG inhibition by ligand-based and receptor-based approaches [33]. A recent study that concentrates to suggest workflow to predict the binding modes of hERG binders and their liability [34]. Their findings suggest that the docking based scoring of hERG binders is not effective compared to MD-based MM/GBSA scoring. Furthermore, the authors conclude that with their suggested workflow would help to design and optimize molecules against hERG inhibition. In addition to molecular docking studies, MD simulation method included to provide more detailed picture of the hERG inhibition. Negami et al used MD-CAFEE absolute binding free energy method to predict binding affinities of molecules to hERG, and showed their methodology successfully predict experimental binding affinities with 0.73 kcal/mol RMSE [35]. Dickson et al used the first experimental hERG structure and MD simulations were used to assess different channel conformations to be utilized in ensemble docking studies [36]. In another study, Luo et al conducted an in silico protocol which combines, molecular docking, MD simulation and free energy calculations to shed light on to the binding modes of fluoroquinolones in the central cavity of hERG [37].

A careful review of the studies cited above reveals that most of the small molecule studies in the literature are aimed at understanding hERG blocking properties. Studies with toxins have addressed partial inhibition of hERG and have been performed using a binding site located in the upper part of the selectivity filter. In the first part of this work, toxin-hERG interactions were studied at the atomic level for the first time. In the second part, a two-step protocol was applied. In the first step, the binding modes and energies of small molecules (drug-like and peptide-like) in the central binding site of hERG were determined. The molecules that showed weak binding to the central cavity were selected and used in the second step. In the second step, the affinity of these selected molecules to the upper part of the selectivity filter was estimated by

molecular docking and the obtained poses were submitted to MD simulations to understand their partial hERG blocking mechanisms and energies.

1.1 The Aim and the Scope of the Thesis

This thesis has two objectives, the first of which is to elucidate the interactions between the spider toxins BeKm-1 and BmTx3b and the closed-state hERG channel at the atomic level. The second aim is to investigate the open-state hERG interactions of *de novo* peptides, peptidomimetics and FDA molecules formed with BeKm-1 and BmTx3b amino acids, which play an active role in the binding obtained in the first part, this time at the atomic level. For this purpose, molecular docking and molecular dynamics simulations were used. Understanding the mechanism of partial inhibition of hERG, rather than inhibition from the internal cavity, which causes cardiotoxicity and sudden cardiac death, will allow hERG to be inhibited for therapeutic purposes. In particular, hERG is known to cause cell proliferation in different types of cancer. Therapeutic targeting of hERG in these cancer types is very important. For this purpose, with this thesis study, a flow chart for molecule screening to be used for therapeutic purposes has been proposed to the literature. This flowchart is based on partial inhibition of the hERG channel. Molecules that are too large to fit into the inner cavity will be docked directly to the upper part of the selective filter, while molecules that can inhibit the inner cavity will be docked first to the inner cavity and then those that show low binding in this region will be docked to the upper part of the selective filter to determine their binding affinity. For toxin molecules, those that bind with high affinity to the upper part of the selective filter, *de novo* peptides, peptidomimetics and FDA approved molecules that bind with low affinity to the inner cavity and high affinity to the upper part of the selective filter will be determined and channel-peptide interactions will be studied at the atomic level by molecular dynamics simulation. This will identify molecular determinants of partial hERG inhibition and provide guidance for further studies.

1.2 Innovation Potential of the Thesis

Inhibition of the hERG channel without stopping potassium flow is a potential therapeutic for cancer (such as glioblastoma and breast cancer) and dementia. The molecules that cause long QT syndrome and subsequent sudden cardiac death by

stopping the flow of potassium and their mechanisms of action are well known in the literature. However, the partial inhibition of hERG, which is therapeutically important in some forms of cancer and dementia, has not been explained at the atomic level. To this end, this thesis has studied the interaction between closed-state hERG and spider toxins at the atomic level and proposed a flowchart for possible therapeutic applications. Therefore, the innovative aspect of this thesis is the detailed elucidation of the hERG interactions of BeKm-1 and BmTx3b toxins. The information that obtained from hERG- BeKm-1 and hERG-BmTx3b interactions, was used to design *de novo* peptides. The designed *de novo* peptides were investigated on open-state hERG. In addition to *de novo* peptides, peptidomimetics and FDA-approved molecules were included in the study to increase the number of molecules studied. We believe that the data obtained in the thesis study will provide guidance for hERG inhibition for therapeutic purposes. In this way, we expect to be able to eliminate various types of disease without causing sudden cardiac death.

2. METHODS

2.1 Protein Preparation

2.1.1 Protein preparation in Chapter 3

BeKm-1 (PDB ID, 1J5J) and BmTx3b peptides (PDB ID, 1M2S) have been retrieved from protein data bank server [38]. The atomic coordinates of hERG1 channel were obtained from our previously reported study [1]. Protein and peptide structures were prepared using Protein Preparation module implemented in the Schrodinger's Maestro Molecular Modeling package. During protein and peptide preparation, missing hydrogen atoms were added, disulfide bonds are formed followed by energy minimization and optimization by OPLS2005 force field. Protonation states of amino acid residues were determined at the physiological pH 7.4 with the PROPKA [39, 40].

2.1.2 Protein preparation in Chapter 4

Open-state of hERG was downloaded from RCSB with the PDB ID 5VA1 [10]. This structure lacks the potassium ions and coordinating water molecules, to model the structure correctly, 4 potassium ions and 3 water molecules were taken from closed-state model of hERG. Protein preparation wizard was used to prepare the protein structure by adding missing atoms, and hydrogens [39]. Subsequently obtained structure was minimizedstructure was minimized.

2.2 Ligand Preparation in Chapter 4

25 *de novo* peptides were generated based on the decomposition energies that obtained in the first part of the thesis. N and C terminal cappings were added to each *de novo* peptides. The protonation states of the peptides were set according to pH 7.4. 36711 peptidomimetic compounds were downloaded from ChemDiv [41]. 6733 FDA approved and the drugs that are in clinical trials were obtained from NCI. These molecules were prepared at pH 7.4 using LigPrep module of Schrodinger Molecular Modeling Suite.

2.3 Protein-Protein Docking (Chapter 3)

2.3.1 Docking of (BeKm-1 or BmTx3b) scorpion toxins to hERG1

The BeKm-1 toxin belongs to γ-KTxs family and has 36 amino acids with the sequence of RPTDIKCSESYQCFPVCKSRFGKTNGRCVNGFCDCF. It is cross-linked by three disulfide bridges, Cys7-Cys28, Cys13-Cys33 and Cys17-Cys35. The BmTx3b toxin belongs to α-KTxs family and contains 37 residues with the sequence of FGLIDVKCFASSECWTACKKVTGSGQGKCQNNQCRCY. It is also cross-linked by three disulfide bridges, Cys8-Cys29, Cys14-Cys34 and Cys18-Cys36. These disulfide bridges enhance the internal conformational stability by decreasing the flexibility of protein.

In this study, ClusPro2.0 protein-protein docking algorithm has been employed for docking of toxins to the closed state of hERG1 K^+ channel [42-45]. The correct pose predictions of ClusPro has been evaluated and validated previously in the CAPRI challenge [46]. The protein-protein docking protocol employs fast fourier transform (FFT)-based sampling. 30-poses for each toxins were requested in docking [44]. ClusPro includes 4 different types of ranking scoring schemes (i.e., balanced, electrostatic favored, hydrophobic-favored and van der Waals (vdW) + electrostatics) [42]. Here, protein-protein complex models have been identified based on vdW + electrostatics interactions scoring functions. The obtained docking poses were then compared with the available experimental results from literature for the hERG1/BeKm-1 [28, 31] and hERG1/BmTx3B [32, 47] interactions.

2.3.2 MD simulations

The channel/toxin docking poses were used as initial structures in MD simulations. Both apo and holo forms of the hERG1 K^+ channels immersed into the dipalmitoylphosphatidylcholine (DPPC) lipid bilayer using OPM (Orientations of Proteins in Membranes) server [48]. MD simulations were carried out using Gromacs 5.1 package [49, 50]. CHARMM36 force field [51] was employed in all MD simulations. Protein/membrane systems were prepared using CHARMM-GUI [52], in an explicit solvent, using TIP3P water model [53]. The cut-off distance of 12 Å was used for the calculation of vdW and electrostatic interactions. The particle-mesh Ewald (PME) [54] was implemented for the calculation of the long-range electrostatic interactions. LINCS algorithm [55] was used to constrain atoms. All systems were

solvated from extracellular and intracellular regions of the membrane with TIP3P water model using water layer thickness of 20 Å. The simulation box contained channel/toxin complex, 256 DPPC molecules, 3 K^+ ions at the selectivity filter, pore water molecules in the intracellular cavity, solvated by 0.15 M KCl aqueous salt solution. Structures were minimized and equilibrated by gradually decreasing harmonic constraints initially 10.0 kcal mol^{-1} $Å^{-2}$ and 5.0 kcal mol^{-1} $Å^{-2}$ to 0.5 and 0.1 kcal mol^{-1} $Å^{-2}$ for the backbone and side chains, respectively. Simulation time was over 2 ns for equilibration and 100 ns production. As minimization method, steepest descent algorithm with Verlet cut-off scheme [56] were used. Equilibrations were done with V-rescale thermostat [57] and Berendsen barostat [58]. At production step, V-rescale thermostat and Parrinello-Rahman coupling algorithm [59] with semiisotropic pressure scaling were performed in all MD simulations for constant pressure of 1 atm at 310 K, in NPT ensemble. Each simulation was repeated by 3 times starting from different velocity distributions.

2.3.3 The Molecular Mechanics/Poisson-Boltmann Surface Area (MM/PBSA) calculations

In biological systems, binding or interaction free energies can be estimated by MM/PBSA method [60]. Here, MM/PBSA analysis was performed using MD simulations with Gromacs 5.1 package [49, 50] to calculate the binding free energies of the studied toxins at the hERG1 K^+ channel. Binding free energies of the toxins (protein with ligand) in solvent are calculated as given in equation (2.1) [61];

$$\Delta G_{bind} = \Delta G_{complex} - (\Delta G_{protein} + \Delta G_{ligand}) \quad (2.1)$$

where, $\Delta G_{complex}$, $\Delta G_{protein}$, ΔG_{Ligand} are the free energy changes of the protein-ligand complex in solvent, isolated protein in solvent, and the isolated ligand in solvent, respectively. ΔG_{bind} consists of enthalpic and entropic terms (Equation (2.2));

$$\Delta G_{bind} = \Delta H - T\Delta S \quad (2.2)$$

ΔH is expressed as a sum of molecular mechanics (MM) interactions energy between protein and the ligand (ΔE_{MM}) and the solvation free energy (ΔG_{sol}), as given in Equation (2.3).

$$\Delta H = \Delta E_{MM} + \Delta G_{sol} \quad (2.3)$$

ΔE_{MM} is the sum of electrostatic (ΔE_{elec}) and vdW (ΔE_{vdW}) interactions between interacting parts and it is given in Equation (2.4).

$$\Delta E_{MM} = \Delta E_{elec} + \Delta E_{vdW} \quad (2.4)$$

The solvation free energy ΔG_{sol} has two components (Equation (5)).

$$\Delta G_{sol} = \Delta G_P + \Delta G_{NP} \quad (2.5)$$

where, ΔG_P defines the polar solvation energy calculated by Poisson−Boltzmann (PB) method and ΔG_{NP} describes non-polar solvation energy which is predicted through estimation of the solvent-accessible surface area (SASA) as given in Equation (6).

$$\Delta G_{NP} = \gamma SASA + \beta \quad (2.6)$$

where, γ is the coefficient related to surface tension of the solvent and β is the fitting parameter and default values were used in our calculations.

2.3.4 Decomposition binding energy

The binding energy can be decomposed on a per residue basis by the *g_mmpbsa* tool [61]. E_{MM}, G_P and G_{NP} are the energy components of individual atoms which they calculated for bound and unbound forms, and their contribution to the binding energy $\Delta R_X^{BE}$of residue X is calculated according to Equation (2.7).

$$\Delta R_X^{BE} = \sum_{i=1}^{n} \left(A_i^{bound} - A_i^{free}\right) \quad (2.7)$$

where, $A_i^{complex}$and A_i^{free} are the energy of i^{th} atom in residue X with bound and unbound forms respectively. n is the total number of atoms in the residue. Thus, binding energy for total number of residues in either protein-protein or protein-ligand complex can be given by Equation (2.8).

$$\Delta G_{binding} = \sum_{x=1}^{m} \Delta R_X^{BE} \quad (2.8)$$

where m is the total number of residues in the target structure.

2.3.5 Decomposition binding energy

Alanine scanning mutagenesis is often used method to identify residues contributing most to the protein-protein interactions [62]. In this study, wild type and Ala-mutated toxins were docked to hERG1 K^+ channel with ClusPro 2.0 [43-46]. For Alanine-scanning mutagenesis study, binding free energy values were recorded based on vdW + electrostatics interaction results and ΔΔGbind values were determined with Equation (2.9).

$$\Delta\Delta G_{bind} = |\Delta G_{mutant\ bind} - \Delta G_{wild\ type\ bind}| \quad (2.9)$$

2.4 Ligand-Protein Docking (Chapter 4)

2.4.1 Molecular docking

Two grids were generated for the internal cavity and top of the selectivity filter. The aminoacids for the internal cavity was selected based on the literature knowledge. Following residues were selected to generate the internal cavity grid file; 623, 624, 652, 653, 656 [1, 33]. The cut-off docking score for the selection of weak binders at the internal cavity was set to -4.580 kcal/mol. This score was obtained in well-known central cavity blocker, Dofetilide in our docking simulations. This cut-off was applied both in Peptidomimetics and FDA molecules selection for MD. For the top of the selectivity filter grid file following residues were selected; 582, 583, 585, 588, 592, 628, 631 [63, 64]. For the *de novo* peptides Glide SP-peptide docking was used [65]. For the peptidomimetics and FDA compounds Glide-SP was used [66, 67]. residues in the target structure.

2.4.2 Molecular dynamics simulations

Obtained docking poses were first uploaded to Orientations of Proteins in Membranes (OPM) server [68]. Oriented structures were inserted in POPC model membrane in Desmond. 0.15 mM KCl salt concentration was used to neutralize the simulation medium. TIP3P water model was used to solvate the system in the simulation box. The temperature of the system was set to 310 K and controlled by Nose-Hoover thermostat [69], and the pressure of the system was set to 1.01325 bar and controlled with Martyna-Tobias-Klein (MTK) barostat [70]. MD simulations were conducted for 100

ns and Desmond MD engine was used to simulate and collect 1000 frames for each complex [71].

3. ELUCIDATION OF INTERACTION MECHANISM OF HERG1 POTASSIUM CHANNEL WITH SCORPION TOXINS BeKm-1 AND BmTx3b[1]

In this part of the thesis, we investigated the molecular interactions between hERG1 K^+ channel and the scorpion toxins BeKm-1 and BmTx3b [64]. These toxins were considered for their therapeutic potentials against the evolution of metastasis [72, 73] and they have 35% sequence identity, 48% sequence similarity and 51% homology between them. Structurally they are very similar, when they align to each other, root-mean square deviation (RMSD) is found 1.32 Å. (Figure 3.1). The sequence alignment was generated by Multiple Sequence Viewer tool of Maestro and the structure alignment was generated by Protein Structure Alignment tool.

Figure 3.1 : (a) The sequence alignment of BeKm-1 (1J5J) and BmTx3b (1M2S). **(b)** The structure alignment of BeKm-1 (green) and BmTx3b (magenta). RMSD, 1.32 Å, alignment score, 0.06.

3.1 Protein-Protein Docking (Docking of scorpion toxins (BeKm-1 or BmTx3b) to hERG channel)

Cluspro 2.0 docking program were used to predict docked poses to understand the interaction of hERG1 and the scorpion toxins. Two low energy poses which fit with experimental results for each toxin were selected (in total 4 poses, Figure 3.2). Tables 3.1 and 3.2 show the number of members in each cluster of docking poses of toxins and their corresponding docking scores.

---

[1] This chapter is based on the paper 'Colak Gunay, B., Yurtsever, M., Durdagi, S. (2020), Elucidation of interaction mechanism of hERG1 potassium channel with scorpion toxins BeKm-1 and BmTx3b. Journal of Molecular Graphics and Modelling, 96, 107504. Doi: 10.1016/j.jmgm.2019.107504'

Table 3.1 : Docked complexes of hERG1 and BeKm-1 taken from Cluspro docking server.

Cluster	Members	Representative	Weighted Score
0	322	Center	-185.3
0	322	Lowest Energy	-248.2
1	219	Center	-181.0
1	219	Lowest Energy	-248.2
2	116	Center	-180.1
2	116	Lowest Energy	-256.1
3	115	Center	-180.1
3	115	Lowest Energy	-255.9
4	113	Center	-204.9
4	113	Lowest Energy	-269.4
5	113	Center	-204.9
5	113	Lowest Energy	-269.3
6	2	Center	-180.3
6	2	Lowest Energy	-192.0

Table 3.2 : Docked complexes of hERG1 and BmTx3b taken from Cluspro docking server.

Cluster	Members	Representative	Weighted Score
0	226	Lowest Energy	-244.7
0	226	Center	-188.8
1	194	Lowest Energy	-244.6
1	194	Center	-171.4
2	94	Lowest Energy	-220.9
2	94	Center	-175.4
3	92	Lowest Energy	-244.6
3	92	Center	-172.1
4	67	Lowest Energy	-199
4	67	Center	-171.9
5	66	Lowest Energy	-244.7
5	66	Center	-172
6	63	Lowest Energy	-199
6	63	Center	-171.9
7	58	Lowest Energy	-196.3
7	58	Center	-184.4
8	52	Lowest Energy	-196.2
8	52	Center	-184.3
9	42	Lowest Energy	-211.1
9	42	Center	-175.2
10	18	Lowest Energy	-194.1
10	18	Center	-188.7
11	17	Lowest Energy	-194.1
11	17	Center	-188.6
12	6	Lowest Energy	-190.3

Table 3.2 (continued) : Docked complexes of hERG1 and BmTx3b taken from Cluspro docking server.

Cluster	Members	Representative	Weighted Score
12	6	Center	-185.6
13	5	Center	-185.6
13	5	Lowest Energy	-185.6

The crucial residues for strong hERG1/toxin interactions were compared with literature. BeKm-1 is known as hERG1 channel's spesific scorpion toxin and it selectively binds to closed state of hERG1 channel (Figure 3.2) [16]. Residues of BeKm-1 are located in the α-helix and the following loop makes interaction with the outer vestibule of hERG1 channel. Its interaction mechanism is different from other γ-KTxs family [19]. According to experimental studies in literature, the interactions between S631/K18, S631/R20, Q592/R20, I583/Y11 and R582/F14 were expected [16]. Our protein-protein docking poses cover most of these interactions (Figure 3.2).

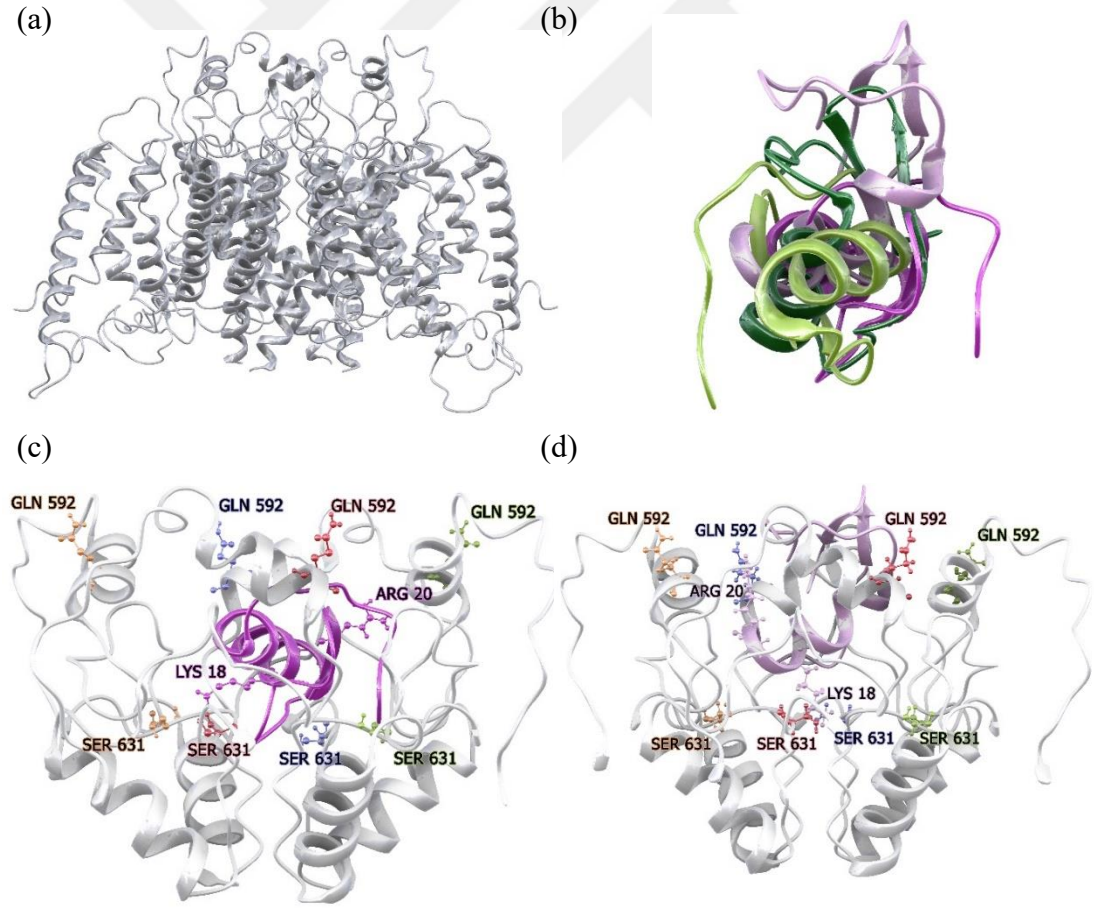

Figure 3.2 : (a) 3D structure model of closed state hERG K^+ ion channel used in the current study. **(b)** Two different low energy conformations of BeKm-1 (pale and dark pink) and BmTx3b (pale and dark green) toxins at the binding site. **(c, d)** first and second docking poses of hERG1/BeKm-1 complexes. **(e, f)** first and second docking poses for the hERG1/BmTx3b complexes.

(e) (f)

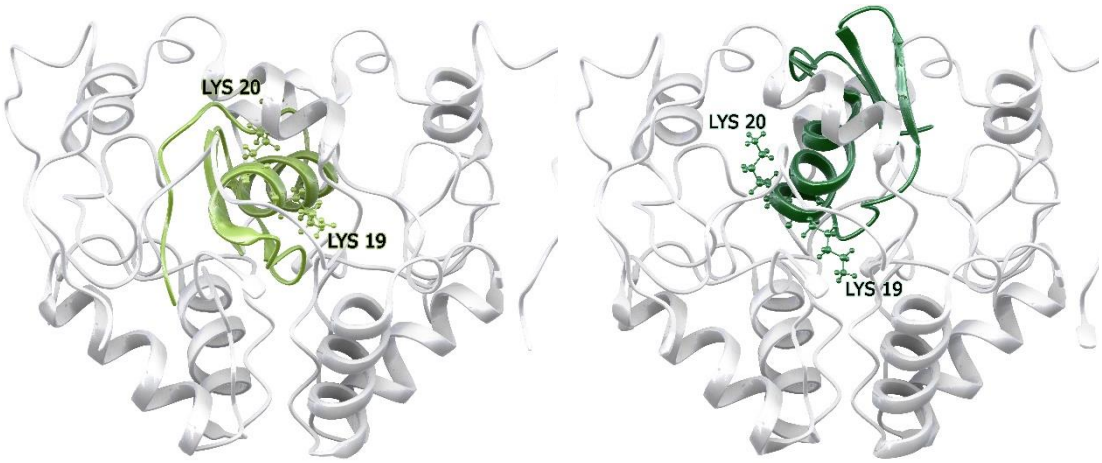

Figure 3.2 (continued) : (a) 3D structure model of closed state hERG K^+ ion channel used in the current study. **(b)** Two different low energy conformations of BeKm-1 (pale and dark pink) and BmTx3b (pale and dark green) toxins at the binding site. **(c, d)** first and second docking poses of hERG1/BeKm-1 complexes. **(e, f)** first and second docking poses for the hERG1/BmTx3b complexes.

BmTx3b is α-KTx and has two different faces (A and B). Face-A side residues K19 and K20 are placed in the α-helix and Face-B side residues K28 and Y37 are placed in the β-sheet. BmTx3b interacts with outer vestibule of hERG1 channel from the Face-A side. In the obtained docking poses (Figure 3.2), the expected interactions from Face-A side were also observed. In order to investigate the time-dependent molecular mechanism of toxin/channel interactions, classical all-atom MD simulations were applied.

(a) (b)

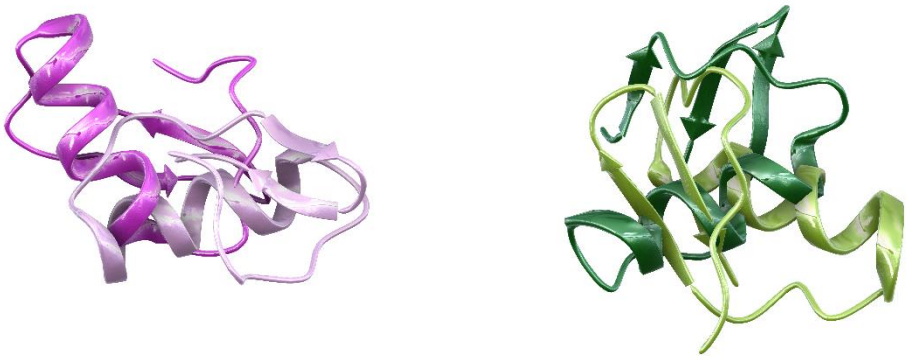

Figure 3.3 : (a) Structural view of the initial poses (i.e., top-docking pose: dark pink; second-best pose: pale pink), of BeKm-1 at the docked complexes (**b)** Structural view of the starting poses (i.e., top-pose: dark green, second-best pose: pale green) of BmTx3b at the docked complexes.

When the selected docking poses of toxins (i.e., top pose and second best) were compared, large conformational differences can be seen in both toxins (Figures 3.3 and 3.4). RMSD values between two used docking poses were found as 13.30 and 12.63 Å for BeKm-1 and BmTx3b toxins, respectively.

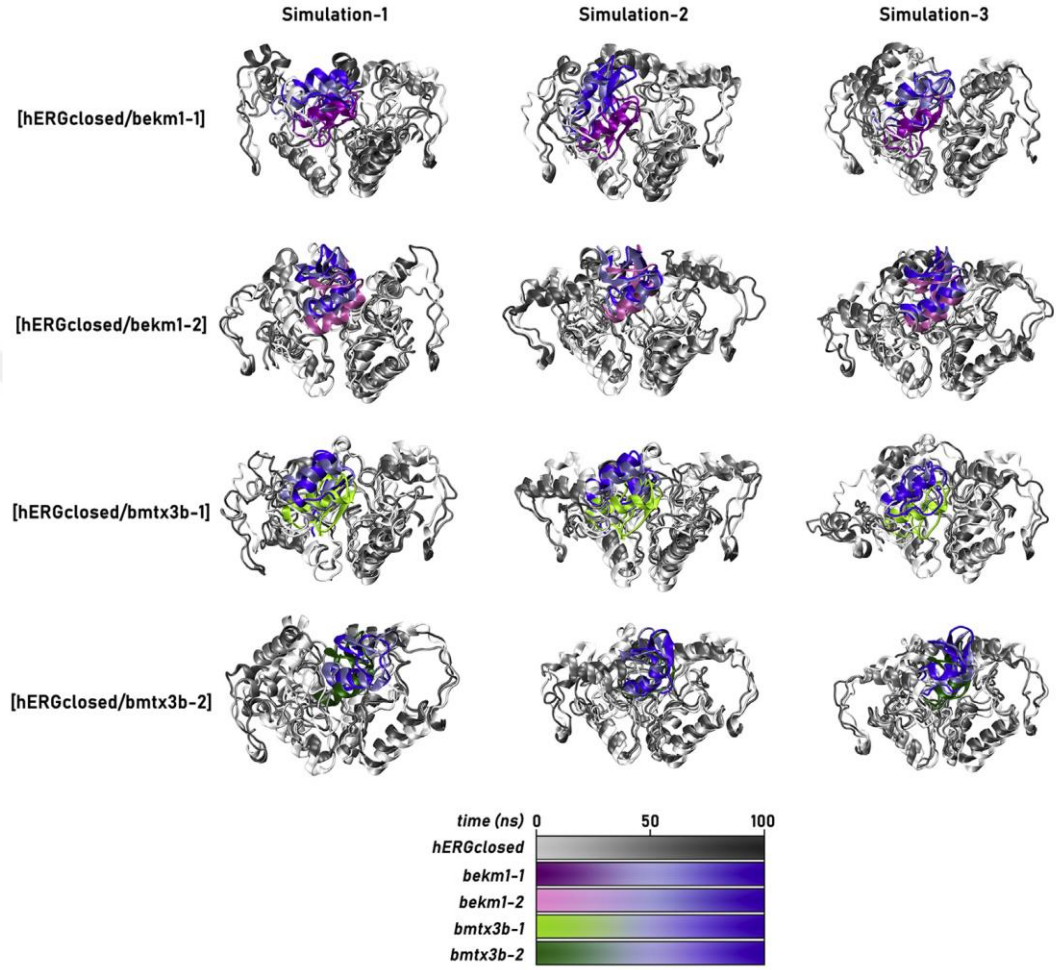

Figure 3.4 : Color-scaled changes of conformations of both toxins throughout the MD simulations.

3.2 MD Simulations

In order to investigate the molecular mechanism of toxin/channel interactions, classical all-atom MD simulations were performed in the closed state of the hERG1 [$hERG_{closed}$] (apo form) and closed form hERG1/toxin complexes [$hERG_{closed}$/BeKm1-1], [$hERG_{closed}$/BeKm1-2], [$hERG_{closed}$/BmTx3b-1] and [$hERG_{closed}$/BmTx3b-2] (holo form) for 100 ns using Gromacs 5.1 program. Each simulation was repeated by three times with different starting velocity distributions. In total, 1.5 μs MD simulations were performed.

3.2.1 RMSD and root-mean square fluctiations (RMSF) analyses of complexes

3.2.1.1 RMSD analyses

RMSD analyzes were calculated throughout the MD trajectory file (10.000 frames for each simulation were collected) based on backbone atoms using VMD program. In Figure A.1, change in the RMSD values of hERG1 channel, given as an average of three independent simulations in each complex are plotted. Results showed that the RMSD values do not change significantly after 20 ns of MD simulations. The individual RMSD values from each simulation for hERG1/toxin complexes are given in Figure A.1. It is clearly seen that the RMSD values of apo form is lower than of the holo form in each case. All complexes are structurally stable in their conformation after reaching the plateau at the RMSD graph.

RMSD values of toxins in each protein-toxin complex as an average of three independent simulations were also depicted in Figure A.1. Although average RMSD values for both of first (top-docking pose) starting conformations of BeKm-1 and BmTx3b toxins to the protein structure were identified with larger changes (i.e., around 7 Å) in conformations compared to their initial structures throughout the simulations, corresponding effects for the second starting poses have smaller values (i.e., around 5 Å) throughout the simulations. All toxin conformations reach to a plateau region after 50-ns at the RMSD-time graph. It must be noted that RMSD graphs for both channel and toxin show average values of three independent runs for each simulation. Corresponding RMSD plots of each individual simulation have been provided in Figure A.1 (b-m)

RMSD plots which belong to only toxins throughout MD simulations were also considered. (Figure 3.6). While the average RMSDs of top-pose of BeKm-1 at the binding site of the channel have around 8 Å, corresponding values for the BmTx3b toxin are around 7 Å. Second-top poses have smaller average RMSD changes throughout the simulations for both toxins (i.e., around 4 Å).

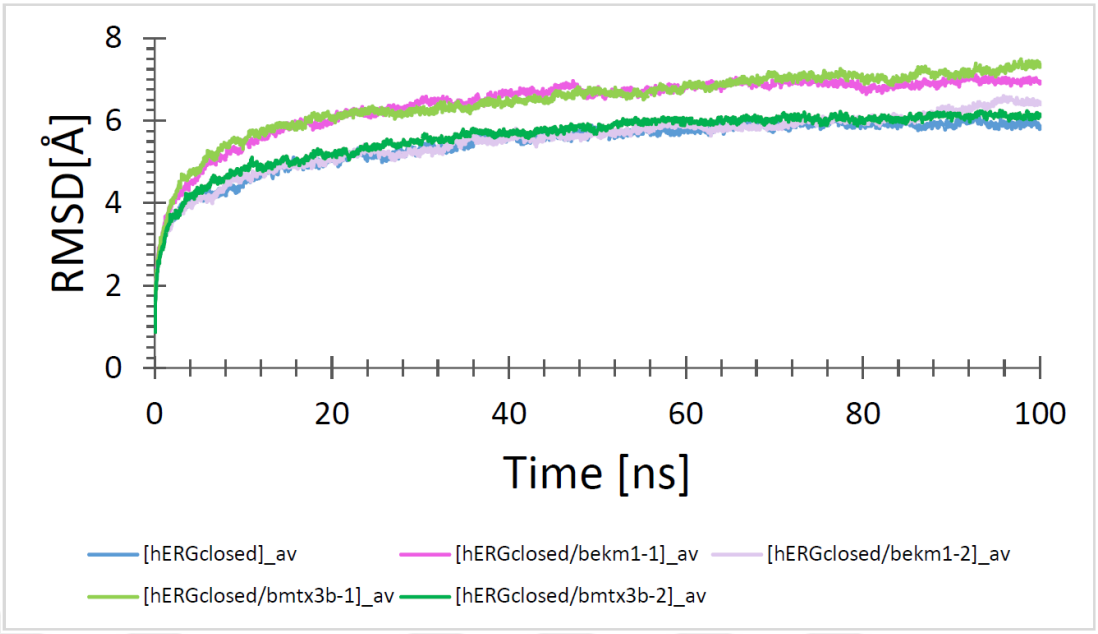

Figure 3.5 : Average RMSD graphs for apo and holo form of complexes.

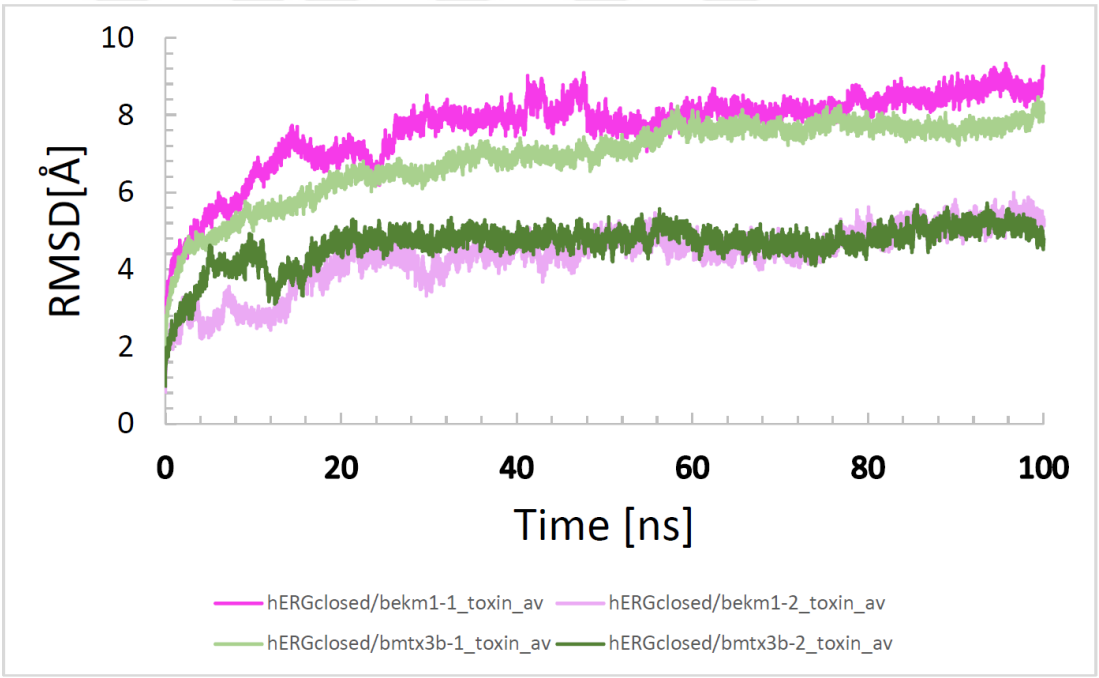

Figure 3.6 : Average RMSD graphs for toxins in complexes.

In order to better represents the conformational change of both toxins throughout the MD simulations, in Figure A.1, time-dependent conformational changes of both toxins are depicted using time-dependent color scales.

3.2.1.2 RMSF analyses

RMSF analysis for each simulation was calculated on Cα atoms using Gromacs trajectory file (10000 frames were used in analysis for each simulation). RMSF figures in Figure A.2 clearly show that no significant changes in hERG1 channel were observed during simulations. As it is expected in S5-pore domain of hERG1, higher fluctuations on apo form compared to holo forms of hERG1 channel were observed. RMSF studies were also studied only for toxins and corresponding figures are provided in Figure 3.7.

a) The RMSF graphs of BeKm-1 toxin in hERG1 close state

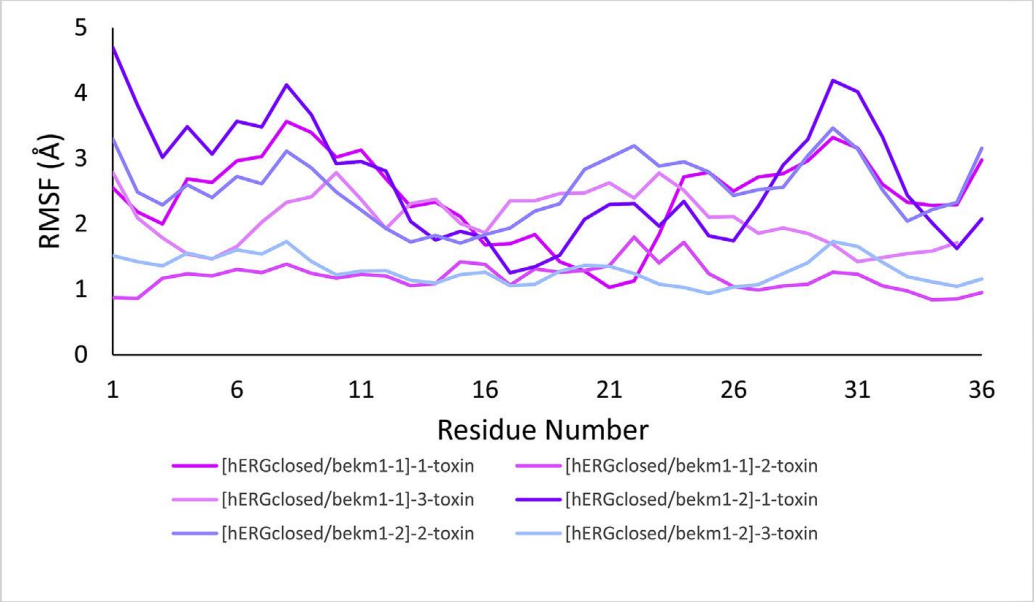

b) The RMSF graphs of BmTx3b toxin in hERG1 close state

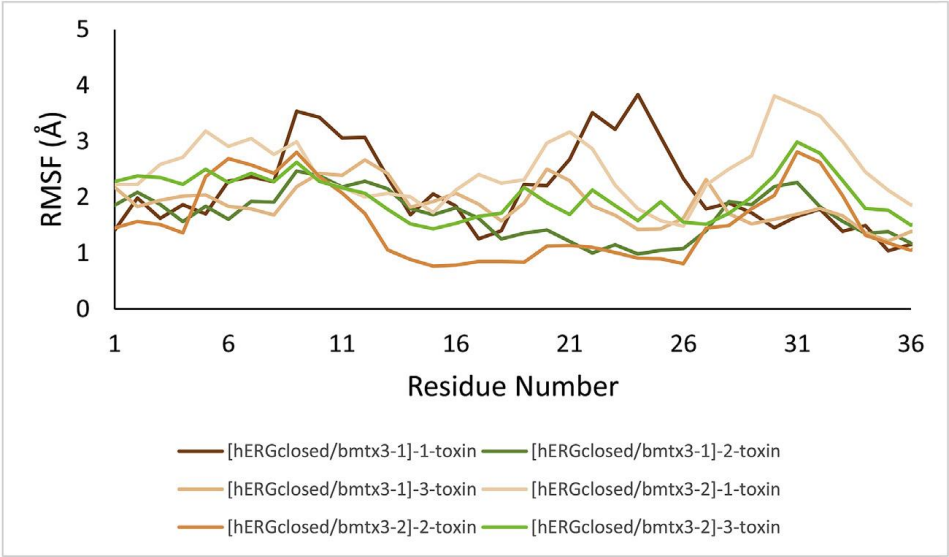

Figure 3.7 : RMSF graphs of BeKm-1 (a); and BmTx3b (b) toxins at the hERG1 closed state.

The smallest RMSF values in the first pose of BeKm-1 during the simulations mainly observed in following residues 21, 31 and 35. Corresponding region of the first pose of BmTx3b were found in residues 24, 25 and 35.

3.3 MM/PBSA Ligand Binding and Decomposition Energy Analyses

MM/PBSA calculations were carried out to calculate the binding free energies of toxins in the hERG1/toxin complexes to understand the interaction pattern of hERG1 with BeKm-1 and BmTx3b and also in order to identify hot spot residues of toxins in complex formation. In these calculations, we first considered the impact of the dielectric constant of the media by changing the dielectric constant, ε. Binding free energies (including vdW, electrostatic, polar solvation and SASA energy contributions) in different dielectric media for hERG/BeKm-1 and hERG/BmTx3B complexes were calculated and given in and Figure 3.8 and Figure A.5.

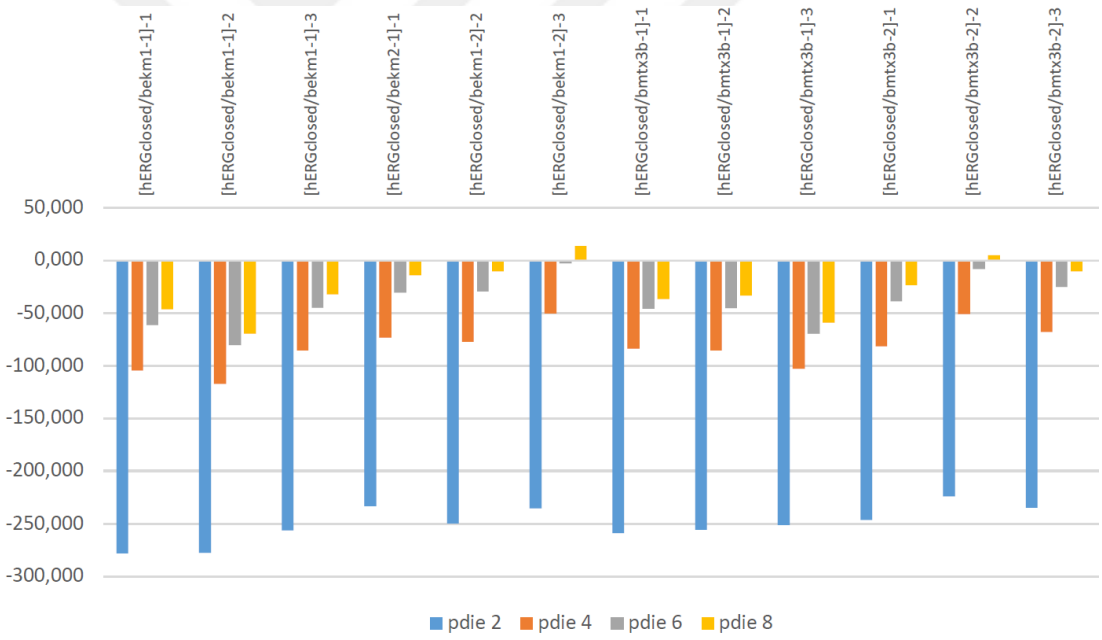

Figure 3.8 : Free Binding Energy Results of hERG/BeKm-1 and hERG/BmTx3b complexes (3 times repeated MD simulations with two different conformation of toxins) using different dielectric constants (values are in kcal/mol).

Table 3.3 shows average binding free energy analysis of toxins considering the ε = 4, which is the most commonly used dielectric constant value for proteins and it is believed to account for electronic polarization and small backbone fluctuation [74]. Results show that in both poses of toxins, top-starting docking poses have stronger binding interactions during the simulations.

Table 3.3 : Average free binding energy results of hERG/BeKm-1 and hERG/BmTx3b complexes (for two different conformation of toxins, ε = 4), values are in kcal/mol.

[hERG/BeKm-1-1]-av	[hERG/BeKm-1-2]-av	[hERG/BmTx3b-1]-av	[hERG/BmTx3b-2]-av
-102.22	-67.00	-90.55	-66.55

Calculated decomposition energies showing the free energy of binding per residue in each toxin are depicted in Figures 3.9 and 3.10. It can be clearly seen that R1, K6, K18, R20, K23 and R27 residues favor the binding of BeKm-1 whereas F1, K7, K19, K20, K28, and R35 favor the binding of BmTx3b to hERG1. In contrast to the nonpolar solvation interactions, the polar solvation interactions were found to make unfavorable contributions to the total binding energies with positive ΔG values.

Although hERG1 forms hydrogen bond and electrostatic interactions with the residues D4, E9, D34 in BeKm-1, their contributions are not enough to overcome large desolvation penalties. Crucial residues playing role in toxin binding were compared with literature data. In the literature, crucial amino acids for BeKm-1/hERG1 interactions were reported to be K18 and R20 [28]. In our studies, in addition to K18 and R20; R1, K6, K23, and R27 were also found to be critical for strong interactions. In literature, K19 and K20 were reported to be crucial for BmTx3b/hERG1 interactions [32]. In our calculations, not only K19 and K20, but also F1, K7, K28, and R35 residues were observed to be important in binding. Figures A.3 and A.4, represent 2D and 3D toxin-channel interactions in atomic details. Figure A.3 (ii) shows the interaction between hERG and BeKm1. GLU575, ASP591, GLN592, GLY604, ASN629, and ASN635 from chain X were contributed to stabilization of BeKm-1 around SF region. SER599 and LEU602 from chain Z were formed interactions with the toxin. For the stabilization of BeKm-1, two chains were involved in the non-covalent interactios. Figure A.4 (ii) shows the interactions between BmTx3b and hERG. ASP591, and ASN629 from chain T, SER600, PHE619, SER620, PHE627, SER631, and LYS638 from chain X, ASP591 and GLN592 from chain Y, and ASP591, SER599, and GLY628 from chain Z were contributed to BmTx3b stabilization around SF region. BmTx3b was stabilized with the contribution of all chains from the hERG side.

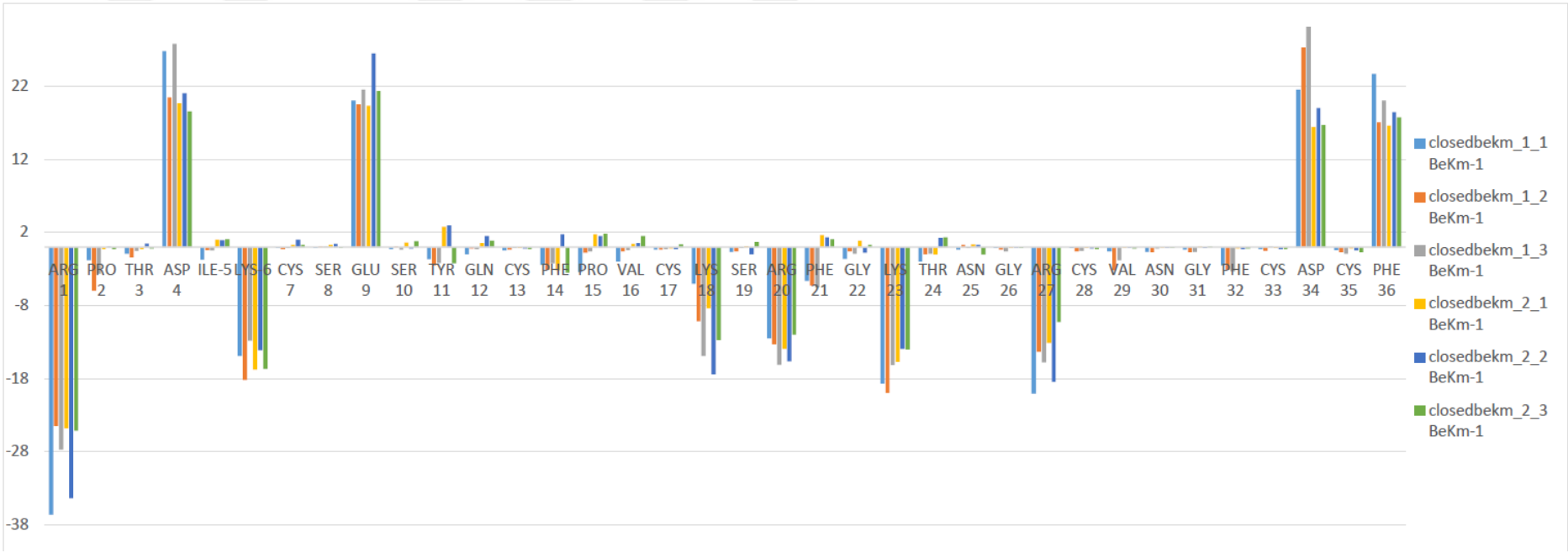

Figure 3.9 : Free Binding Energy Results per each residues of BeKm-1 (values are in kcal/mol).

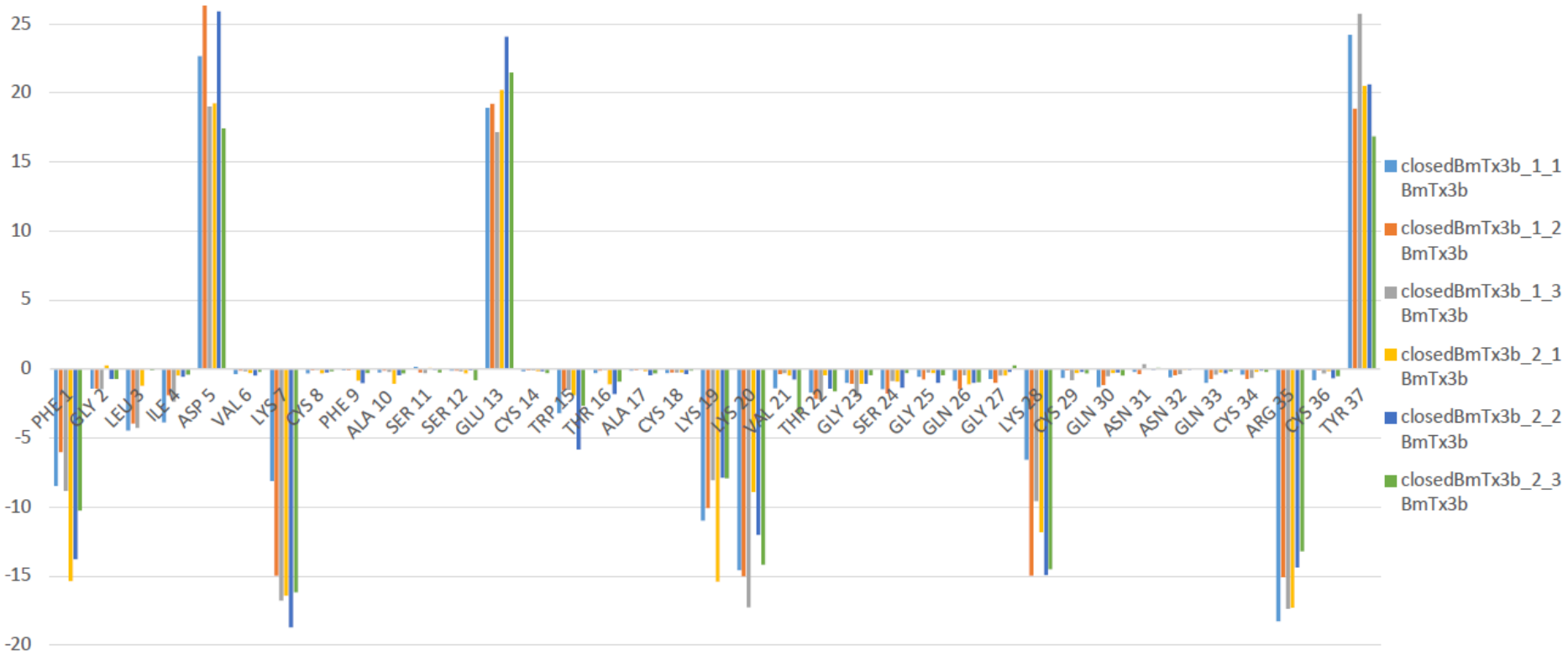

Figure 3.10 : Free Binding Energy Results per each residues of BmTx3b (values are in kcal/mol).

Table 3.4 : The hERG residues that contributed to BeKm-1 and BmTx3b binding.

BeKm-1	BmTx3b
Z:LEU602	X:PHE627
Z:SER599	X:SER620
X:GLN592	X:PHE619
X:ASP591	Z:SER599
X:GLU575	Z:ASP591
X:GLY604	X:SER600
X:ASN635	T:ASN629
X:ASN629	T:ASP591
	Y:ASP591
	Y:GLN592
	Z:GLY628
	X:SER631
	X:LYS638

3.4 *In Silico* Alanine Mutagenesis Study

In this part, 36 residues of BeKm-1 and 37 residues for BmTx3b were mutated with Alanine one at a time. Then, wild and mutated toxins were docked to hERG1 channel. The contribution of each residue of both toxins into the docking score were shown in the ΔΔG plots (Figures 3.11 and 3.12). The in silico Alanine mutagenesis analysis results of hERG-toxin complexes are in good agreement with both MM/PBSA results and the literature [28, 32] regarding to the active residues.

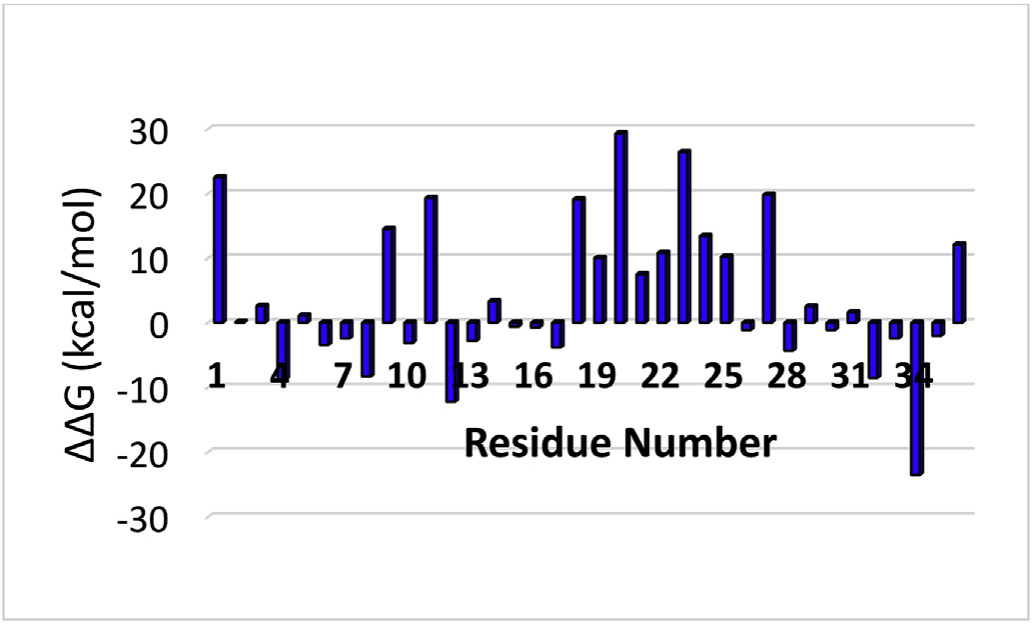

Figure 3.11 : *In Silico* Alanine Mutagenesis results for hERG-BeKm-1 complex.

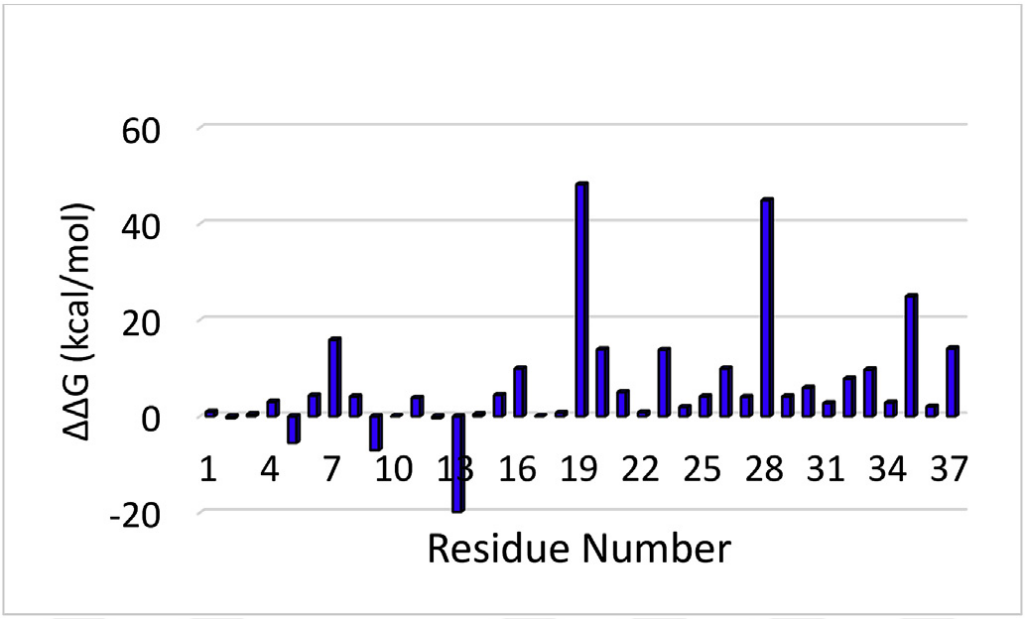

Figure 3.12 : *In Silico* Alanine Mutagenesis results for hERG-BmTx3b complex.

3.5 Conclusions

Although there are a few studies in the literature about the toxin/hERG channel interactions, in the current study a comprehensive approach has been applied. Here, we used whole S1-S6 domains (both PD and VSD parts) of hERG1 channel, in other studies mainly only PD region, so partial parts of the channel were used.

In this study, two toxins BeKm-1 and BmTx3b have been interacted with hERG1 K^+ channel using different molecular modeling approaches including protein-protein docking, classical all-atom MD simulations and post-processing MD analyses as well as in silico Alanine scanning mutagenesis. The crucial residues of toxins playing an important role in binding mechanisms have been highlighted. Based on the analyses, we explored that R1, K6, K18, R20, K23 and R27 residues in BeKm-1 and F1, K7, K19, K20, K28 and R35 residues in BmTx3b are responsible from strong interactions with the closed-state hERG1 K^+ channel. Since the crucial residues from studied toxins sides as well as target protein side as well as nonbonded chemical interactions between them are detailed and highlighted in the current study, this information can be used in designing of better therapeutics which mimics the toxins. Thus, the results of this study can be used by medicinal chemists in the designing of diverse therapeutic applications of natural or synthetic peptides targeting the closed state hERG1 K^+ channels.

4. ATOMIC LEVEL INVESTIGATION OF PARTIAL INHIBITION MECHANISM OF OPEN-STATE HERG WITH *DE NOVO* PEPTIDES, PEPTİDOMIMETICS AND FDA APPROVED PART DRUGS

In this part of the thesis, we screened a library of *de novo* peptides (designed from the toxins BeKm-1 and BmTx3b in the first publication and amino acids that play an important role in the interaction with hERG), peptide-like molecules (peptidomimetics) and FDA-approved molecules. In this screening, the recently revealed open structure of hERG was used. In this structure, two different binding sites were targeted: the inner cavity and the top of the selectivity filter. The grid region consisting of amino acids 623, 624, 652, 653, and 656 was selected for the inner cavity region and amino acids 582, 583, 585, 588, 592, 628, and 631 were selected for the top of the selectivity filter. Molecular docking was then simulated first in the inner cavity region, where molecules with low binding energy were selected and docked to the upper part of the selective filter. As a result of these docking simulations, the ΔΔG was obtained by subtracting the docking score obtained in the inner cavity from the docking score obtained in the upper part of the selective filter. According to the ΔΔG scores, molecular dynamics simulations were performed by selecting the best scoring de novo peptides, peptidomimetics, and FDA-approved molecules. For peptidomimetics and FDA-approved molecules, the molecules that bind most tightly to the top of the selective filter were also selected and included in the MD simulations.

In this section, the obtained docking scores, amino acids involved in the interaction, MD trajectories, simulation interaction plots were evaluated. The binding modes of the molecules selected for the MD simulation were examined in detail, and the stability of the simulation starting poses was evaluated by discussing whether they were maintained throughout the simulation. The RMSD values of the protein and the RMSD changes of the ligand with respect to both the protein and its own atoms were plotted and interpreted throughout the simulation. Finally, the potential mechanisms of partial hERG inhibition by the three library molecules studied (de novo peptides,

peptidomimetics, and FD approved) were elucidated by discussing the conservation rates of the amino acid interactions involved in binding during the simulation.

Table 4.1 : Top 25 *de novo* peptides sorted according to ΔΔG scores.

de novo Peptides	Selectivity Filter ΔG (kcal/mol)	Internal Cavity ΔG (kcal/mol)	ΔΔG (kcal/mol)
QGKCQN_1m2s	-8.73	-5.67	-3.06
TNGRCV_1j5j	-8.52	-6.08	-2.44
DIKCS_1j5j	-6.61	-4.67	-1.94
KCQNNQ_1m2s	-8.13	-6.40	-1.73
WTACKKVTG_1m2s	-8.20	-6.65	-1.55
GKTNG_1j5j	-5.99	-4.95	-1.04
QNNQCR_1m2s	-7.67	-6.73	-0.94
VNGFC_1j5j	-6.10	-5.17	-0.93
SYQCFP_1j5j	-8.54	-7.68	-0.86
KSRF_1j5j	-6.10	-5.25	-0.85
CWTACK_1m2s	-7.13	-6.34	-0.78
KTNGR_1j5j	-6.80	-6.16	-0.64
YQCF_1j5j	-7.51	-6.88	-0.63
CKSRFG_1j5j	-8.31	-7.91	-0.40
VKCFAS_1m2s	-7.73	-7.35	-0.39
SRFGKT_1j5j	-6.14	-5.85	-0.29
WTACKK_1m2s	-8.63	-8.41	-0.22
VTGSGQ_1m2s	-5.89	-5.74	-0.15
FPVCK_1j5j	-7.41	-7.45	0.03
KKVTGS_1m2s	-6.31	-6.40	0.09
NNQCRC_1m2s	-8.20	-8.48	0.28
GLIDVK_1m2s	-4.80	-5.32	0.52
RPTDIK_1j5j	-5.61	-6.39	0.79
KCSESY_1j5j	-7.57	-8.94	1.37
KSRFGK_1j5j	-6.82	-8.42	1.60

We defined a metric (ΔΔG) to select best *de novo* peptides according to their docking scores in two different binding sites. ΔΔG is obtained by subtracting the internal cavity (IC) docking score from selectivity filter (SF) docking score. The lower ΔΔG shows the molecules tends to bind SF more tightly compared to IC. We applied cut-off value as -1.00 kcal/mol, and the molecules that have the ΔΔG lower than this cut-off selected for the MD simulations. Three peptides from 1M2S, and three peptides from 1J5J were selected, in total six molecules were simulated. These were QGKCQN, KCQNNQ, and WTACKKVTG (from 1M2S), and TNGRCV, DIKCS, and GKTNG (from 1J5J). Table 4.1 summarizes the ΔΔG values for all generated de novo peptides (25 de novo molecules) based on their affinities which were obtained in the first part of this thesis study. QGKCQN peptide was the best binder among all according to ΔΔG values. Although WTACKK and SYQCFP were the two most tightly bound peptides

compared to others (the best second and third molecules after QGKCQN), the low binding energies of these two peptides in the IC resulted in high ΔΔG scores. These two peptides were not selected to be used in the simulations. FPVCK, KKVTGS, NNQCRC, GLIDVK, RPTDIK, KCSESY, and KSRFGK peptides were observed to have higher binding affinities in the IC compared to SF, and ΔΔG scores were positive. For the IC, KCSESY was found as the tightest molecules and DIKCS was found as the weakest binder, and for the SF, QGKCQN was the tightest and GLIDVK was the weakest *de novo* peptides.

Table 4.2 : Top 25 peptidomimetics sorted according to ΔΔG scores.

Peptidomimetics	Selectivity Filter ΔG (kcal/mol)	Internal Cavity ΔG (kcal/mol)	ΔΔG (kcal/mol)
C28H27ClN4O4	-5.85	-0.40	-5.45
C27H24N4O4	-6.57	-1.51	-5.06
C24H33N5O4	-5.07	-0.05	-5.03
C25H33N5O4	-5.09	-0.24	-4.85
C25H29N5O5S	-5.06	-0.25	-4.81
C25H28N4O4	-5.30	-0.84	-4.46
C22H21FN4O4S	-5.18	-0.81	-4.37
C27H31N5O2	-5.94	-1.67	-4.27
C24H31N5O5	-4.30	-0.06	-4.24
C26H23ClN4O4	-5.54	-1.35	-4.19
C24H25N3O4	-4.98	-0.82	-4.16
C24H28ClN3O3	-5.73	-1.59	-4.15
C25H28ClN5O5S	-4.81	-0.68	-4.14
C26H24N4O5	-5.74	-1.66	-4.09
C29H30N4O5	-6.42	-2.34	-4.08
C28H32N4O3	-4.36	-0.33	-4.03
C31H32N4O5	-5.42	-1.43	-3.99
C27H25ClN4O4	-6.27	-2.32	-3.95
C26H33N5O5	-5.07	-1.15	-3.92
C27H25FN4O4	-5.84	-1.95	-3.89
C25H31N5O3	-5.33	-1.47	-3.87
C27H30N4O4	-5.86	-2.00	-3.86
C26H38N6O2S	-5.42	-1.57	-3.85
C30H30N4O4	-4.15	-0.31	-3.84
C27H23FN4O4	-6.38	-2.58	-3.80

Table 4.2 lists the ΔΔG scores for the top 25 peptidomimetic molecules. For the peptidomimetics, we used -4.50 kcal/mol, and the molecules that have lower ΔΔG than the cut-off were selected and proceeded to MD simulations. Following molecules were selected; C28H27ClN4O4, C27H24N4O4, C24H33N5O4, C25H33N5O4, and C25H29N5O5S. Among these selected molecules, C28H27ClN4O4 has the lowest ΔΔG among all.

Table 4.3 : The docking scores in IC and SF for the first 25 peptidomimetics according to ΔG in the SF.

Peptidomimetics	Selectivity Filter ΔG (kcal/mol)	Internal Cavity ΔG (kcal/mol)	ΔΔG (kcal/mol)
C28H27ClN4O4	-6.83	-3.08	-3.75
C29H28N4O4	-6.73	-2.97	-3.76
C29H30N4O5	-6.59	-3.83	-2.76
C27H24N4O4	-6.57	-1.51	-5.06
C21H22N4O4	-6.56	-4.07	-2.49
C28H26N4O6	-6.54	-4.00	-2.55
C20H17N3O3	-6.47	-4.33	-2.14
C28H27ClN4O4	-6.46	-4.11	-2.35
C26H24N4O5	-6.45	-2.81	-3.64
C29H30N4O5	-6.42	-2.34	-4.08
C27H23FN4O4	-6.41	-2.64	-3.77
C27H29N3O3S	-6.39	-3.86	-2.54
C27H25FN4O4	-6.39	-3.51	-2.89
C27H23FN4O4	-6.38	-2.58	-3.80
C27H36N6O2	-6.37	-4.14	-2.23
C19H18N4O2	-6.34	-4.30	-2.03
C26H28N4O3	-6.34	-4.55	-1.79
C28H28N4O5	-6.30	-3.36	-2.94
C29H28N4O5	-6.30	-4.29	-2.02
C26H31N3O3	-6.27	-4.23	-2.05
C27H25ClN4O4	-6.27	-2.32	-3.95
C29H30N4O5	-6.26	-4.12	-2.14
C27H23FN4O4	-6.26	-4.57	-1.69
C27H25ClN4O4	-6.24	-2.76	-3.48
C26H24F2N4O2S	-6.23	-3.70	-2.53

Table 4.3 lists the top 25 peptidomimetic molecules according to their docking scores in SF. Top 5 molecules were selected; C28H27ClN4O4, C29H28N4O4, C29H30N4O5, C27H24N4O4, and C21H22N4O4. Among these selected molecules, C28H27ClN4O4 was the tightest binder to the SF.

Table 4.4 : Top 25 FDA molecules sorted according to ΔΔG scores.

FDA Molecules	Selectivity Filter ΔG (kcal/mol)	Internal Cavity ΔG (kcal/mol)	ΔΔG (kcal/mol)
Stallimycin	-5.79	-0.34	-5.45
Iopamidol	-6.80	-1.92	-4.88
Broclepride	-7.01	-2.61	-4.41
Pimelautide	-5.28	-1.06	-4.22
Tienoxolol	-6.16	-2.08	-4.08
Icospiramide	-5.46	-1.67	-3.80
Clebopride	-6.22	-2.47	-3.75
Mioflazinum	-6.85	-3.56	-3.29
Anidoxime	-5.50	-2.25	-3.25

Table 4.4 (continued) : Top 25 FDA molecules sorted according to ΔΔG scores.

FDA Molecules	Selectivity Filter ΔG (kcal/mol)	Internal Cavity ΔG (kcal/mol)	ΔΔG (kcal/mol)
Batanopride	-5.91	-2.67	-3.24
Denipride	-6.00	-2.80	-3.20
Darapladib	-7.10	-3.91	-3.20
Tiprostanide	-6.50	-3.41	-3.10
Novobiocin	-5.51	-2.44	-3.06
Procarbazine	-4.38	-1.35	-3.03
Imanixil	-4.78	-1.80	-2.99
orlistat	-3.25	-0.31	-2.94
Cinitapride	-5.06	-2.21	-2.85
Pirepolol	-6.00	-3.26	-2.74
Ioversol	-6.32	-3.76	-2.56
Diperedon	-6.02	-3.47	-2.55
Nifuroxazide	-4.88	-2.34	-2.54
Sapropterin	-6.27	-3.73	-2.54
Bucromarone	-4.06	-1.53	-2.53
Ioglicic acid	-4.26	-1.73	-2.53

Table 4.4 lists the ΔΔG scores for the top 25 FDA molecules. For the FDA molecules, we used -4.00 kcal/mol, and the molecules that have lower ΔΔG than the cut-off were selected and proceeded to MD simulations. Following molecules were selected; Stallimycin, Iopamidol, Broclepride, Pimelautide, and Tienoxolol. Among these selected molecules, Stallimycin has the lowest ΔΔG among all.

Table 4.5 : The docking scores in IC and SF for the first 25 FDA molecules according to ΔG in the SF.

FDA Molecules	Selectivity Filter ΔG (kcal/mol)	Internal Cavity ΔG (kcal/mol)	ΔΔG (kcal/mol)
Darapladib	-7.10	-3.91	-3.20
Broclepride	-7.01	-2.61	-4.41
Mioflazinum	-6.85	-3.56	-3.29
Iopamidol	-6.80	-1.92	-4.88
Isoetarine	-6.61	-4.53	-2.08
Tiprostanide	-6.50	-3.41	-3.10
Haloperidol	-6.32	-4.46	-1.87
Metkephamid	-6.32	-4.50	-1.82
Ioversol	-6.32	-3.76	-2.56
Sapropterin	-6.27	-3.73	-2.54
Clebopride	-6.22	-2.47	-3.75
Rebimastat	-6.21	-4.38	-1.82
Hydracarbazinum	-6.18	-4.54	-1.64
pantethine	-6.18	-3.69	-2.49
Tienoxolol	-6.16	-2.08	-4.08
Methylene blue	-6.08	-4.53	-1.55
Trazolopride	-6.06	-4.34	-1.71

Table 4.5 (continued): The docking scores in IC and SF for the first 25 FDA molecules according to ΔG in the SF.

FDA Molecules	Selectivity Filter ΔG (kcal/mol)	Internal Cavity ΔG (kcal/mol)	ΔΔG (kcal/mol)
Dioxifedrine	-6.05	-4.51	-1.54
Diperedon	-6.02	-3.47	-2.55
Iopromide	-6.02	-3.91	-2.11
Pirepolol	-6.00	-3.26	-2.74
Denipride	-6.00	-2.80	-3.20
Cloxacepride	-5.94	-3.79	-2.15
Batanopride	-5.91	-2.67	-3.24
Mdl-035	-5.90	-4.48	-1.42

Table 4.5 lists the top 25 FDA molecules according to their docking scores in SF. Top 5 molecules were; Darapladib, Broclepride, Mioflazinum, Iopamidol, and Isoetarine. However, when sorting according to ΔΔG *scores* was performed, Broclepride and Iopamidol were in the selected molecules, so these two were not selected again. Selected molecules were Darapladib, Mioflazinum and Isoetarine. Among these selected molecules, Darapladib was the tightest binder to the SF.

Figure 4.1 shows the docking poses in the SF region for all selected *de novo* peptides. Panel A shows the binding mode of the DICKS in SF region. The residues from chain B and C formed interactions with the peptide. These were ASN588, ASP591, and GLY628 from chain B, GLN592 and ASN629 from chain C. Panel B shows the interactions between GKTNG and hERG. ASN588, GLN592, GLY628, and ASN633 from chain A, GLY628 from chain B, ASN588, and SER631 from chain D formed interactions with the peptide. Panel C shows the interactions between KCQNNQ and hERG, where ASP580, ARG582, ASN588, and GLY628 from chain A, and ASN588, ASP591, GLN592, PHE627, and ASN633 from chain B contributed. Panel D shows the interactions between QGKCQN and hERG. Five non-covalent interactions were observed between peptide and the channel, the contributions of hERG residues were the following ASN588 from chain A, ASP580, and ASP591 from chain B, ASP591 and GLN592 from chain C. The interactions between TNGRCV and hERG is given in panel E. GLY628, and ASN633 from chain A, ASN588, GLY628, and ASN629 from chain B, ASN633 from chain C, and ASN629 from chain D were found in the interaction network of the *de novo* peptide at the SF region. Panel F shows the interactions between WTACKKVTG and hERG, where ASN588, ASP591, and ASN633 from chain A, GLY628 from chain B, ASN629 from chain C, and ASP580 from chain D contributed.

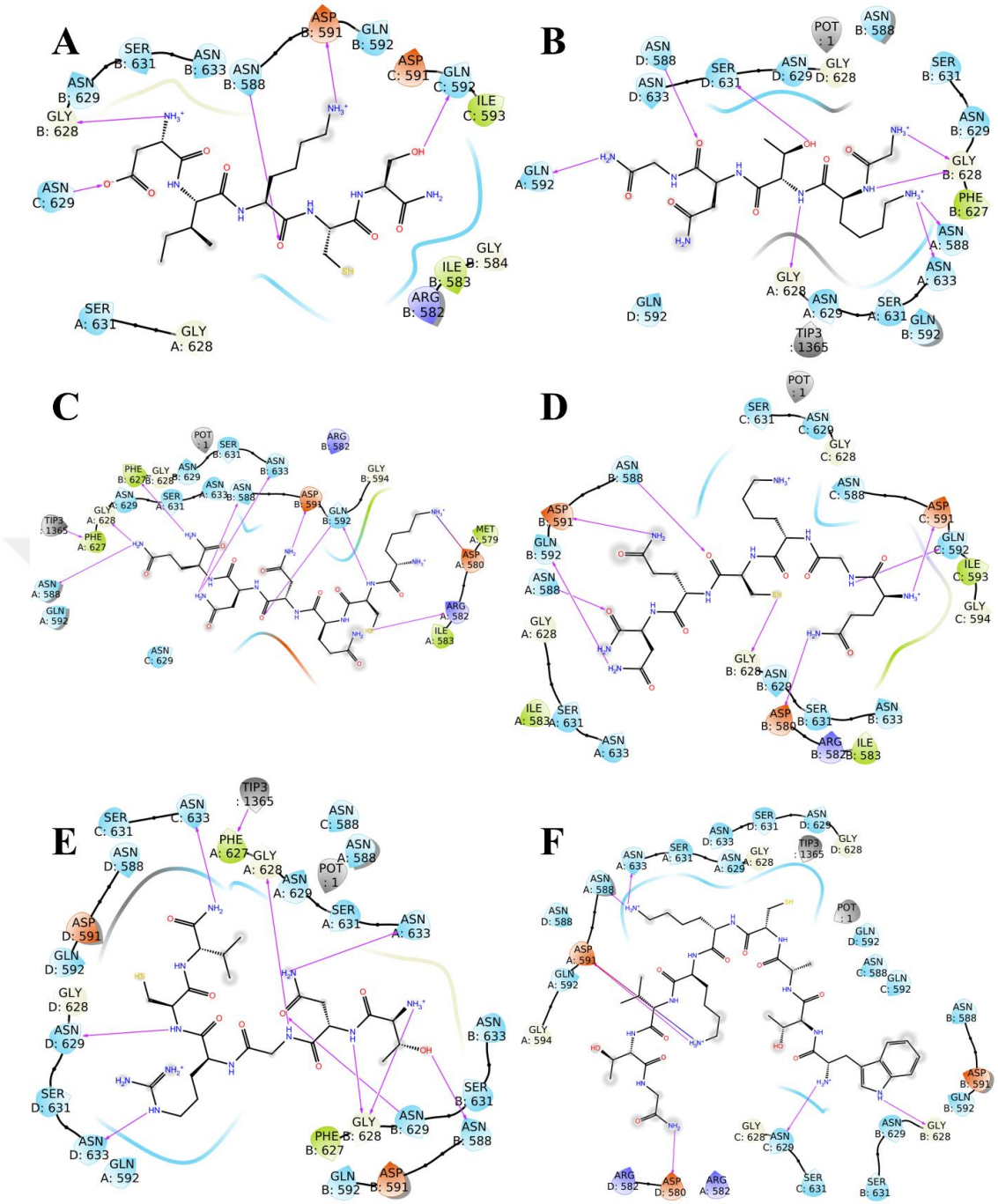

Figure 4.1 : Docking poses for the selected *de novo* molecules. (A) DIKCS, (B) GKTNG, (C) KCQNNQ, (D) QGKCQN, (E) TNGRCV, and (F) WTACKKVTG.

Figure 4.2 shows the docking poses in the SF region for all selected peptidomimetics according to their ΔΔG scores. Panel A shows the binding mode of the C28H27ClN4O4 in SF region. GLY628 from chain A, ASN633 from chain C, ASN588 from chain D, and potassium ion from the SF were contributed to C28H27ClN4O4 binding. Panel B shows the interactions between hERG and C27H24N4O4. GLY628 from chain B, ASN588 and ASN633 from chain D contributed to stabilize C27H24N4O4 in the SF region. The interactions between

C24H33N5O4 and hERG are given in Panel C, where ASN588 and GLY628 from chain C, and ASN629 from chain D, and the potassium ion from SF were contributed. GLY628 from chain D formed two interactions with C25H33N5O4, and this binding mode is given in Panel D. Panel E shows the interactions between C25H29N5O5S and hERG, where ASN588, and GLY628 from chain C, and potassium ion from SF, GLN592, and ASN629 from chain D found to be contributed.

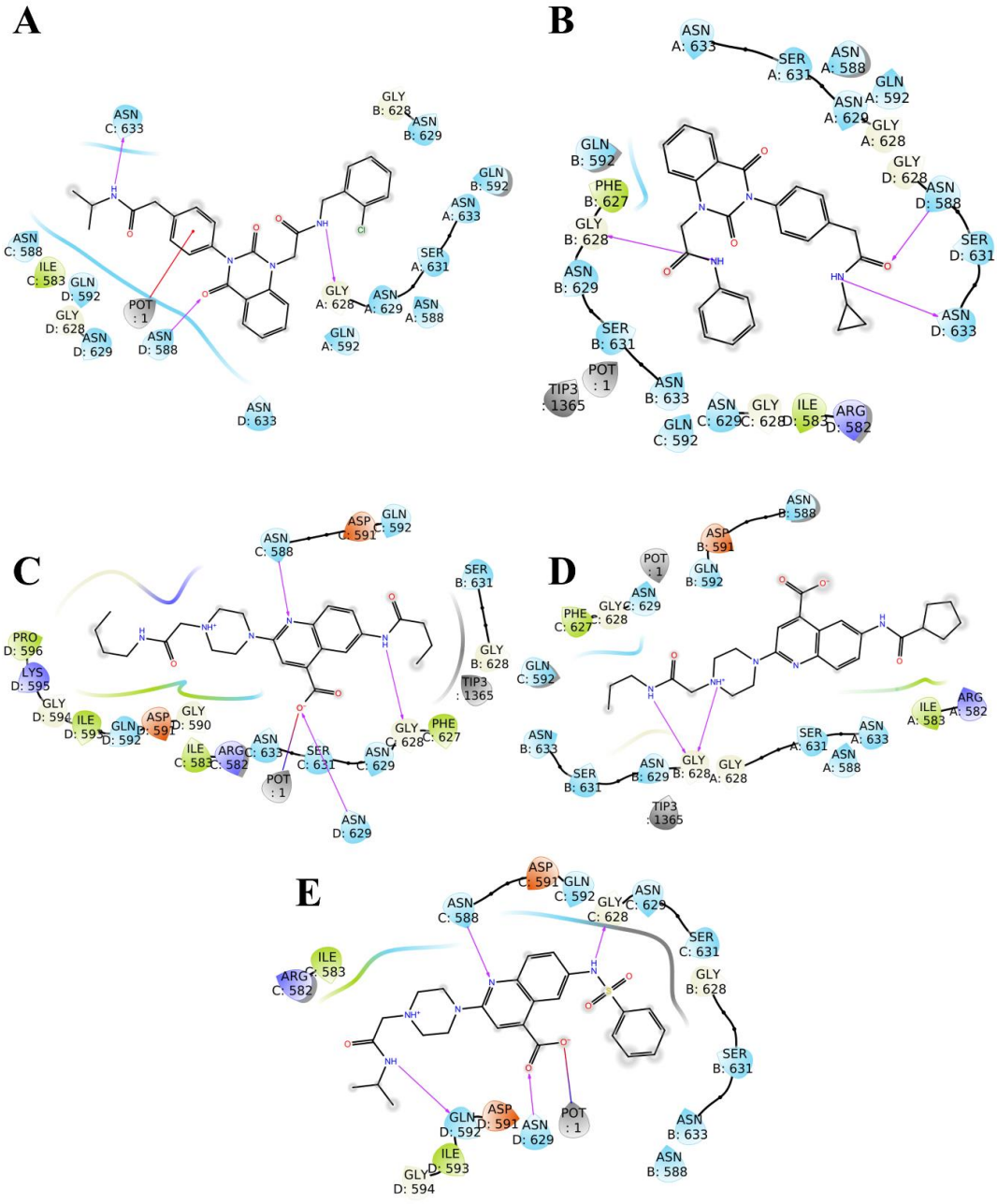

Figure 4.2 : Docking poses for the selected peptidomimetics according to their ΔΔG scores. (A) C28H27ClN4O4, (B) C27H24N4O4, (C) C24H33N5O4, (D) C25H33N5O4, and (E) C25H29N5O5S.

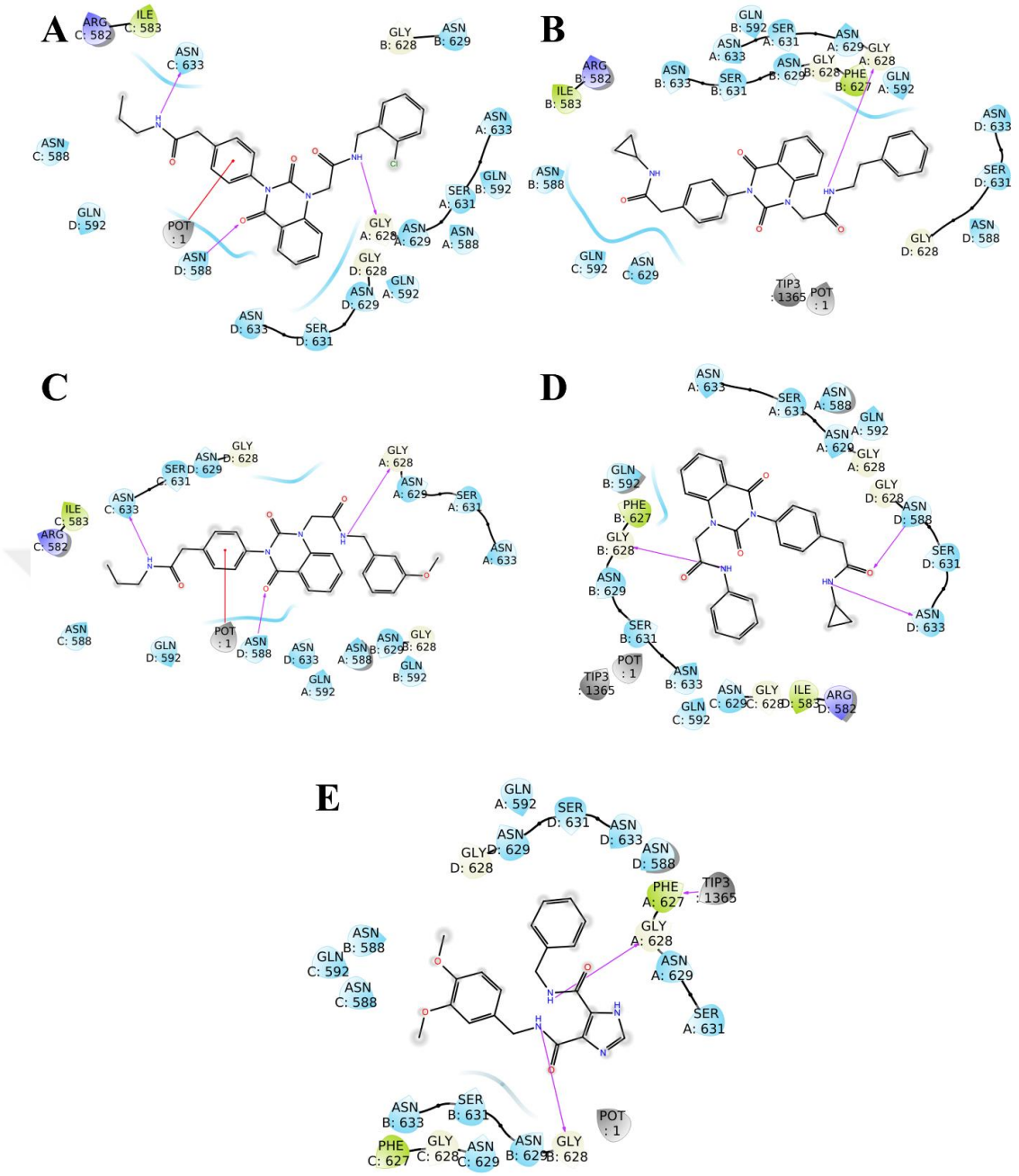

Figure 4.3 : Docking poses for the selected peptidomimetics according to their ΔG scores in the SF. (A) C28H27ClN4O4, (B) C29H28N4O4, (C) C29H30N4O5, (D) C27H24N4O4, and (E) C21H22N4O4.

Figure 4.3 shows the docking poses in the SF region for all selected peptidomimetics according to their ΔG scores in SF. Panel A shows the binding mode of the C28H27ClN4O4 in SF region. GLY628 from chain A, ASN633 from chain C, ASN588 from chain D, and potassium ion from the SF were contributed to C28H27ClN4O4 binding. Panel B shows the interactions between hERG and C29H28N4O4. Only one interaction was observed where GLY628 from chain B contributed. The interactions between C29H30N4O5 and hERG are given in Panel C,

where GLY628 from chain A, and the potassium ion from SF were contributed. GLY628 from chain B, and ASN588, and ASN633 from chain D formed three interactions with C27H24N4O4, and this binding mode is given in Panel D. Panel E shows the interactions between C21H22N4O4 and hERG, where GLY628 from chain A and B found to be contributed.

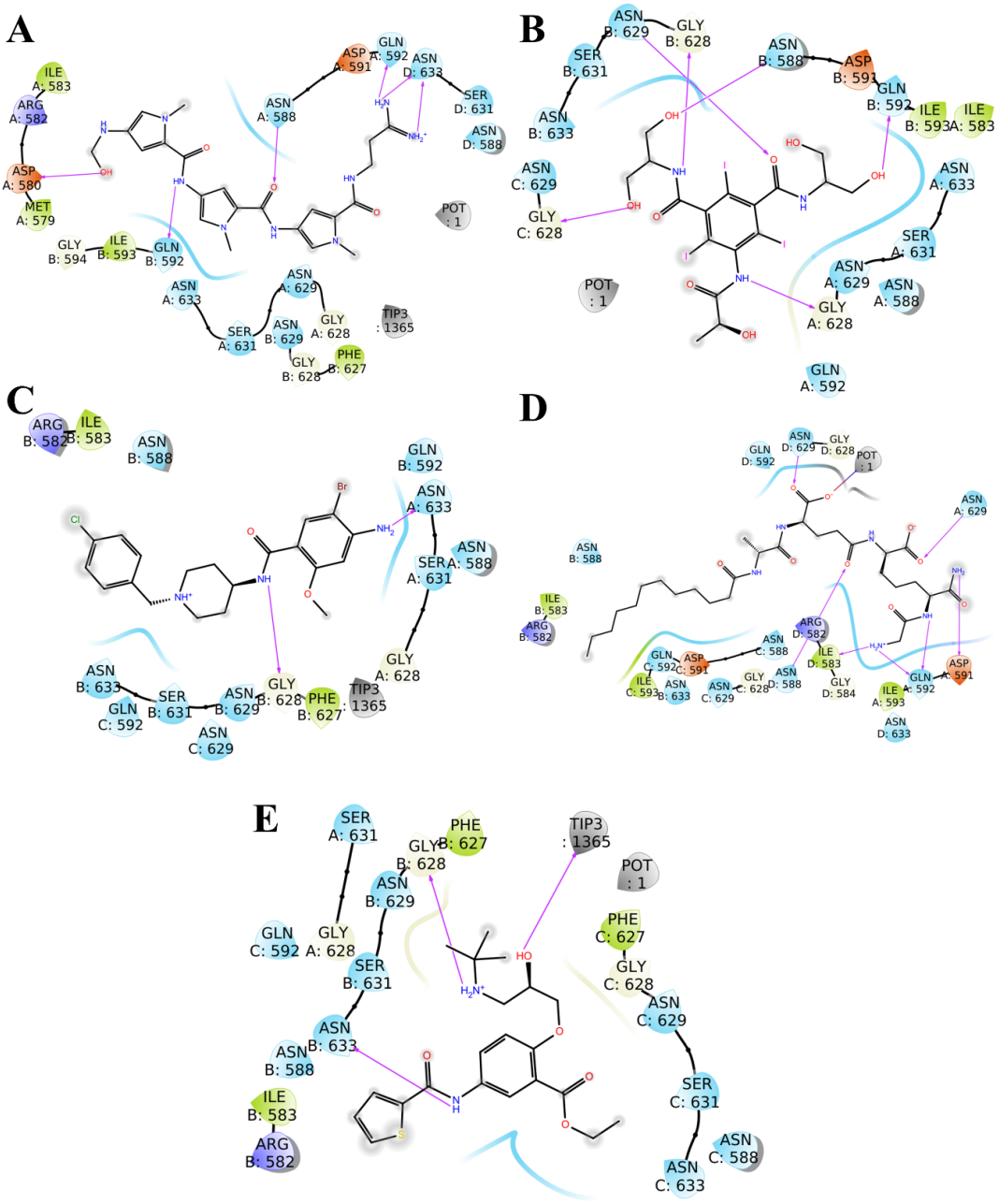

Figure 4.4 : Docking poses for the selected FDA molecules according to their ΔΔG scores. (A) Stallimycin, (B) Iopamidol, (C) Broclepride, (D) Pimelautide, and (E) Tienoxolol.

Figure 4.4 shows the docking poses in the SF region for all selected FDA molecules according to their ΔΔG scores. Panel A shows the binding mode of the Stallimycin in

SF region. ASP580, ASN588, and GLN592 from chain A, GLN592, and ASN633 from chain B were contributed for the stabilization of Stallimycin in SF region. Panel B shows the interactions between hERG and Iopamidol. GLY628 from chain A, ASN588, GLN592, GLY628, and ASN629 from chain B, and GLY628 from chain C formed interactions with the Iopamidol. The interactions between Broclepride and hERG are given in Panel C, where ASN633 from chain A and GLY628 from chain B were contributed. ASP591, GLN592, and ASN629 from chain A, ILE583, ASN588, and ASN629 from chain D, and potassium from SF formed seven interactions with Pimelautide, and this binding mode is given in Panel D. Panel E shows the interactions between Tienoxolol and hERG, where GLY628, and ASN633 from chain B, and water molecule from SF were found to be contributed.

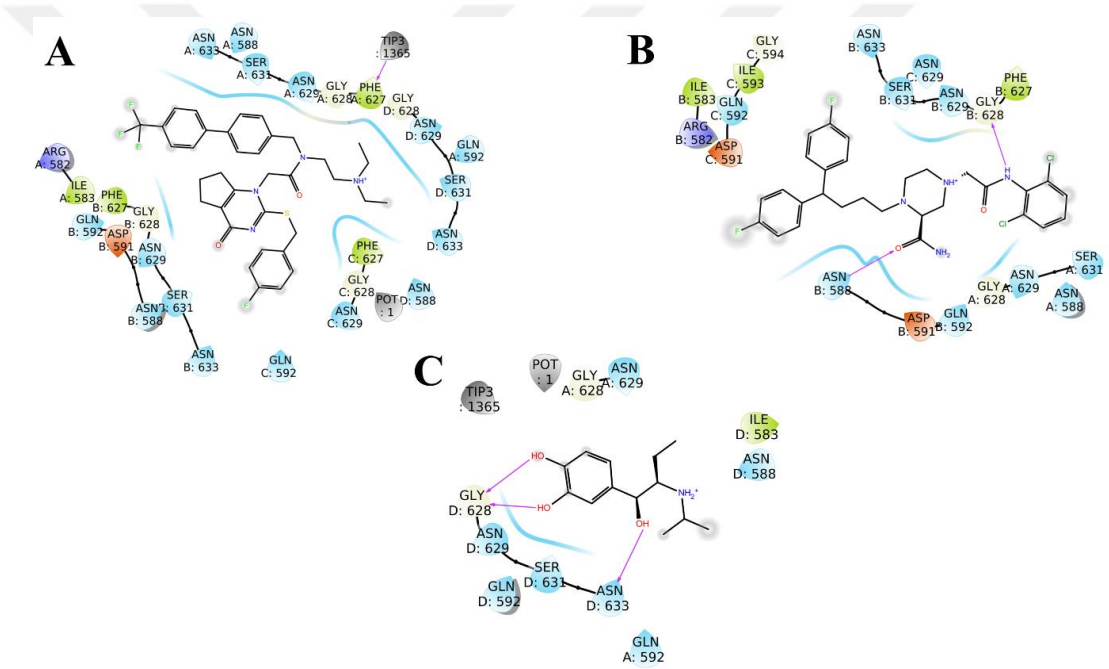

Figure 4.5 : Docking poses for the selected FDA molecules according to their ΔG scores in the SF. (A) Darapladib, (B) Mioflazinum, and (C) Isoetarine.

Figure 5 shows the docking poses in the SF region for all selected FDA molecules according to their ΔG scores in SF. Table 5 lists the ΔG scores, since Broclepride (2nd best based on docking score in SF) and Iopamidol (4th best based on docking score in SF) were selected based on their ΔΔG scores, so these binding poses were not included in the comparison of molecules according to ΔG scores. Panel A shows the binding mode of the Darapladib, and no direct bonding was observed, however shape complementarity of the molecule in the SF region was satisfactory to observe -7.10 kcal/mol docking score. The interactions between Mioflazinum and hERG is depicted

in panel B, where ASN588 from chain A, and GLY628 from chain B contributed binding. Isoetarine binding mode is given in Panel C, GLY628, and ASN633 from chain D formed three interactions with hERG.

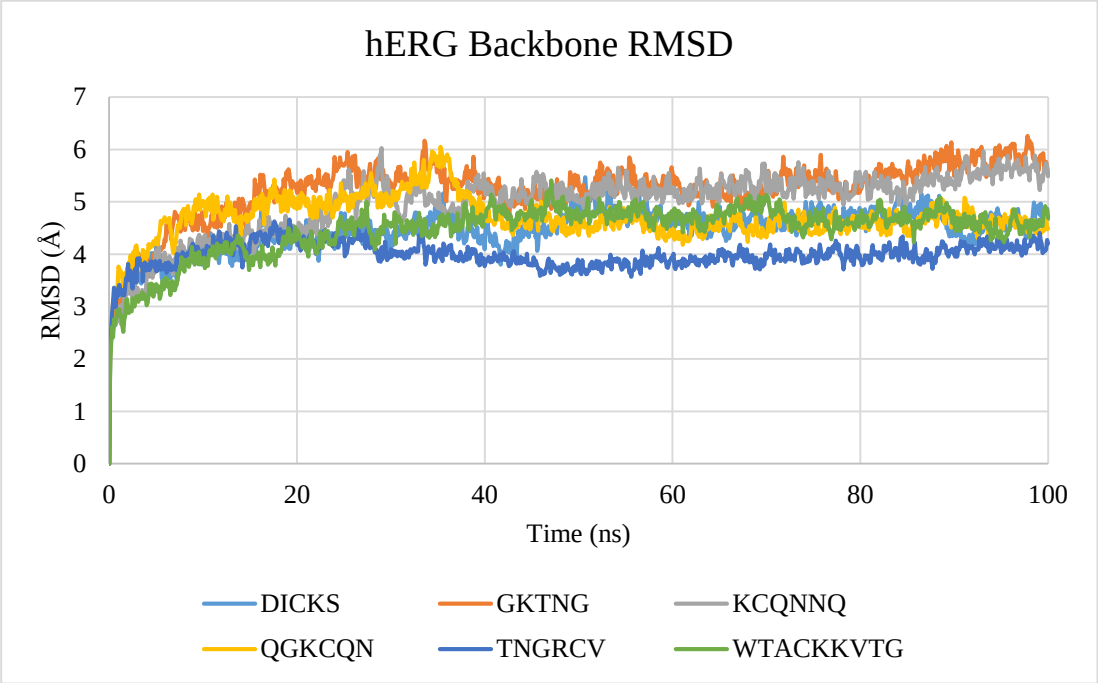

Figure 4.6 : Backbone RMSD values for hERG in *de novo* peptide complexes.

Figure 4.6 shows the root mean squared deviation (RMSD) values for the backbone atoms in the de novo peptide – hERG complexes. All complexes reached plateau after first 20 ns. The BB RMSD averages and the standard deviations (SD) were given in Table 4.6 for the BB atoms of hERG for the selected de novo peptide complexes.

Table 4.6 : Backbone RMSD averages and the SDs for the hERG complexes with selected *de novo* peptides.

	DIKCS	GKTNG	KCQNNQ	QGKCQN	TNGRCV	WTACKKVTG
Averages	4.46	5.24	4.98	4.69	3.98	4.46
SD (±)	0.43	0.57	0.63	0.42	0.27	0.50

According to Table 4.6, the lowest RMSD value for hERG backbone atoms was observed in TNGRCV-hERG complex (3.98 ± 0.27 Å), and the highest RMSD value was observed in GKTNG-hERG complex (5.24 ± 0.57 Å).

Figure 4.7 shows the LFP RMSD values for the *de novo* peptides. For all peptides different patterns were observed. Among all studied de novo peptides only TNGRCV has LFP RMSD value lower than 5 Å. GKTNG, and WTACKKVTG clearly diffused

away from the SF region. The LFP RMSD averages and the standard deviations (SD) were given in Table 4.7 for the selected *de novo* peptide complexes.

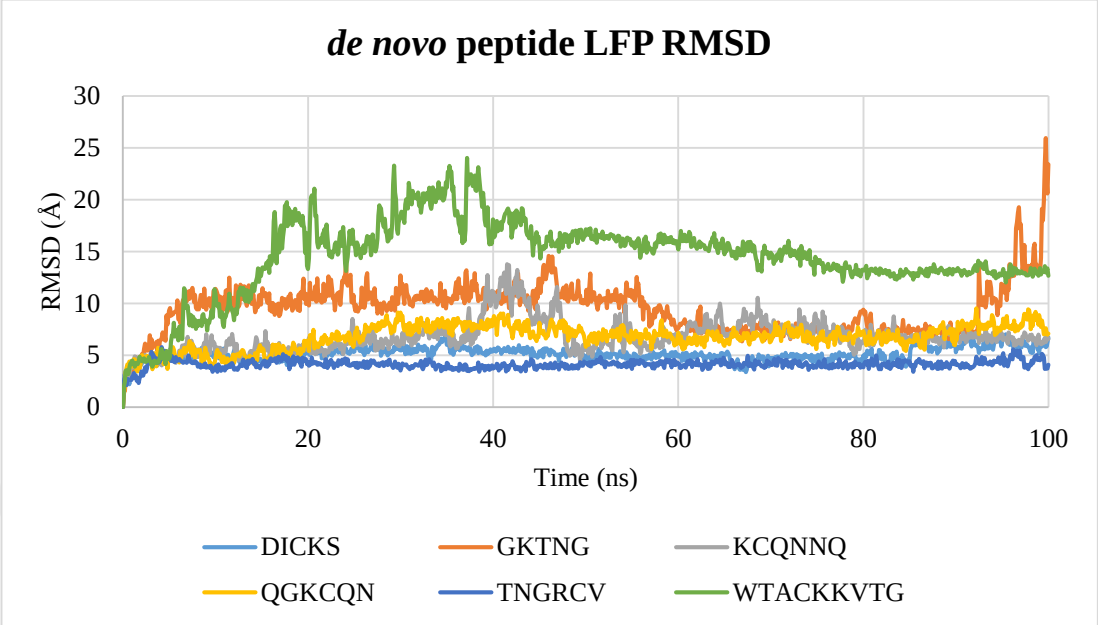

Figure 4.7 : Lig Fit Prot (LFP) RMSD values for *de novo* peptides.

According to Table 4.7, the lowest LFP RMSD value for *de novo* peptides was observed in TNGRCV (4.11 ± 0.42 Å), and the highest LFP RMSD value was observed in WTACKKVTG (14.43 ± 3.80 Å), clearly showing that the peptide diffused away from the SF region.

Table 4.7 : LFP RMSD averages and the SDs for selected *de novo* peptides.

	DIKCS	GKTNG	KCQNNQ	QGKCQN	TNGRCV	WTACKKVTG
Averages	5.14	9.49	6.78	6.74	4.11	14.43
SD (±)	0.67	2.44	1.58	1.19	0.42	3.80

Figure 4.8 shows the LFL RMSD values for the *de novo* peptides. For all peptides different patterns were observed. Among all studied *de novo* peptides only WTACKKVTG and KCQNNQ have LFP RMSD value higher than 3 Å. The LFP RMSD averages and the standard deviations (SD) were given in Table 4.8 for the selected *de novo* peptide complexes.

Table 4.8 : LFL RMSD averages and the SDs for selected *de novo* peptides.

	DIKCS	GKTNG	KCQNNQ	QGKCQN	TNGRCV	WTACKKVTG
Averages	1.58	2.38	2.91	2.35	2.34	4.61
SD (±)	0.38	0.41	0.94	0.28	0.28	0.62

According to Table 4.8, the lowest LFL RMSD value for *de novo* peptides was observed in DIKCS (1.58 ± 0.38 Å), and the highest LFL RMSD value was observed in WTACKKVTG (4.61 ± 0.62 Å).

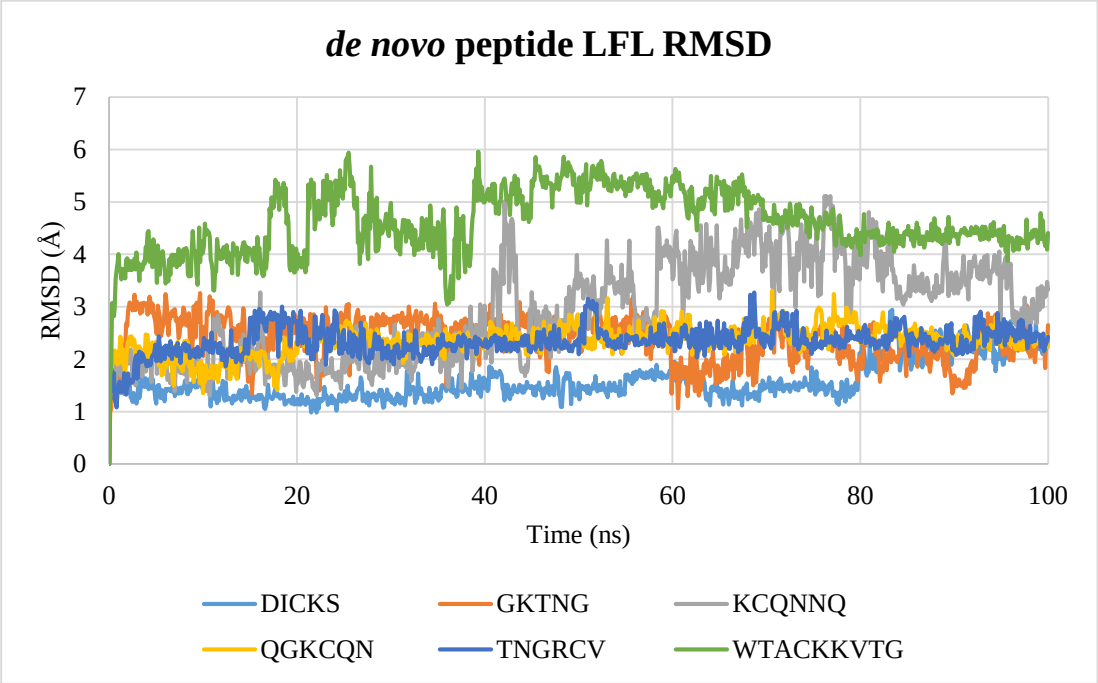

Figure 4.8 : Lig Fit Lig (LFL) RMSD values for de novo peptides.

Figure 4.9 shows the BB RMSD values for the peptidomimetics. For all peptides different patterns were observed. All complexes reached plateau after first 30 ns. The BB RMSD averages and the standard deviations (SD) were given in Table 4.9 for the BB atoms of hERG for the selected de peptidomimetics complexes.

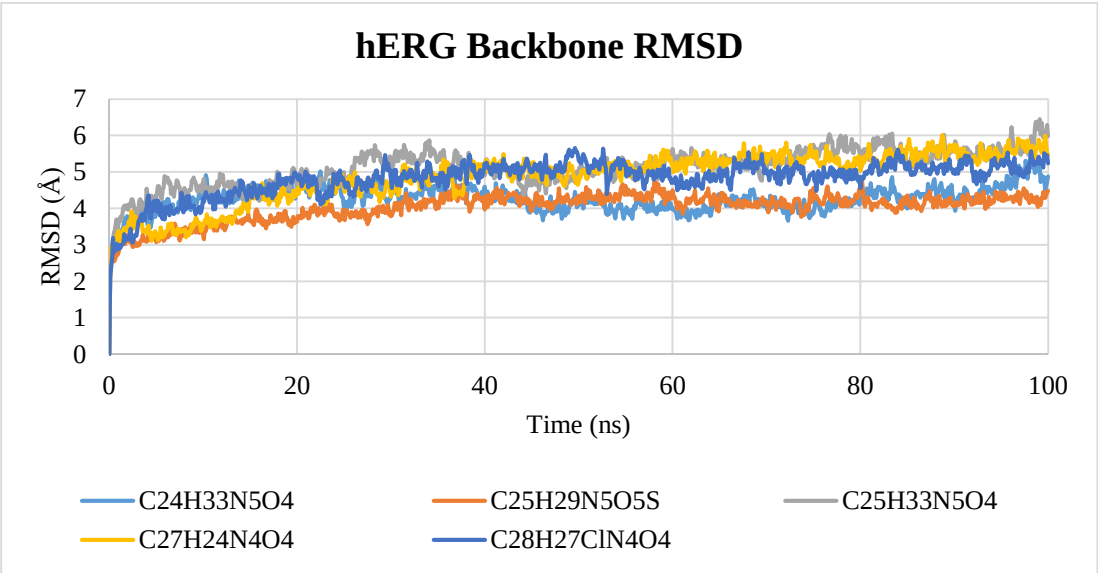

Figure 4.9 : Backbone RMSD values for hERG in peptidomimetics complexes which selected according to ΔΔG scores.

Table 4.9 : Backbone RMSD averages and the SDs for the hERG complexes with selected peptidomimetics based on ΔΔG scores.

	C24H33N5O4	C25H29N5O5S	C25H33N5O4	C27H24N4O4	C28H27ClN4O4
Averages	4.26	4.02	5.11	4.86	4.81
SD (±)	0.37	0.40	0.53	0.71	0.51

According to Table 4.9, the lowest RMSD value for hERG backbone atoms was observed in C25H29N5O5S-hERG complex (4.02 ± 0.40 Å), and the highest RMSD value was observed in C25H33N5O4-hERG complex (5.11 ± 0.53 Å).

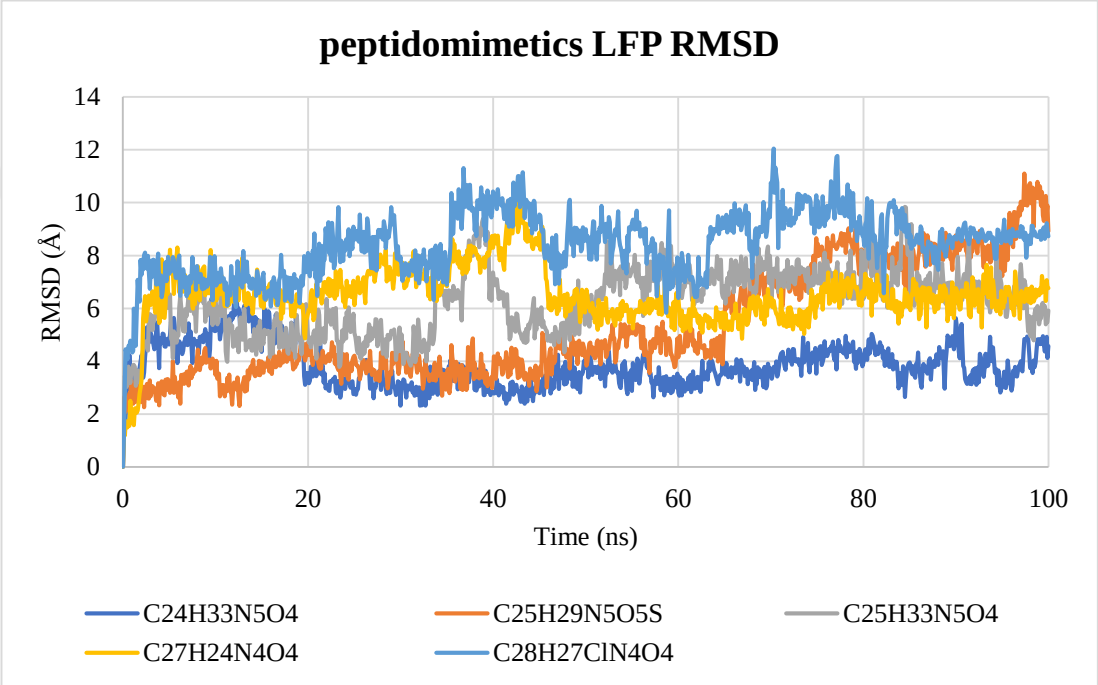

Figure 4.10 : Lig Fit Prot (LFP) RMSD values for peptidomimetics which selected based on ΔΔG scores.

Figure 4.10 shows the LFP RMSD values for the peptidomimetics. For all peptides different patterns were observed. Among all studied de novo peptides only C24H33N5O4 has LFP RMSD value lower than 4 Å. C28H27ClN4O4 clearly diffused away from the SF region. The LFP RMSD averages and the standard deviations (SD) were given in Table 4.10 for the selected peptidomimetics complexes.

Table 4.10 : LFP RMSD averages and the SDs for the peptidomimetics which selected based on ΔΔG scores.

	C24H33N5O4	C25H29N5O5S	C25H33N5O4	C27H24N4O4	C28H27ClN4O4
Averages	3.84	5.33	6.23	6.51	8.40
SD (±)	0.83	2.12	1.25	1.11	1.23

According to Table 4.10, the lowest LFP RMSD value for peptidomimetics was observed in C24H33N5O4 (3.84 ± 0.83 Å), and the highest LFP RMSD value was observed in C28H27ClN4O4 (8.40 ± 1.23 Å), clearly showing that this peptidomimetics diffused away from the SF region.

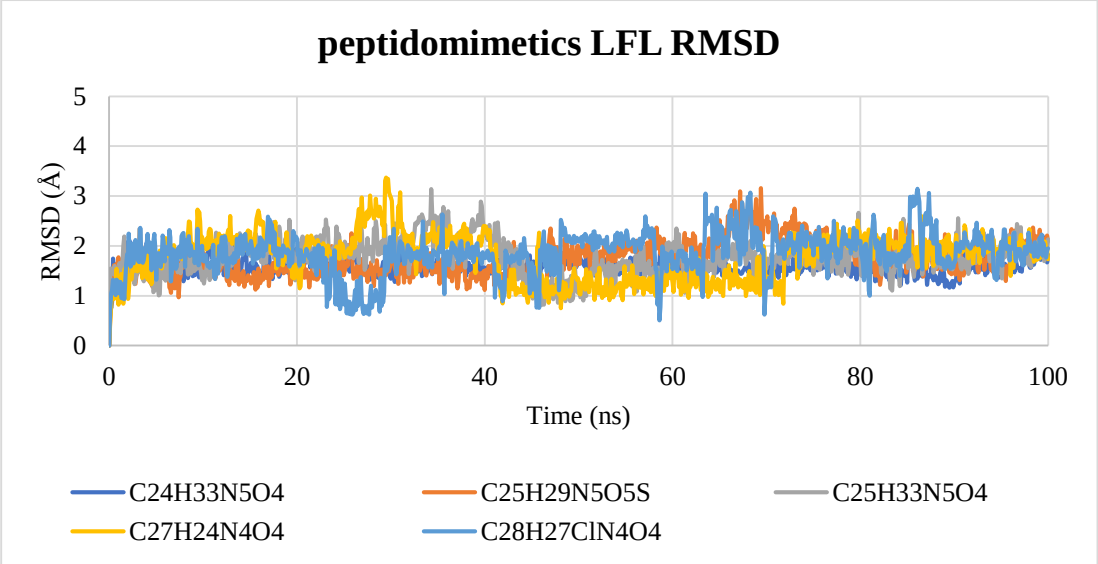

Figure 4.11 : Lig Fit Lig (LFL) RMSD values for peptidomimetics which selected based on ΔΔG scores.

Figure 4.11 shows the LFL RMSD values for the peptidomimetics which selected based on ΔΔG scores. All peptidomimetics displayed LFP RMSD values lower than 3 Å. The LFP RMSD averages and the standard deviations (SD) were given in Table 4.11 for the selected *de novo* peptide complexes.

Table 4.11 : LFL RMSD averages and the SDs for the peptidomimetics which selected based on ΔΔG scores.

	C24H33N5O4	C25H29N5O5S	C25H33N5O4	C27H24N4O4	C28H27ClN4O4
Averages	1.57	1.74	1.77	1.77	1.85
SD (±)	0.17	0.36	0.36	0.47	0.42

According to Table 4.11, the lowest LFL RMSD value for the peptidomimetics was observed in C24H33N5O4 (1.57 ± 0.17 Å), and the highest LFL RMSD value was observed in C28H27ClN4O4 (1.85 ± 0.42 Å).

Figure 4.12 shows the BB RMSD values for the peptidomimetics. For all peptides different patterns were observed. All complexes reached plateau after first 10 ns. The BB RMSD averages and the standard deviations (SD) were given in Table 4.12 for the BB atoms of hERG for the selected peptidomimetics complexes.

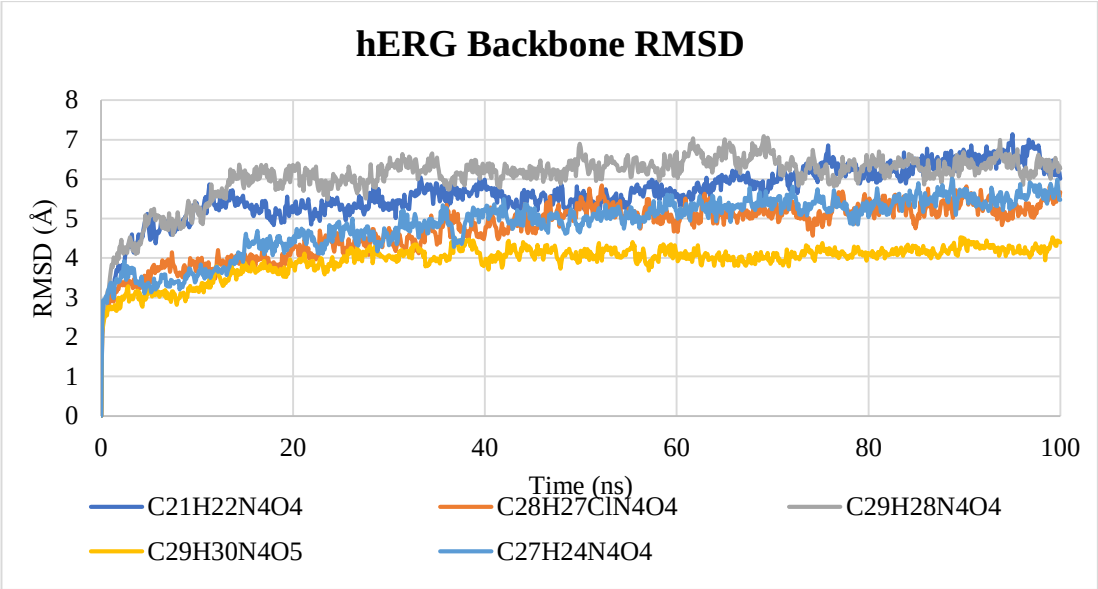

Figure 4.12 : Backbone RMSD values for hERG in peptidomimetics complexes which selected according to ΔG scores in SF.

Table 4.12 : LFL RMSD averages and the SDs for the peptidomimetics which selected based on ΔΔG scores.

	C21H22N4O4	C28H27ClN4O4	C29H28N4O4	C29H30N4O5	C27H24N4O4
Averages	5.65	4.74	6.06	3.94	4.86
SD (±)	0.69	0.67	0.65	0.41	0.71

According to Table 4.12, the lowest RMSD value for hERG backbone atoms was observed in C29H30N4O5-hERG complex (3.94 ± 0.41 Å), and the highest RMSD value was observed in C29H28N4O4-hERG complex (6.06 ± 0.65 Å).

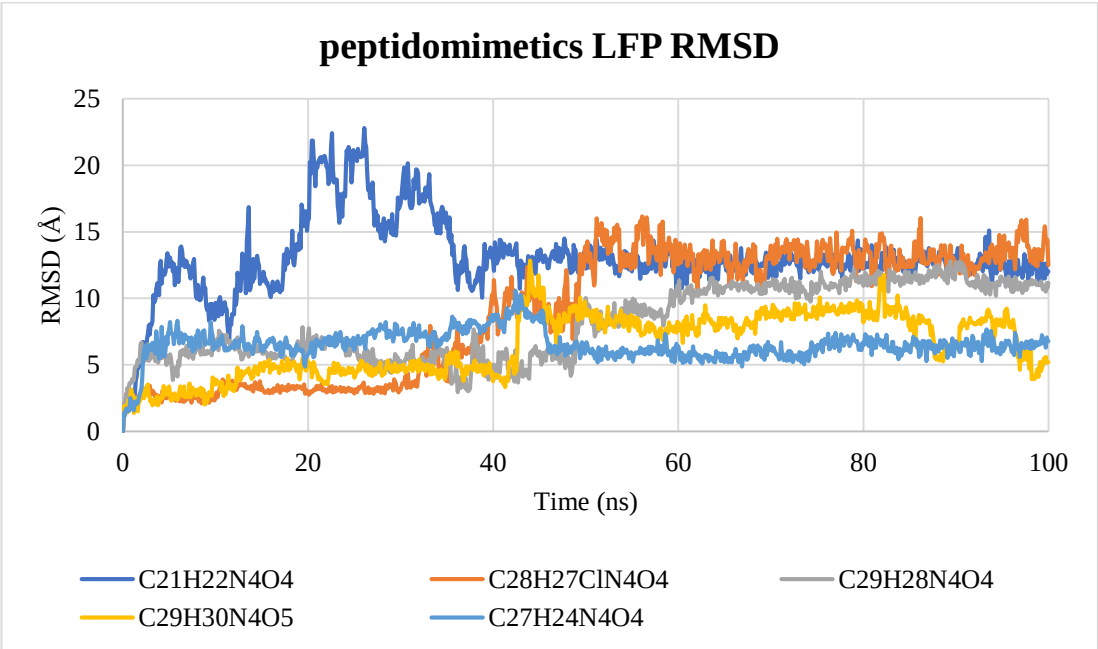

Figure 4.13 : Lig Fit Prot (LFP) RMSD values for peptidomimetics which selected based on ΔG scores in SF.

Figure 4.13 shows the LFP RMSD values for the peptidomimetics which selected based on ΔG scores in SF. For all peptides different patterns were observed. Among all studied peptidomimetics only C29H30N4O5 and C27H24N4O4 have LFP RMSD value lower than 7 Å. C29H28N4O4, C28H27ClN4O4, and C21H22N4O4 clearly diffused away from the SF region. The LFP RMSD averages and the standard deviations (SD) were given in Table 4.13 for the selected peptidomimetics complexes.

Table 4.13 : LFP RMSD averages and the SDs for the peptidomimetics which selected based on ΔG scores in SF.

	C21H22N4O4	C28H27ClN4O4	C29H28N4O4	C29H30N4O5	C27H24N4O4
Averages	1.57	1.74	1.77	1.77	1.85
SD (±)	0.17	0.36	0.36	0.47	0.42

According to Table 4.13, the lowest LFP RMSD value for peptidomimetics was observed in C29H30N4O5 (6.48 ± 2.34 Å), and the highest LFP RMSD value was observed in C21H22N4O4 (13.04 ± 2.93 Å), clearly showing that this peptidomimetics together with C28H27ClN4O4, and C29H28N4O4 diffused away from the SF region.

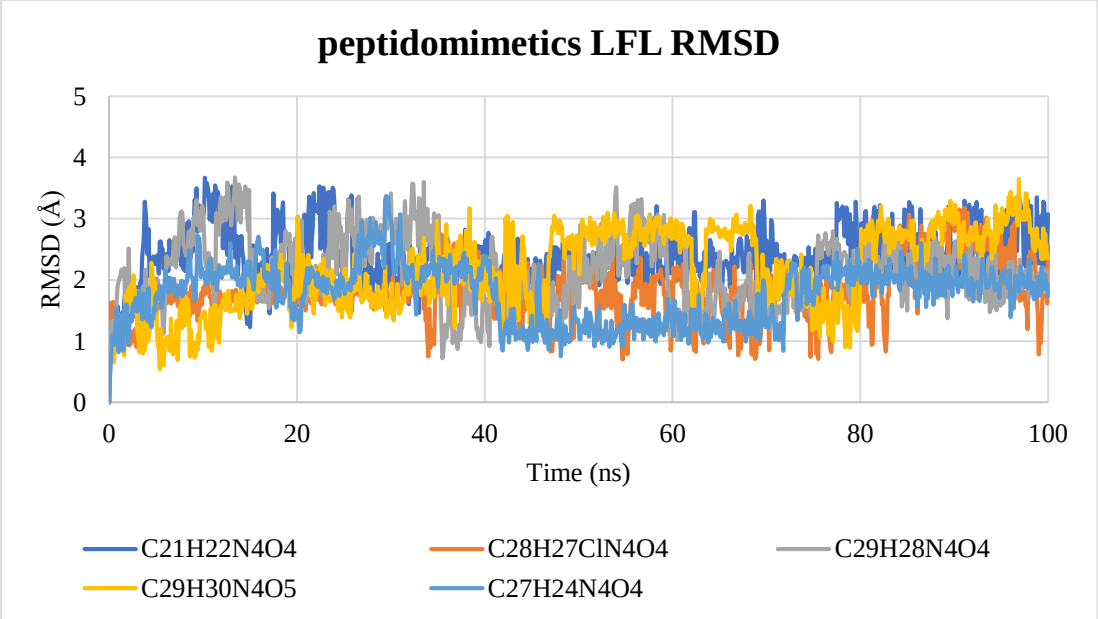

Figure 4.14 : Lig Fit Lig (LFL) RMSD values for peptidomimetics which selected based on ΔG scores in SF.

Figure 4.14 shows the LFL RMSD values for the peptidomimetics which selected based on ΔG scores in SF. All peptidomimetics displayed LFP RMSD values lower

than 2.50 Å. The LFP RMSD averages and the standard deviations (SD) were given in Table 4.14 for the selected peptidomimetics complexes.

Table 4.14 : LFL RMSD averages and the SDs for the peptidomimetics which selected based on ΔG scores in SF.

	C21H22N4O4	C28H27ClN4O4	C29H28N4O4	C29H30N4O5	C27H24N4O4
Averages	2.40	1.83	2.15	2.17	1.77
SD (±)	0.45	0.47	0.58	0.64	0.47

According to Table 4.14, the lowest LFL RMSD value for the peptidomimetics was observed in C27H24N4O4 (1.77 ± 0.47 Å), and the highest LFL RMSD value was observed in C21H22N4O4 (2.40 ± 0.45 Å).

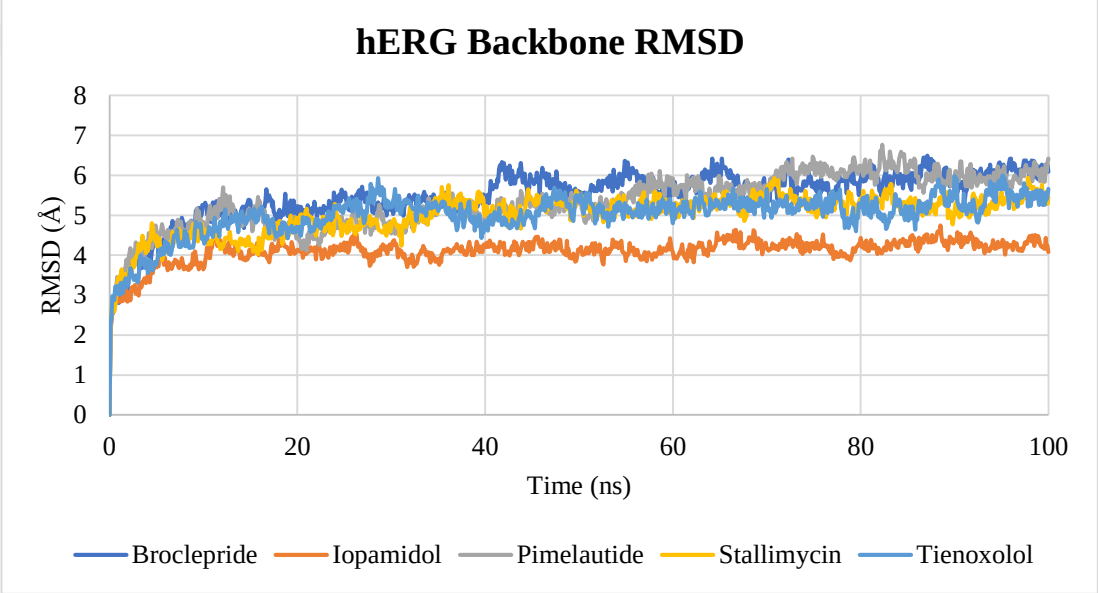

Figure 4.15 : Backbone RMSD values for hERG in FDA molecule complexes which selected according to ΔΔG scores.

Figure 4.15 shows the BB RMSD values for the FDA molecules. All complexes reached plateau after first 40 ns. The BB RMSD averages and the standard deviations (SD) were given in Table 4.15 for the BB atoms of hERG for the selected FDA molecule complexes.

Table 4.15 : Backbone RMSD averages and the SDs for the hERG complexes with selected FDA molecules based on ΔΔG scores.

	Broclepride	Iopamidol	Pimelautide	Stallimycin	Tienoxolol
Averages	5.49	4.10	5.33	5.01	5.01
SD (±)	0.65	0.33	0.69	0.51	0.53

According to Table 4.15, the lowest RMSD value for hERG backbone atoms was observed in Iopamidol-hERG complex (4.10 ± 0.33 Å), and the highest RMSD value was observed in Pimelautide-hERG complex (5.33 ± 0.69 Å).

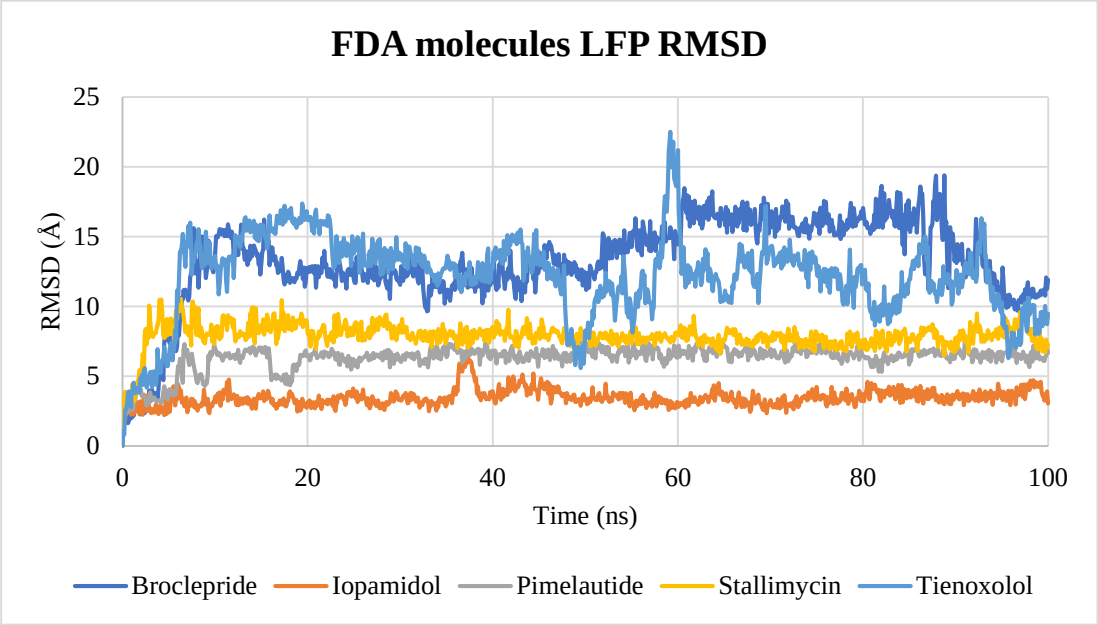

Figure 4.16 : Lig Fit Prot (LFP) RMSD values for FDA molecules which selected based on ΔΔG scores.

Figure 4.16 shows the LFP RMSD values for the FDA molecules which selected based on ΔΔG scores. All studied FDA molecules displayed different LFP RMSD patterns. Among all studied molecules only Iopamidol has LFP RMSD value lower than 5 Å. Broclepride and Tienoxolol clearly diffused away from the SF region. The LFP RMSD averages and the standard deviations (SD) were given in Table 4.16 for the selected FDA molecule complexes.

Table 4.16 : LFP RMSD averages and the SDs for the FDA molecules which selected based on ΔΔG scores.

	Broclepride	Iopamidol	Pimelautide	Stallimycin	Tienoxolol
Averages	13.26	3.46	6.30	7.90	12.17
SD (±)	3.12	0.59	0.91	0.92	2.95

According to Table 4.16, the lowest LFP RMSD value for FDA molecules was observed in Iopamidol (3.46 ± 0.59 Å), and the highest LFP RMSD value was observed in Broclepride (13.26 ± 3.12 Å), clearly showing that this molecule diffused away from the SF region.

Figure 4.17 shows the LFL RMSD values for the FDA molecules which selected based on ΔΔG scores. All studied FDA molecules displayed different LFL RMSD patterns.

Among all studied molecules only Pimelautide has LFP RMSD value higher than 3 Å. The LFL RMSD averages and the standard deviations (SD) were given in Table 4.17 for the selected FDA molecule complexes.

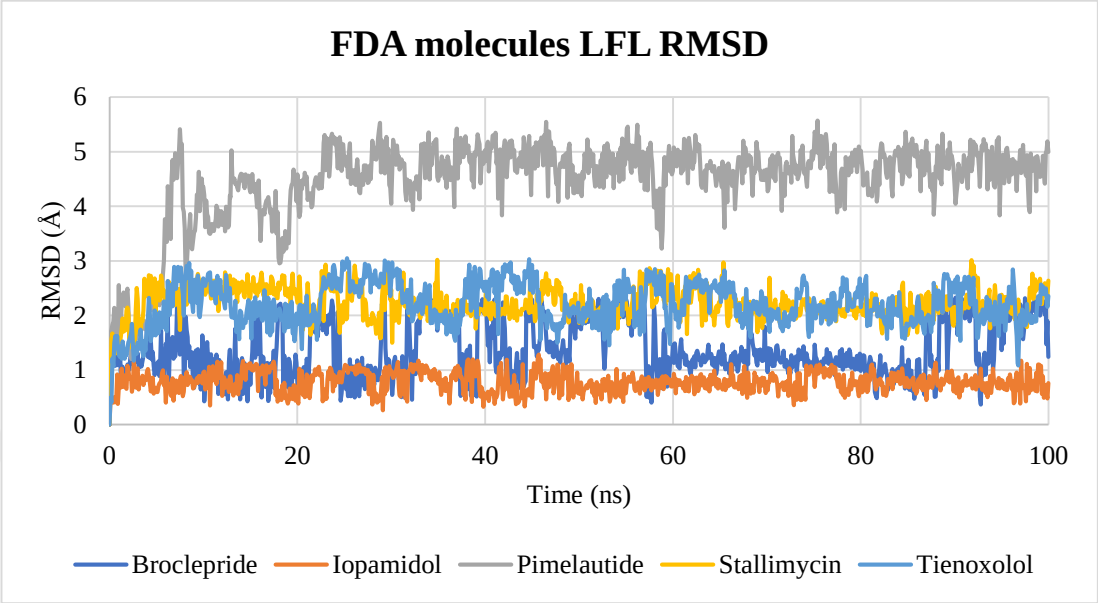

Figure 4.17 : Lig Fit Lig (LFL) RMSD values for FDA molecules which selected based on ΔΔG scores.

Table 4.17 : LFL RMSD averages and the SDs for the FDA molecules which selected based on ΔΔG scores.

	Broclepride	Iopamidol	Pimelautide	Stallimycin	Tienoxolol
Averages	1.37	0.78	4.47	2.23	2.21
SD (±)	0.50	0.19	0.78	0.29	0.40

According to Table 4.17, the lowest LFL RMSD value for peptidomimetics was observed in Iopamidol (0.78 ± 0.19 Å), and the highest LFL RMSD value was observed in Pimelautide (4.47 ± 0.78 Å).

Figure 4.18 shows the BB RMSD values for the FDA molecules. All complexes reached plateau after first 60 ns. The BB RMSD averages and the standard deviations (SD) were given in Table 4.18 for the BB atoms of hERG for the selected FDA molecule complexes.

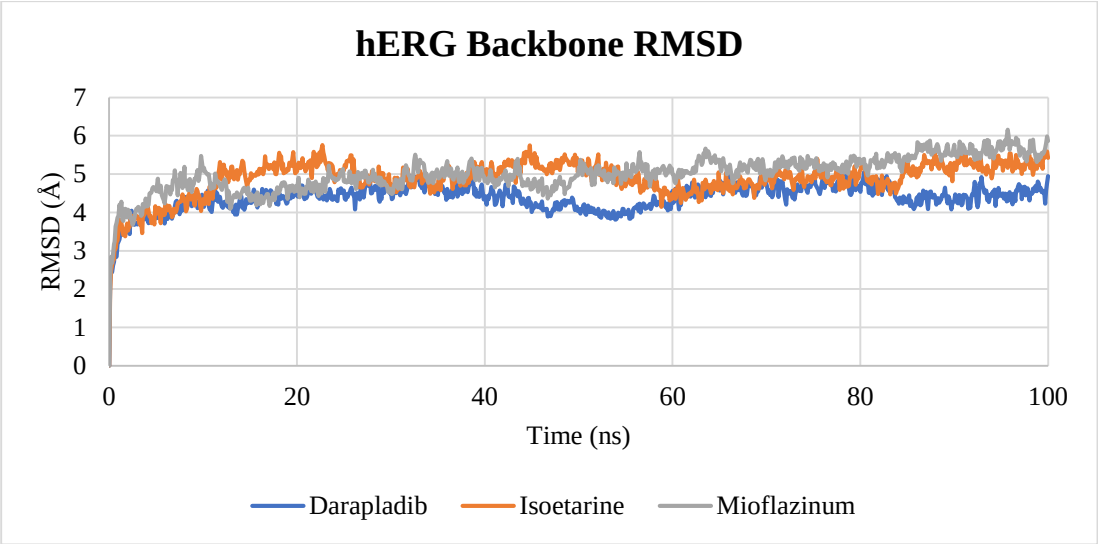

Figure 4.18 : Backbone RMSD values for hERG in FDA molecule complexes which selected according to ΔG scores in SF.

Table 4.18 : Backbone RMSD averages and the SDs for the hERG complexes with selected FDA molecules based on ΔG scores in SF.

	Darapladib	Isoetarine	Mioflazinum
Averages	4.38	4.88	5.00
SD (±)	0.36	0.47	0.48

According to Table 4.18, the lowest RMSD value for hERG backbone atoms was observed in Darapladib-hERG complex (4.38 ± 0.36 Å), and the highest RMSD value was observed in Mioflazinum-hERG complex (5.00 ± 0.48 Å). dolore magna.

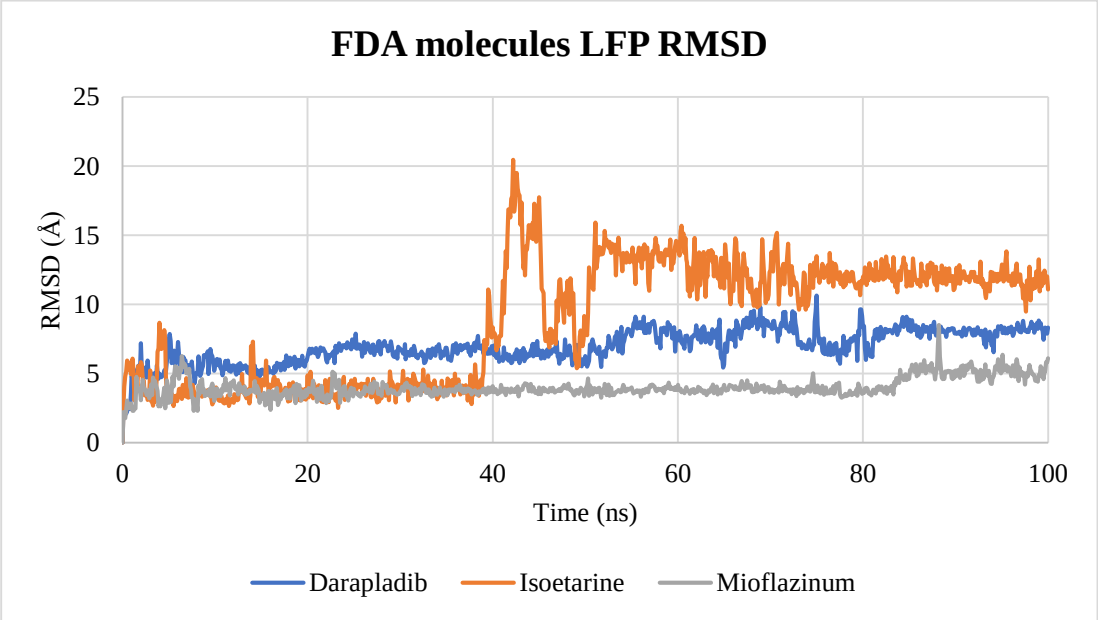

Figure 4.19 : Lig Fit Prot (LFP) RMSD values for FDA molecules which selected based on ΔG scores in SF.

Figure 4.19 shows the LFP RMSD values for the FDA molecules which selected based on ΔG scores in SF. All studied FDA molecules displayed different LFP RMSD patterns. Among all studied molecules only Mioflazinum has LFP RMSD value lower than 4 Å. Darapladib and Isoetarine clearly diffused away from the SF region. The LFP RMSD averages and the standard deviations (SD) were given in Table 4.19 for the selected FDA molecule complexes.

Table 4.19 : LFP RMSD averages and the SDs for the FDA molecules which selected based on ΔG scores in SF.

	Darapladib	Isoetarine	Mioflazinum
Averages	6.95	8.93	3.99
SD (±)	1.22	4.33	0.69

According to Table 4.19, the lowest LFP RMSD value for FDA molecules was observed in Iopamidol (3.99 ± 0.69 Å), and the highest LFP RMSD value was observed in Broclepride (8.93 ± 4.33 Å), clearly showing that this molecule diffused away from the SF region.

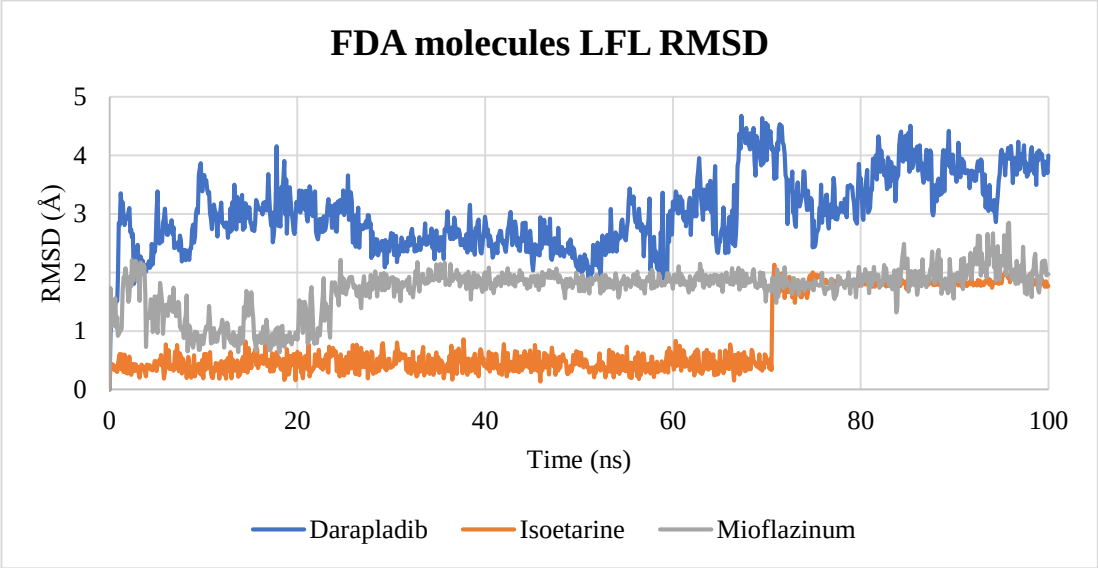

Figure 4.20 : Lig Fit Lig (LFL) RMSD values for FDA molecules which selected based on ΔG scores in SF.

Figure 4.20 shows the LFL RMSD values for the FDA molecules which selected based on ΔG scores in SF. All studied FDA molecules displayed different LFL RMSD patterns. Among all studied molecules only Darapladib has LFP RMSD value higher than 3 Å. The LFL RMSD averages and the standard deviations (SD) were given in Table 4.20 for the selected FDA molecule complexes.

Table 4.20 : LFL RMSD averages and the SDs for the FDA molecules which selected based on ΔG scores in SF.

	Darapladib	Isoetarine	Mioflazinum
Averages	3.02	0.85	1.71
SD (±)	0.63	0.64	0.39

According to Table 4.20, the lowest LFL RMSD value for peptidomimetics was observed in Isoetarine (0.85 ± 0.64 Å), and the highest LFL RMSD value was observed in Darapladib (3.02 ± 0.63 Å).

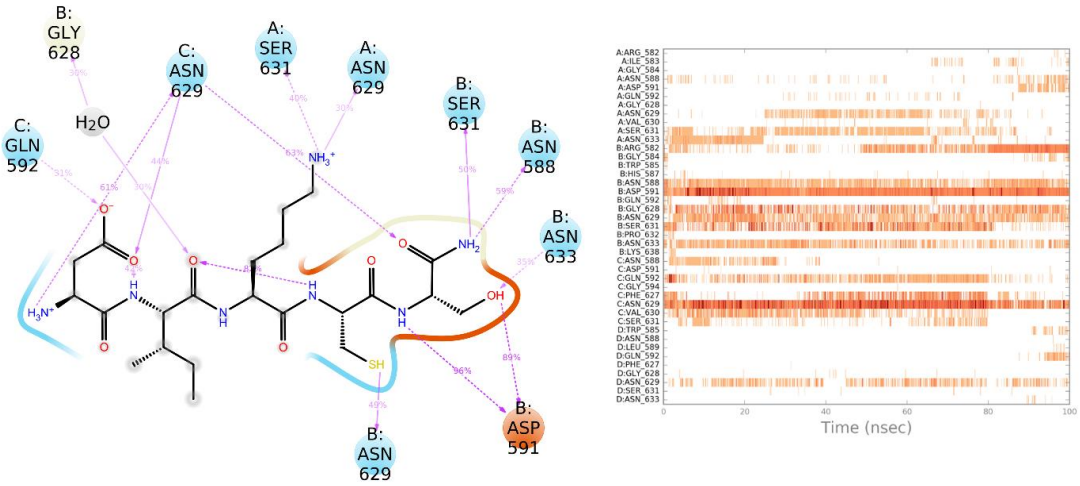

Figure 4.21 : Simulation interaction diagram for DIKCS, percentages of the conservation (left panel), conservation of the interaction throughout trajectory (right panel, darker color shows higher number of interactions).

The interactions that observed in the docking pose of DIKCS was compared with the MD simulation trajectory. Figure 4.21 shows the conservation of the interactions as percentages. On the right panel, the conservation of the interactions throughout the MD trajectory was depicted. The darker the color, the higher the number of interactions, for example, ASN629 from chain A formed less interactions compared to ASN629 from chain C. DIKCS conserved all interactions with the hERG which observed in the docking pose, moreover following interactions ASN629, and SER631 from chain A, ASN629, SER631, and ASN633 from chain B formed during MD simulation.

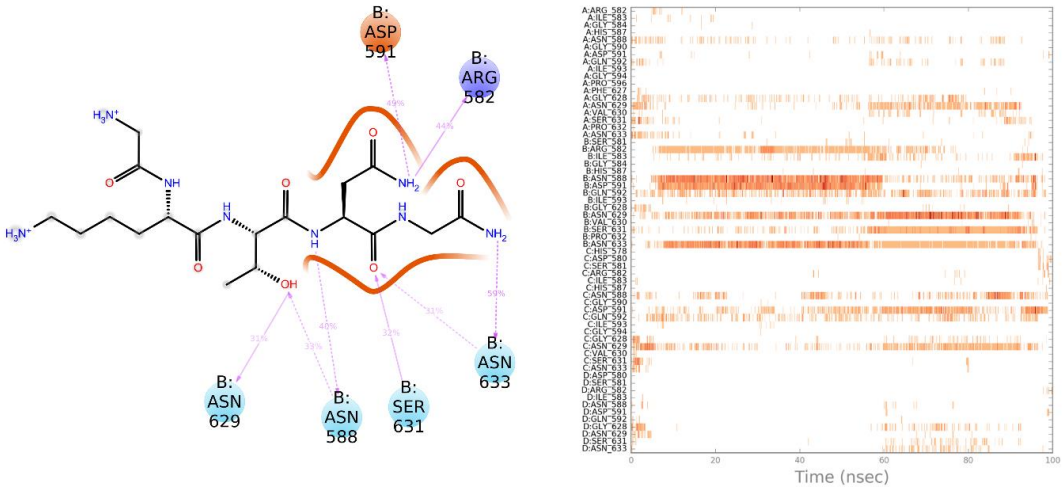

Figure 4.22 : Simulation interaction diagram for GKTNG.

Figure 4.22 shows the interaction diagram for the GKTNG. In docking pose, there were interactions between GKTNG and hERG, via contributions from chain A, B, and D. However, all interactions that were observed in docking pose were lost in the MD simulation (see Figure 4.1B). However, following interactions were formed during MD simulation, ARG582, ASN588, ASP591, ASN629, SER631, and ASN633. All these residues were from chain B, so in GKTNG binding chain B dominated the interactions.

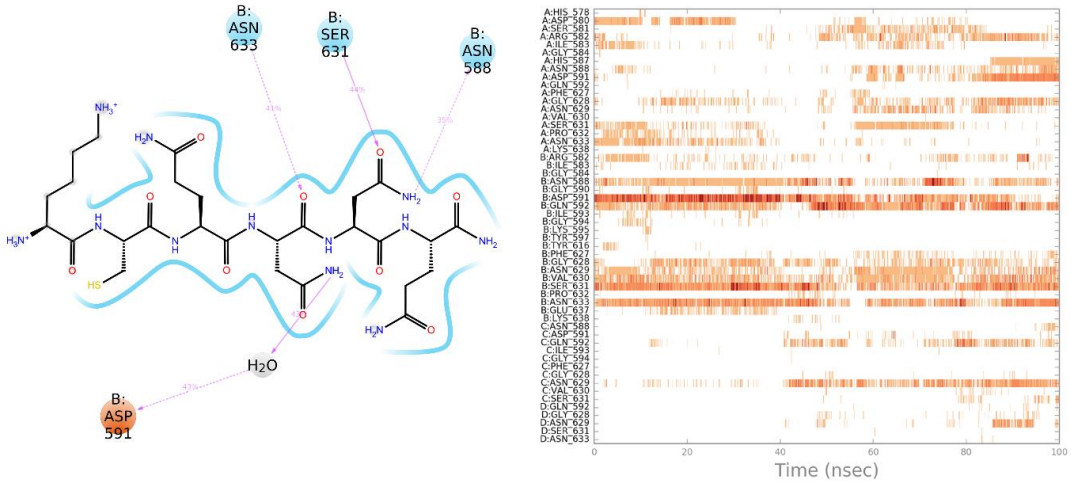

Figure 4.23 : Simulation interaction diagram for KCQNNQ.

The interactions between KCQNNQ and hERG and their conservation percentages were given in Figure 4.23. During MD simulations, all interactions from chain A were lost, together with GLN592, and PHE627 interactions from chain B. ASP591, ASN588, and ASN633 interactions from chain A were conserved, where the ASP591 interaction formed via water bridge. SER631 from chain B formed a new interaction with the *de novo* peptide KCQNNQ.

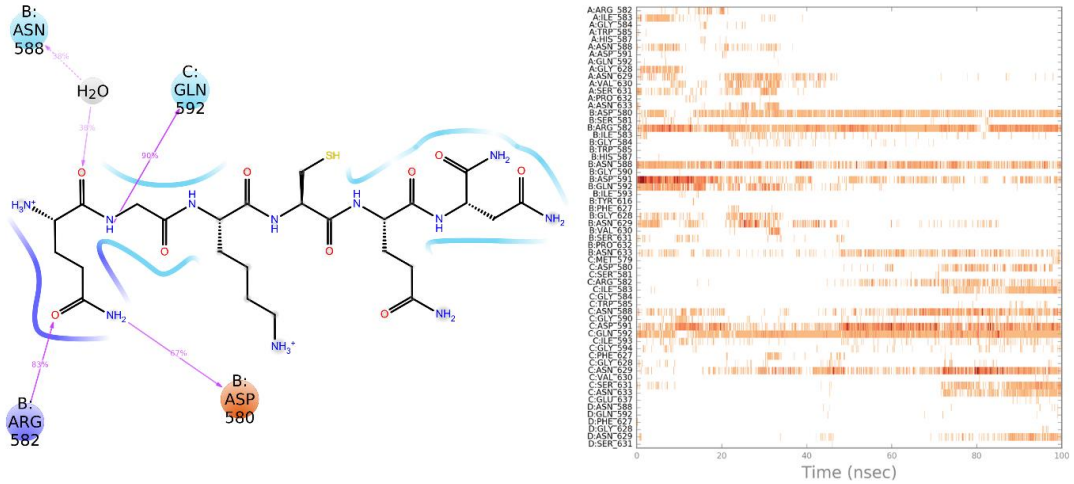

Figure 4.24 : Simulation interaction diagram for QGKCQN.

The interaction diagram between de novo peptide QGKCQN with hERG is given in Figure 4.24. The interactions with QGKCQN with ASN588 from chain A, ASP591, and GLY629 from chain B, and ASP591 from chain C were lost during MD simulations. ASN588 from chain B was shifted as an interaction via water bridge. No new interaction was formed throughout the MD simulation.

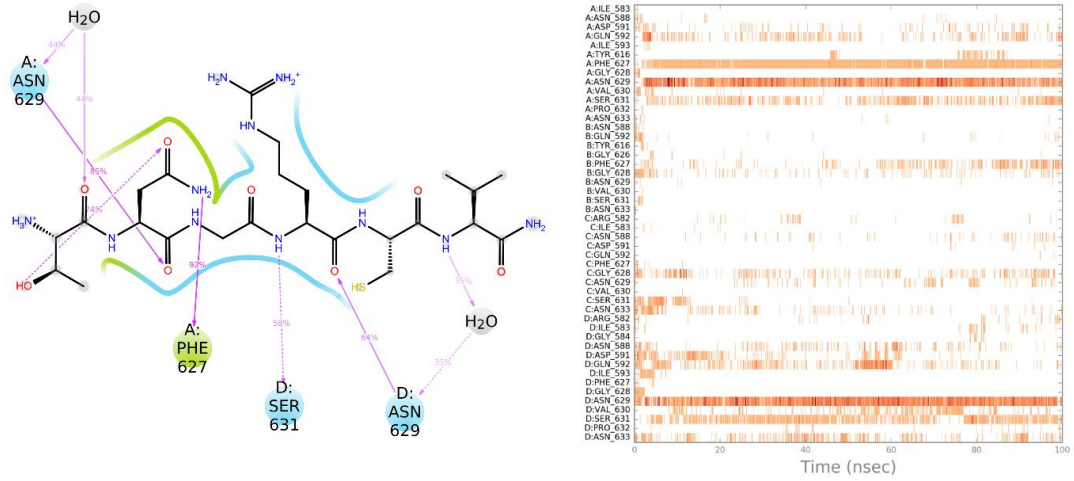

Figure 4.25 : Simulation interaction diagram for TNGRCV.

All the interactions (except ASN629 from chain D) that observed in docking pose were lost in MD simulation. However, PHE627, and ASN629 from chain A, and SER631 from chain D formed during MD simulation. Figure 4.25 shows the interactions between *de novo* peptide TNGRCV and hERG.

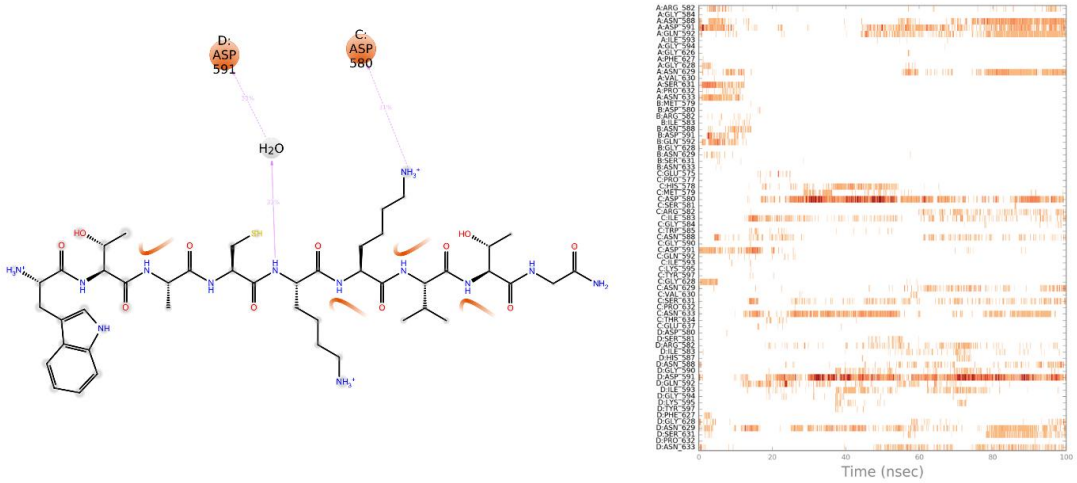

Figure 4.26 : Simulation interaction diagram for WTACKKVTG.

Figure 4.26 shows the WTACKKVTG interactions with hERG. In docking pose, ASN588, ASN591, and ASN633 from chain A, GLY628 from chain B, and ASP580 from chain D contributed to the *de novo* peptide WTACKKVTG stabilization. However, none of them were conserved during the MD simulation, instead ASP580 from chain C, and ASP591 from chain D formed interactions with hERG.

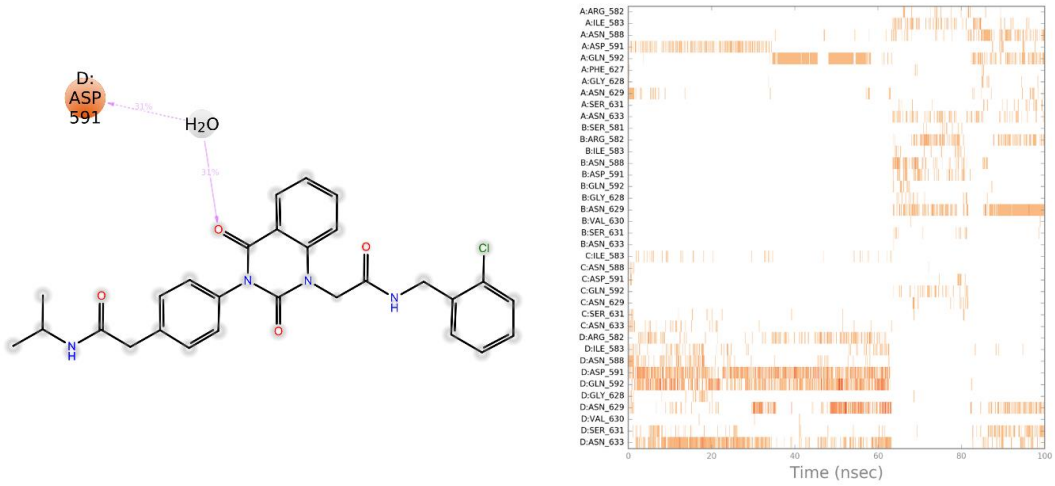

Figure 4.27 : Simulation interaction diagram for C28H27ClN4O4.

C28H27CLN4O4 was the top peptidomimetic compound according to ΔΔG score. This molecule formed interactions with hERG through GLY628 from chain A, ASN633 from chain C, and ASN588 from chain D, and potassium ion from SF. However, none of these were conserved, the molecule moved away from starting pose, and only ASP591 from chain D formed interactions via water bridge. Figure 4.27 shows the interactions between C28H27ClN4O4 and hERG.

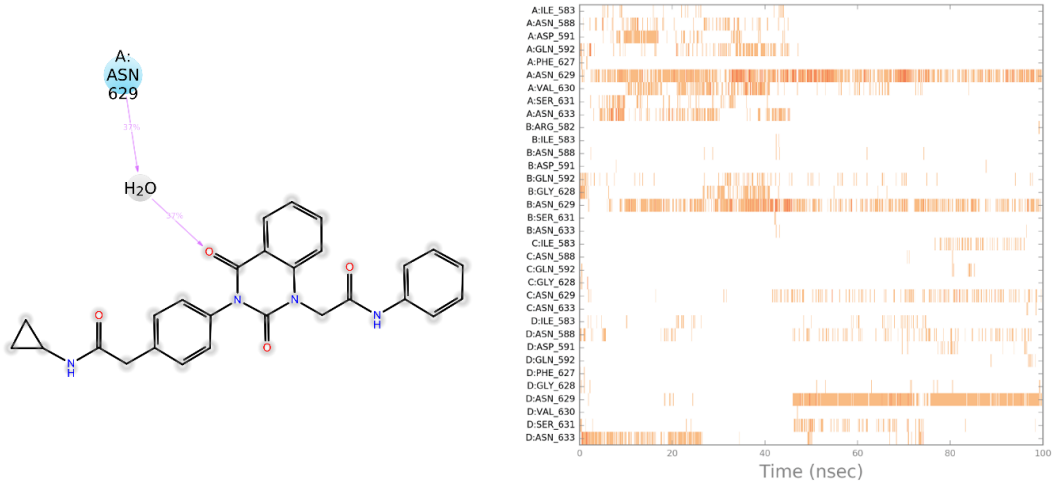

Figure 4.28 : Simulation interaction diagram for C27H24N4O4.

Second top molecule according to ΔΔG score was C27H24N4O4. All interactions that observed in docking pose were lost during MD, instead ASN629 from chain A formed an interaction via water bridge. Figure 4.28 shows the interaction between C27H24N4O4 and hERG.

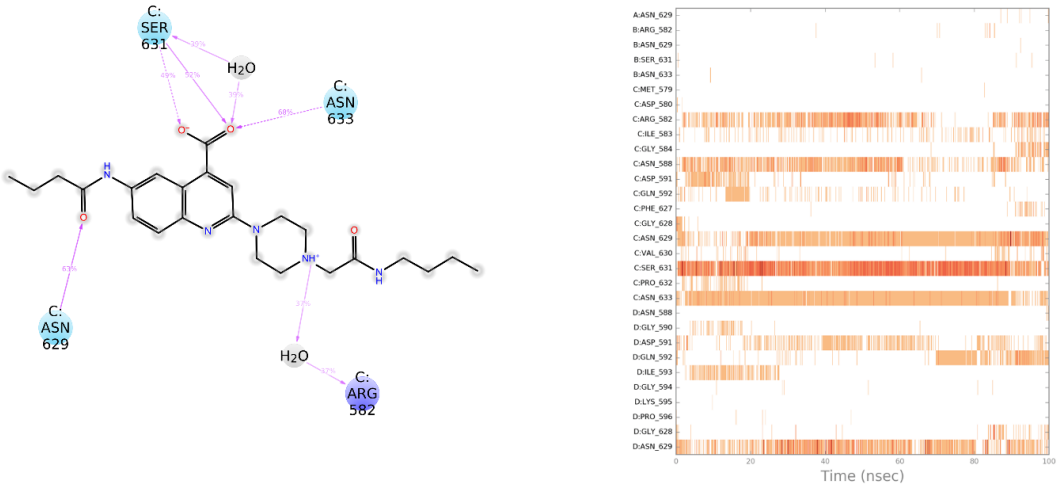

Figure 4.29 : Simulation interaction diagram for C24H33N5O4.

Similar the first and second best peptidomimetics, C24H33N5O4 lost all interactions with hERG that observed in docking pose, however the stabilization of the peptidomimetics were maintained by ARG582, ASN629, SER631, and ASN633 from chain C. The interactions between C24H33N5O4 and hERG depicted in Figure 4.29.

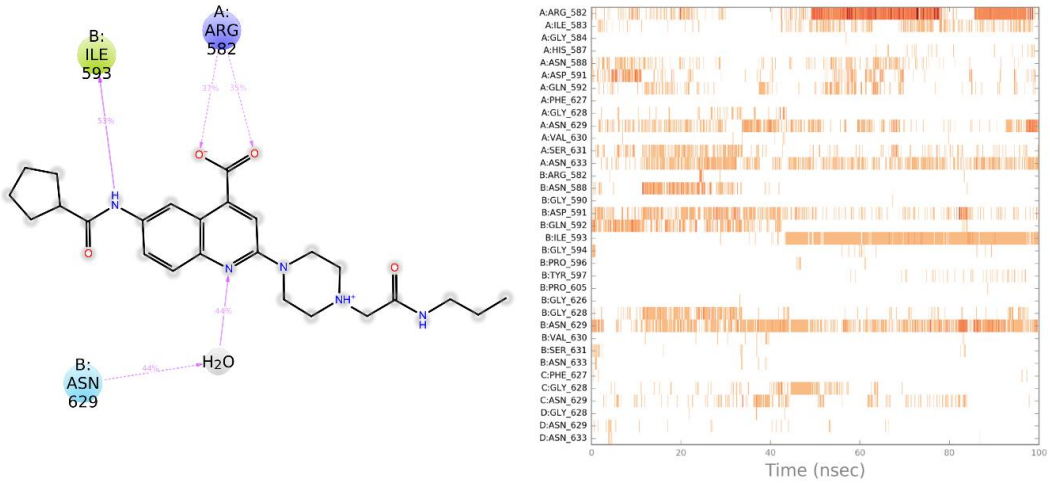

Figure 4.30 : Simulation interaction diagram for C25H33N5O4.

Figure 4.30 shows the interactions with C25H33N5O4 and hERG. The only contributing residue in the docking pose lost the interactions with C25H33N5O4, however the peptidomimetic compound were stabilized through interactions of ARG582 from chain A, ILE593, and ASN629 from chain B during MD simulation.

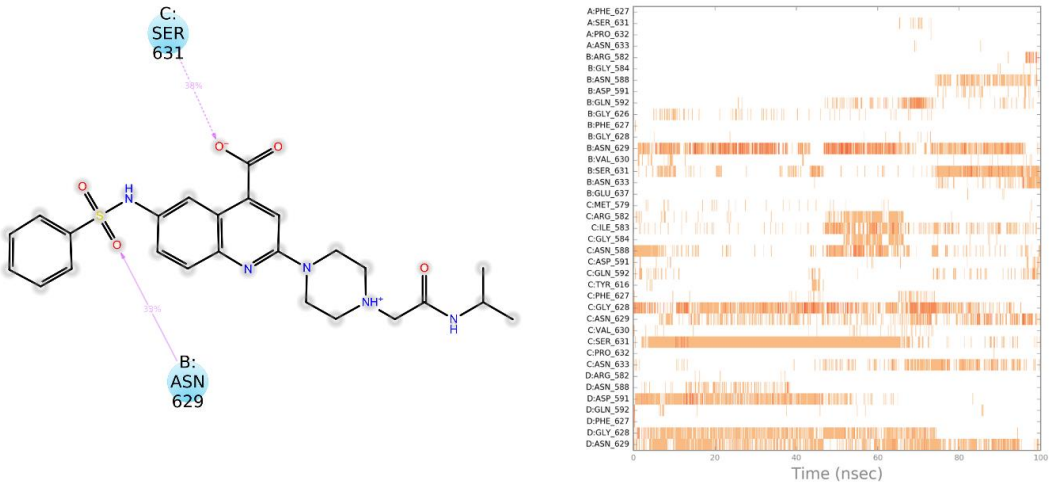

Figure 4.31 : Simulation interaction diagram for C25H29N5O5S.

C25H29N5O5S was the top fifth molecule (last top one) that selected according to ΔΔG score. Similar to first four peptidomimetics, the interactions that observed in docking pose were lost during MD simulation. ASN629 from chain B, and SER631 from chain C were contributed C25H29N5O5S stabilization. Figure 4.31 shows the interactions between C25H29N5O5S and hERG.

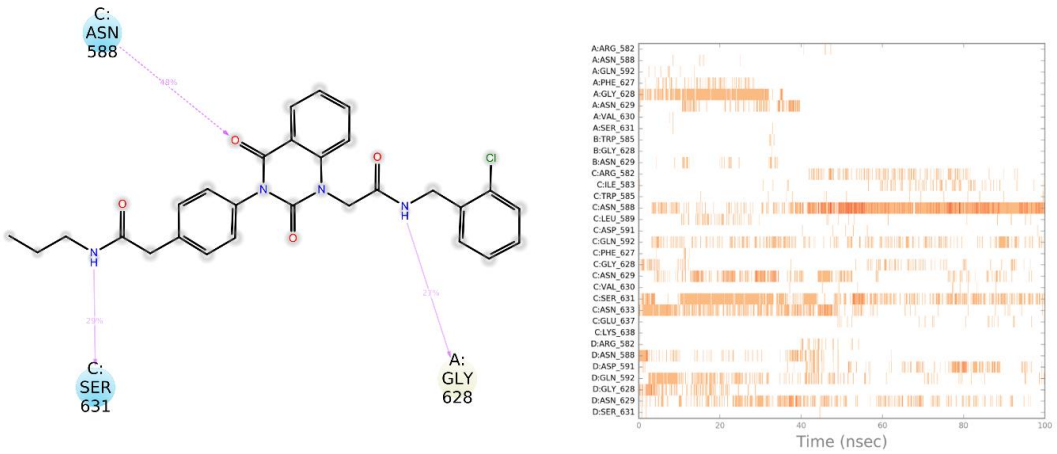

Figure 4.32 : Simulation interaction diagram for C28H27ClN4O4.

Figure 4.32 shows the interactions with C28H27ClN4O4 and hERG. C28H27ClN4O4 was selected as the best binder (top lowest) in SF with -6.83 kcal/mol. GLY628 from chain A was maintained in MD simulations, while others were lost. ASN588 and SER631 from chain C formed two new interactions and these interactions were conserved 48, and 29%, respectively during MD simulation.

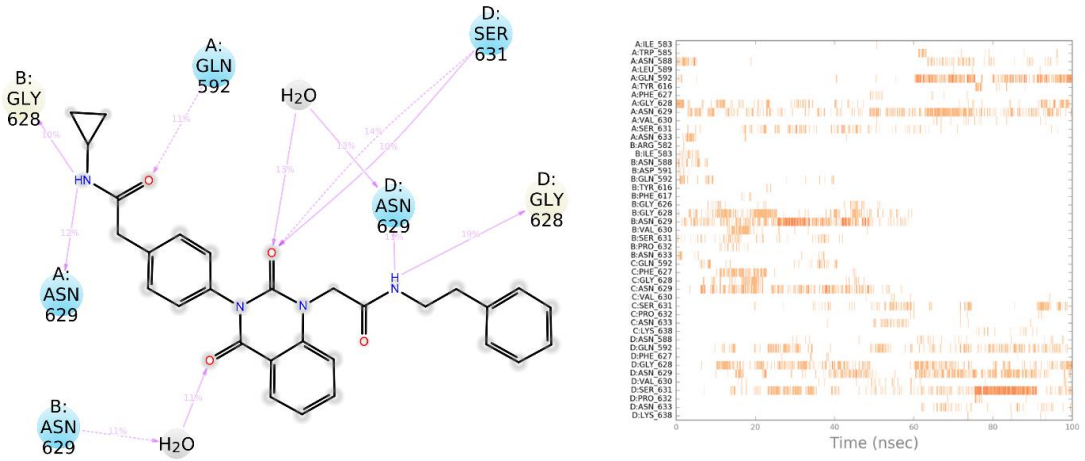

Figure 4.33 : Simulation interaction diagram for C29H28N4O4.

In the docking pose of C29H28N4O4, one interaction was observed between the peptidomimetics and hERG. This interaction was lost in MD, however, GLN592, ASN629 from chain A, GLY628, ASN629 from chain B, GLY628, ASN629, and SER631 from chain D formed new interactions with C29H28N4O4. Figure 4.33 shows the interactions between the peptidomimetic and hERG.

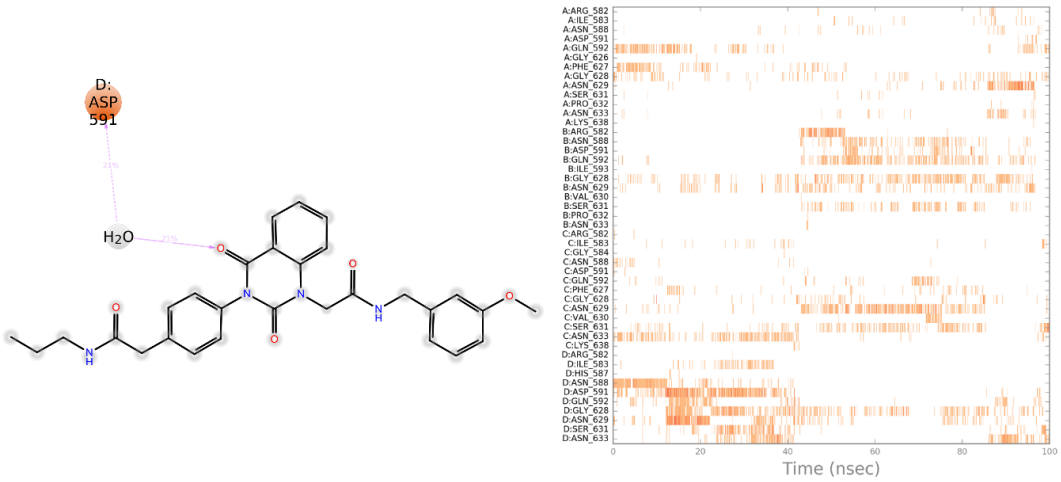

Figure 4.34 : Simulation interaction diagram for C29H30N4O5.

C29H30N4O5 was the top-third peptidomimetics when sorted according to docking scores in SF. Figure 4.34 shows the interactions between C29H30N4O5 and hERG throughout the MD simulation. All four interactions that observed in docking pose were lost, however, ASP591 was formed an interaction via water bridge with the peptidomimetic compound.

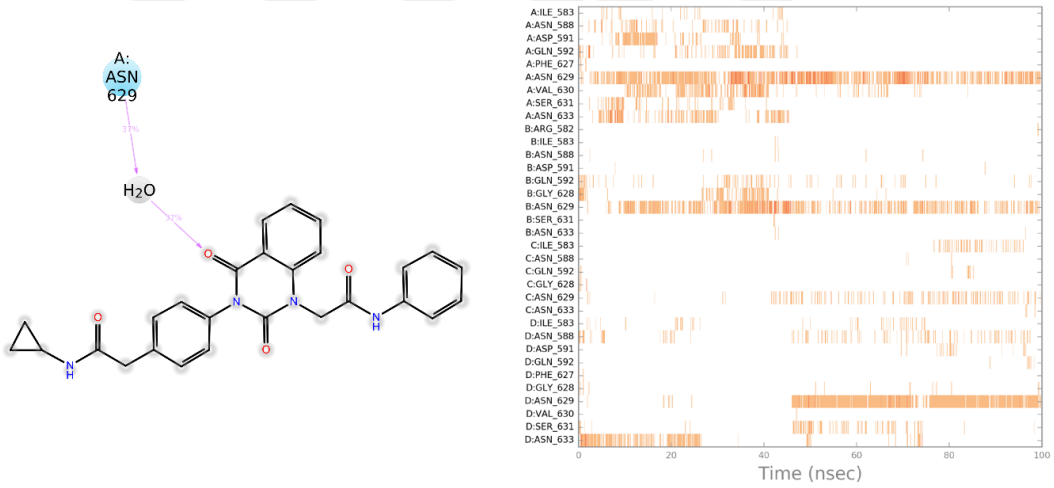

Figure 4.35 : Simulation interaction diagram for C27H24N4O4.

Fourth top molecule according to ΔG score in SF was C27H24N4O4. All interactions that observed in docking pose were lost during MD, instead ASN629 from chain A formed an interaction via water bridge. Figure 4.35 shows the interaction between C27H24N4O4 and hERG.

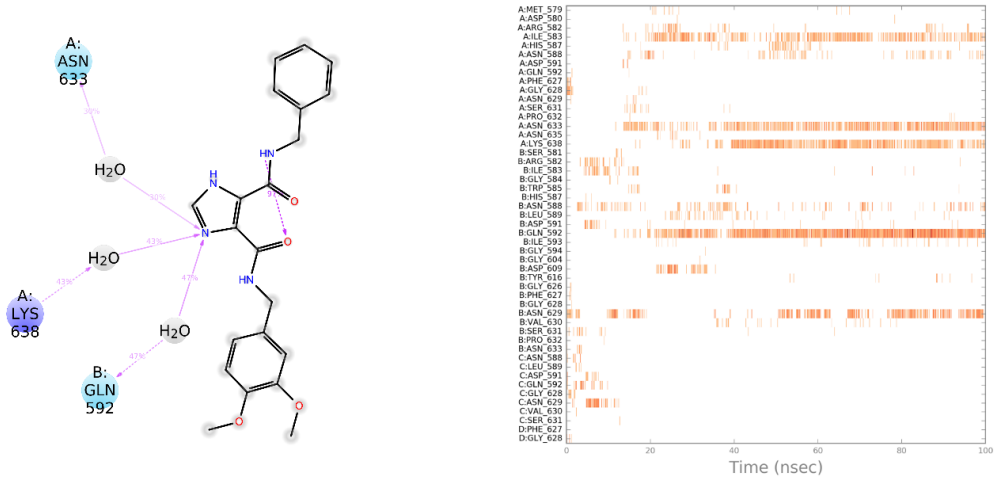

Figure 4.36 : Simulation interaction diagram for C21H22N4O4.

C21H22N4O4 was the last molecule that selected based on ΔG score in SF. GLY628 from chain A and chain B formed two interactions with C21H22N4O4. However, these two interactions were lost during the MD simulation, instead three new interactions were formed via water bridges. These interactions were between ASN633, and LYS638 from chain A, and GLN592 from chain B, and C21H22N4O4. Figure 4.36 shows the interactions and their conservation percentages.

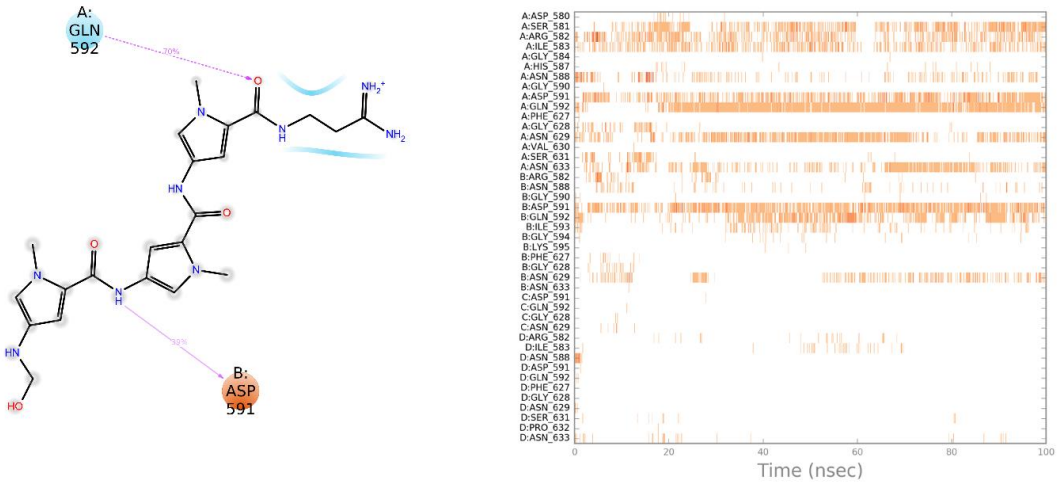

Figure 4.37 : Simulation interaction diagram for Stallimycin.

Figure 4.37 shows the interactions between Stallimycin and hERG. Stallimycin was selected as the best binder (top low scored one) based on the ΔΔG score. All interactions except GLN592 from chain A were lost during the MD simulation. ASP591 from chain B also contributed to binding in 39% of the simulation trajectory.

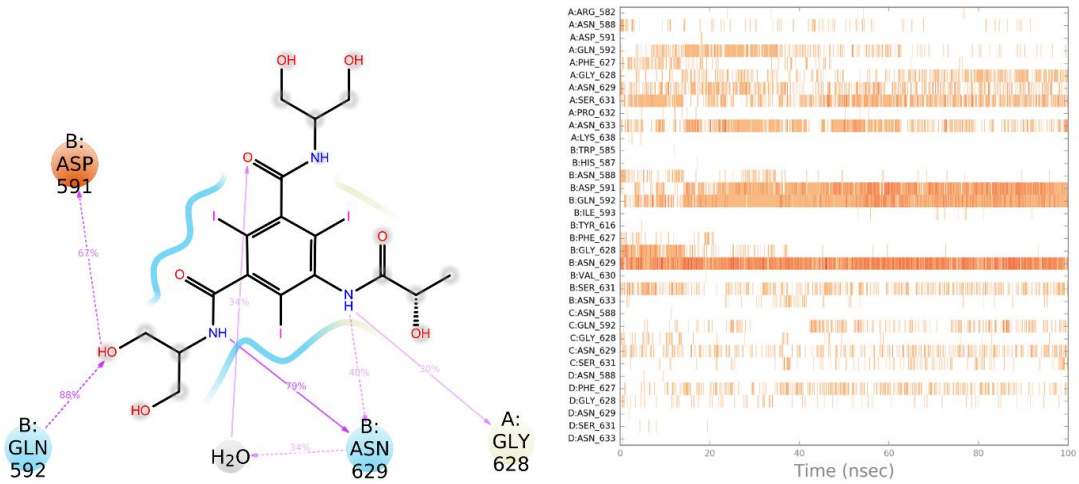

Figure 4.38 : Simulation interaction diagram for Iopamidol.

Figure 4.38 shows the interactions between Iopamidol and hERG. The interactions that observed in the docking pose mostly conserved, and one new interaction between ASP591 from chain B and Iopamidol was formed during the MD simulation. The interactions between hERG and Iopamidol via ASN588 from chain B, and GLY628 from chain C were lost throughout the MD simulation.

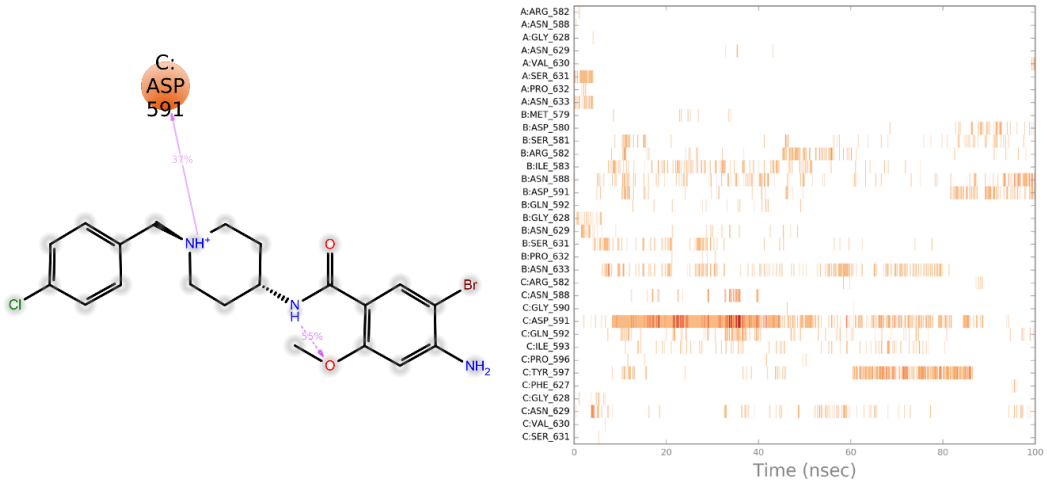

Figure 4.39 : Simulation interaction diagram for Broclepride.

Broclepride was the top third FDA molecule according to ΔΔG score. The interactions and the conservation percentages were given in Figure 4.39. The interactions that observed in the docking pose were lost, ASP591 from chain C was found to be contributed to stabilization of Broclepride during MD simulation.

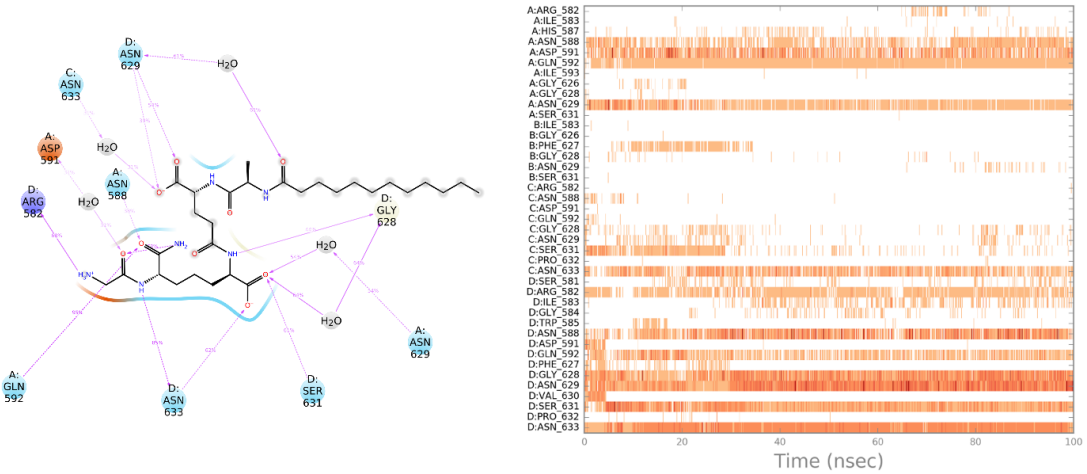

Figure 4.40 : Simulation interaction diagram for Pimelautide.

Figure 4.40 shows the interactions between Pimelautide and hERG. The interactions that observed in the docking pose mostly conserved, ASN588 from chain A, ASN633 from C, ARG582, GLY628, SER631, and ASN633 formed new interactions with the FDA molecule.

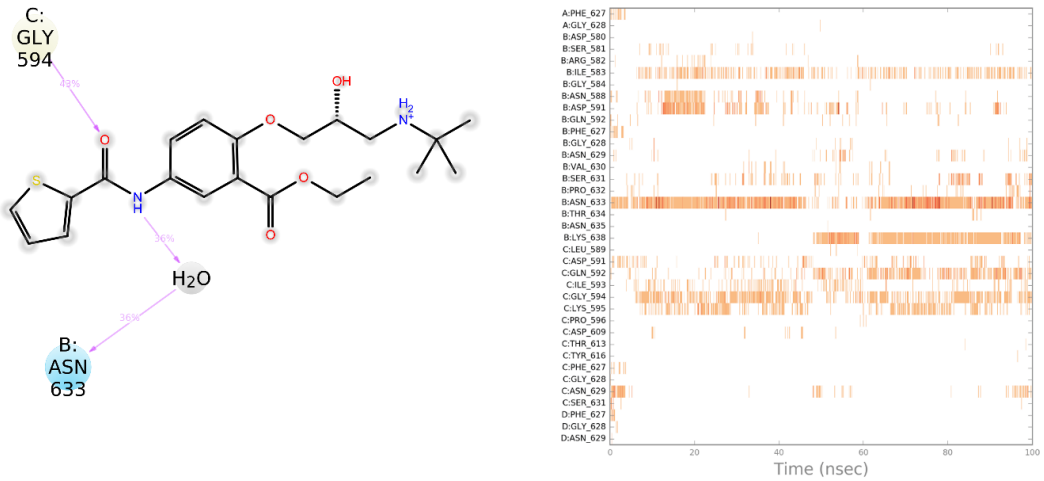

Figure 4.41 : Simulation interaction diagram for Tienoxolol.

Tienoxol was the last molecule that selected based on ΔΔG score. The interactions between GLY628 from chain B, and water molecule from SF and Tienoxolol were lost during MD simulation, however ASN644 from chain B was conserved and GLY594 from chain C contributed to the stabilization of the compound around SF. Figure 4.41 shows the interactions and conservation percentages.

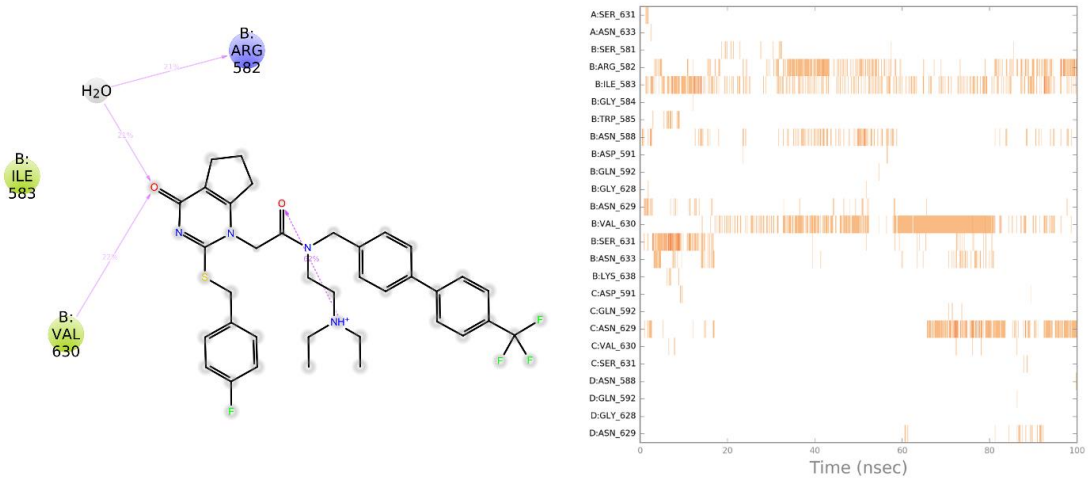

Figure 4.42 : Simulation interaction diagram for Darapladib.

Figure 4.42 shows the interactions between Darapladib and hERG. Darapladib was selected as the top-binder (lowest ΔG score in SF) based on the ΔG score in SF. In the docking pose, Darapladib fitted in the SF without any interaction but according to shape complementarity. During the MD simulation, ARG582 (via water bridge) and VAL630 were formed two interactions with Darapladib.

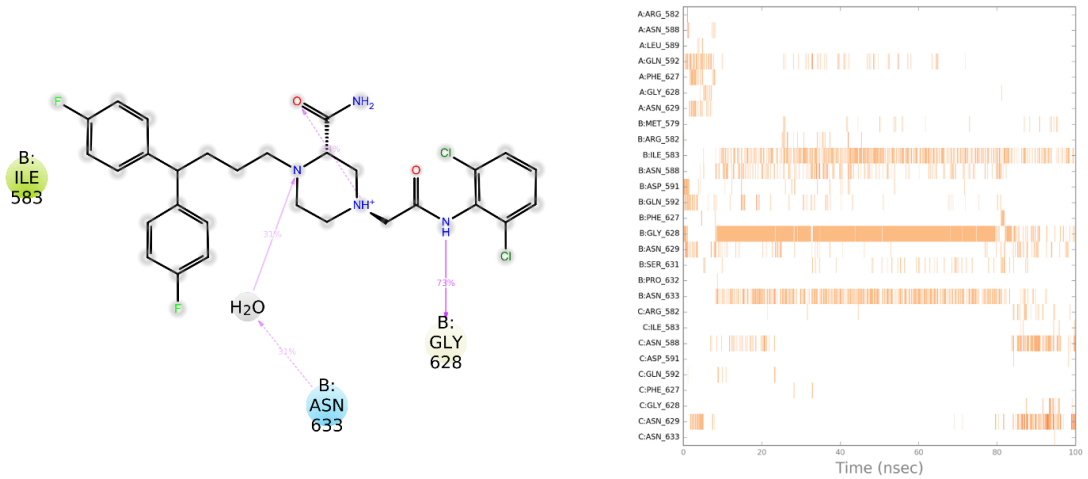

Figure 4.43 : Simulation interaction diagram for Mioflazinum.

The second lowest ΔG score in SF was observed in Mioflazinum. Figure 4.43 shows the interactions between Mioflazinum and hERG. The interaction between Mioflazinum and GLY628 from chain B was conserved, and ASN633 was contributed to stabilization via water bridge. The interaction where ASN588 from chain B was contributed, lost during the MD simulation. citation.

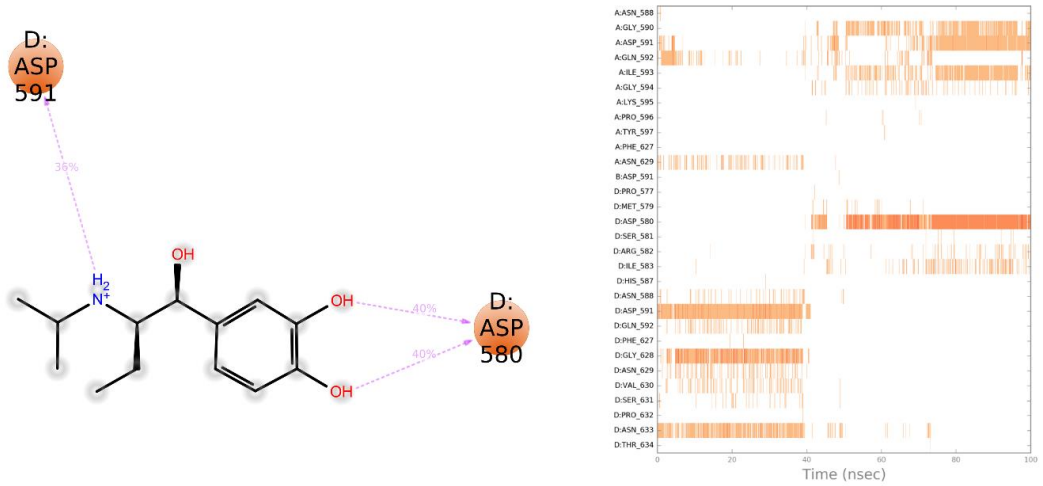

Figure 4.44 : Simulation interaction diagram for Isoetarine.

Figure 4.44 shows the interaction between Isoetarine and hERG. Isoetarine was selected as the 5th molecule according to ΔG score in SF. The interactions that observed in the docking pose were lost during the MD simulation, and three new interactions were formed through ASP580 (two interactions) and ASP591 from chain D.

4.1 Conclusion

In this section, molecular docking and molecular simulations were performed to study the interactions of de novo peptides, peptidomimetics, and FDA-approved molecules with open-state hERG at the atomic level. The toxin-closed-state hERG interactions elucidated by the simulations performed in the previous section provided the rationale for the design of de novo peptides. In addition to the de novo peptides designed with the information obtained here, peptidomimetics and FDA-approved molecules were also used to ensure that the library studied provided the necessary molecular diversity. The goal of this study using the open state of the hERG is to elucidate the details of partial inhibition of an hERG that continues to conduct current despite significantly altered gate kinetics and voltage dependence at the atomic level. Our strategy was to first determine the binding scores of a library of molecules in the inner cavity. It is well known in the literature that molecules bind to the inner cavity region and cause hERG inhibition by stopping the flow of potassium ions. Therefore, molecules with low binding in the inner cavity region (low molecular docking score) were identified and then docked to the top of the selective filter, the region illuminated by toxin-hERG interactions. In order to show the difference in binding energies between the two regions and to more accurately select the molecules to be simulated, the ΔΔG metric

was determined. ΔΔG was obtained by subtracting the binding free energy obtained by docking in the inner cavity from the binding free energy obtained by docking in the upper part of the selective filter. While only the ΔΔG metric was used for de novo molecules, for peptidomimetics and FDA molecules, in addition to ΔΔG, a ranking was made according to the docking scores obtained at the top of the selective filter and a set of molecules was determined by this method. Two of the molecules selected as top de novo peptides (DIKCS and TNGRCV) had lower LFP RMSD values compared to the others. DIKCS maintained all the interactions it formed in the docking pose throughout the simulation, in addition to forming new interactions with hERG. TNGRCV, on the other hand, although it lost most of the interactions observed in the docking pose, remained stable at the binding site by forming interactions to compensate. The other four selected de novo peptides, although they did not have as low LFP values as DIKCS and TNGRCV, established the necessary interactions with other chains of hERG. All de novo peptides were observed to interact either directly with the target amino acids identified as the upper part of the selective filter, or with amino acids in the neighbourhood of these amino acids. Peptidomimetics and FDA molecules were also found to be in contact with amino acids important for interaction with hERG, as shown by atomic level analysis (although the selected molecules generally have high LFP RMSD values), and when this contact is broken, for example for chain A amino acids, it is re-established by other chains. To our knowledge, there is no small molecule screening in the region identified in the literature as the toxin binding site (upper part of the selective filter). It is also very important to find molecules that can shorten the QT interval of hERG in order to increase life-span. These molecules do not cause QT interval prolongation, which leads to death, and they allow hERG inhibition, which is therapeutically necessary in certain conditions such as cancer. However, there is a very important caveat. The targeted inhibition must not cause cardiotoxicity. To this end, molecules with high affinity in the internal cavity were eliminated in our study.

In this study, the partial inhibition of the open-state hERG by small molecules was studied using atomic simulations, and a workflow for therapeutic hERG inhibition targeting studies was proposed. This workflow consists of docking molecules into the inner cavity of the hERG, eliminating those with high affinity in this region, and determining the molecules that provide partial hERG inhibition by docking the

selected molecules into the upper region of the selective filter. Subsequently, the docking poses of these molecules obtained by MD simulations will be refined. Thus, it will be possible to explain the partial hERG inhibition at the atomic level.

5. CONCLUSIONS

The primary aim of this thesis is to clarify the atomic-level interactions between the spider toxins BeKm-1 and BmTx3b and the closed-state hERG channel. The second objective is to investigate the open-state hERG interactions of *de novo* peptides (formed with BeKm-1 and BmTx3b amino acids, which play an active role in the binding obtained in the first part, this time at the atomic level), peptidomimetics and FDA molecules.

In the first part of the thesis, two toxins BeKm-1 and BmTx3b have been interacted with hERG1 K^+ channel using different molecular modeling approaches including protein-protein docking, classical all-atom MD simulations and post-processing MD analyses as well as in silico Alanine scanning mutagenesis. The crucial residues of toxins playing an important role in binding mechanisms have been highlighted. Since the crucial residues from studied toxins sides as well as target protein side as well as nonbonded chemical interactions between them are detailed and highlighted in the current study, this information can be used in designing of better therapeutics which mimics the toxins. Thus, the results of this study can be used by medicinal chemists in the designing of diverse therapeutic applications of natural or synthetic peptides targeting the closed state hERG1 K^+ channels.

In the second part of the thesis, the partial inhibition of the open-state hERG by small molecules was studied using atomic simulations, and a workflow for therapeutic hERG inhibition targeting studies was proposed. This workflow consists of docking molecules into the inner cavity of the hERG, eliminating those with high affinity in this region, and determining the molecules that provide partial hERG inhibition by docking the selected molecules into the upper region of the selective filter. Subsequently, the docking poses of these molecules obtained by MD simulations will be refined. Thus, it will be possible to explain the partial hERG inhibition at the atomic level. Finally, an accurate and detailed understanding of this partial inhibition will pave the way for small molecule therapeutic applications in dementia, glioblastoma and some other cancers, offering a treatment option without the risk of cardiotoxicity.

REFERENCES

[1] **Durdagi, S., Deshpande, S., Duff, H. J. and Noskov, S. Y. (**2012). Modeling of open, closed, and open-inactivated states of the hERG1 channel: structural mechanisms of the state-dependent drug binding. *Journal of Chemical Information and Modelling*, 52(10), 2760-74.

[2] **Kuang, Q., Purhonen, P. and Hebert, H.** (2015). Structure of potassium channels. *Cellular and Molecular Life Sciences*, 72(19), 3677-3693.

[3] **Han, X., Xi, L., Wang, H., Huang, X., Ma, X., Han, Z., … and Ma, D.** (2008). The potassium ion channel opener NS1619 inhibits proliferation and induces apoptosis in A2780 ovarian cancer cells. *Biochemical and Biophysical Research Communications*, 375(2), 205-209.

[4] **Jehle, J., Schweizer, P. A., Katus, H. A. and Thomas, D.** (2011). Novel roles for hERG K+ channels in cell proliferation and apoptosis. *Cell Death & Disease*, 2(8), 193.

[5] **Huang, X. and Jan, L.Y.** (2014). Targeting potassium channels in cancer. *The Journal of Cell Biology*, 206(2), 151-62.

[6] **Vandenberg, J.I., Perry, M. D., Perrin, M. J., Mann, S. A., Ke, Y. and Hill, A. P.** (2012). hERG K+ Channels: Structure, Function, and Clinical Significance. *Physiological Reviews*, 92(3), 1393-1478.

[7] **Börjesson, S. I. and Elinder, F.** (2008). Structure, Function, and Modification of the Voltage Sensor in Voltage-Gated Ion Channels. *Cell Biochemistry and Biophysics*, 52, 149-174.

[8] **Baracaldo-Santamaría, D., Llinas-Caballero, K., Corso-Ramirez, J. M., Restrepo, C. M., Dominguez-Dominguez, C. A., Fonseca-Mendoza, D. J. and Calderon-Ospina, C. A.** (2021). Genetic and Molecular Aspects of Drug-Induced QT Interval Prolongation. *International Journal of Molecular Sciences*, 22, 8090.

[9] **Sanguinetti, M.C. and Tristani-Firouzi, M.** (2006). hERG potassium channels and cardiac arrhythmia. *Nature*, 440(7083), 463-9.

[10] **Wang, W. and MacKinnon, R.** (2017). Cryo-EM Structure of the Open Human Ether-à-go-go-Related K+ Channel hERG. *Cell*, 169(3), 422-430.

[11] **Recanatini, M., Cavalli, A. and Masetti, M.** (2008). Modeling HERG and its interactions with drugs: recent advances in light of current potassium channel simulations. *ChemMedChem*, 3(4), 523-35.

[12] **Ju, P., Pages, G., Riek, R. P., Chen, P., Torres, A. M., Bansal, P. J., … and Vandenberg, J. I.** (2009). The pore domain outer helix contributes to both activation and inactivation of the HERG K+ channel. *Journal of Biological Chemistry*, 284(2), 1000-1008.

[13] **Kutteh, R., Vandenberg, J.I and Kuyucak, S.** (2007). Molecular dynamics and continuum electrostatics studies of inactivation in the HERG potassium channel. *The Journal of Physical Chemistry B*, 111(5), 1090-1098.

[14] **Stansfeld, P.J., Gedeck, P., Gosling, M., Cox, B., Mitcheson, J. S. and Sutcliffe, M. J.** (2007). Drug block of the hERG potassium channel: insight from modeling. *Proteins: Structure, Function, and Bioinformatics*, 68(2), 568-580.

[15] **Subbotina, J., Yarov-Yarovoy, V., Lees-Miller, J., Durdagi, S., Guo, J. and Duff, H. J.** (2010). Structural refinement of the hERG1 pore and voltage-sensing domains with ROSETTA-membrane and molecular dynamics simulations. *Proteins: Structure, Function, and Bioinformatics*, 78(14), 2922-34.

[16] **Tseng, G.N., Sonawane, K. D., Korolkova, Y. V., Zhang, M., Liu, J., Grishin, E. V. and Guy, H. R.** (2007). Probing the outer mouth structure of the HERG channel with peptide toxin footprinting and molecular modeling. *Biophysical Journal*, 92(10), 524-40.

[17] **Zachariae, U., Giordanetto, F. and Leach, A.G.** (2009). Side chain flexibilities in the human ether-a-go-go related gene potassium channel (hERG) together with matched-pair binding studies suggest a new binding mode for channel blockers. *Journal of Medicinal Chemistry*, 52(14). 4266-4276.

[18] **Durdagi, S., Randall, T., Duff, H. J., Chamberlin, A. and Noskov, S. Y.** (2014). Rehabilitating drug-induced long-QT promoters: In-silico design of hERG-neutral cisapride analogues with retained pharmacological activity. *BMC Pharmacology and Toxicology*, 15(1), 14.

[19] **Korolkova, Y.V., Tseng, G.N. and Grishin, E.V.** (2004). Unique interaction of scorpion toxins with the hERG channel. *Journal of Molecular Recognition*, 17(3), 209-17.

[20] **Zhang, M., Korolkova, Y. V., Liu, J., Jinag, M., Grishin, E. V. and Tseng, G.** (2003) BeKm-1 Is a HERG-Specific Toxin that Shares the Structure with ChTx but the Mechanism of Action with ErgTx1. *Biophysical Journal*, 84, 3022–3036.

[21] **Albericio, F. and Kruger, H.G.** (2012). Therapeutic peptides. *Future Medicinal Chemistry*, 4(12), 1527-31.

[22] **Rao, V. R., Perez-Neut, M., Kaja, S. and Gentile, S.** (2015). Voltage-gated ion channels in cancer cell proliferation. *Cancers (Basel)*, 7(2), 849-75.

[23] **Twiner, M. J., Doucette, G. J., Rasky, A., Huang, X., Roth, B. L. and Sanguinetti, M. C.** (2012). The marine algal toxin azaspiracid is an open-state blocker of hERG potassium channels. *Chemical Research in Toxicology*, 25(9), 1975-84.

[24] **Essack, M., Bajic, V. B. and Archer, J. A.** (2012). Conotoxins that confer therapeutic possibilities. *Marine Drugs*, 10(6), 1244-65.

[25] **Calmette, A., Saenz, A. and Costil, L.** (1933). Effects du venin de cobra sur les greffes cancereuses et sur le cancer spontane (adeno-carcinome) de la souris. *Comptes Rendus de l'Academie des Sciences*, 197, 205-210.

[26] **Rodriguez de la Vega, R. C. and Possani, L. D.** (2004). Current views on scorpion toxins specific for K+-channels. *Toxicon*, 43(8), 865-75.

[27] **Lewis, R. J. and Garcia, M. L.** (2003). Therapeutic potential of venom peptides. *Nature Reviews Drug Discovery*, 2(10), 790-802.

[28] **Korolkova, Y. V., Bocharov, E. V., Angelo, K., Maslennikov, I. V., Grinenko, O. V., Lipkin, A. V., … and Grishin, E. V.** (2002). New binding site on common molecular scaffold provides HERG channel specificity of scorpion toxin BeKm-1, *Journal of Biological Chemistry*, 277 (45), 43104-43109.

[29] **Li, M., Wang, Y., Chen, X., Zhang, N., Wu, H. and Hu, G.** (2003). BmTx3B, a novel scorpion toxin from Buthus martensi Karsch, inhibits delayed rectifier potassium current in rat hippocampal neurons, *Acta Pharmacologica Sinica*, 24 (10), 1016-1020.

[30] **Diochot, S., Loret, E., Bruhn, T., Beress, L. and Lazdunski, M.** (2003). APETx1, a new toxin from the sea anemone Anthopleura elegantissima, blocks voltage-gated human ether-a-go-go-related gene potassium channels, *Molecular Pharmacology*, 64 (1), 59-69.

[31] **Yi, H., Cao, Z., Yin, S., Dai, C., Wu, Y. and Li, W.** (2007). Interaction simulation of hERG K+ channel with its specific BeKm-1 peptide: insights into the selectivity of molecular recognition, *Journal of Proteome Research*, 6 (2), 611-620.

[32] **Wang, Y., Chen, X., Zhang, N., Wu, G. and Wu, H.** (2005). The solution structure of BmTx3B, a member of the scorpion toxin subfamily alpha-KTx 16, *Proteins: Structure, Function, and Bioinformatics*, 58 (2), 489-497.

[33] **Durdagi, S., Duff, H. J. and Nuskov, S. Y.** (2011). Combined Receptor and Ligand-Based Approach to the Universal Pharmacophore Model Development for Studies of Drug Blockade to the hERG1 Pore Domain. *Journal of Chemical Information and Modelling*, 51, 2, 463–474.

[34] **Kalyaanamoorthy, S., Lamothe, S. M., Hou, X., Moon, T. C., Kurata, H. T., Houghton, M. and Barakat, K. H.** (2020). A structure-based computational workflow to predict liability and binding modes of small molecules to hERG. *Scientific Reports*, 10, 16262.

[35] **Negami, T., Araki, M., Okuno, Y and Terada, T.** (2019). Calculation of absolute binding free energies between the hERG channel and structurally diverse drugs. *Scientific Reports*, 9, 16586.

[36] **Dickson, C. J., Velez-Vega, C. and Duca, J. S.** (2020). Revealing Molecular Determinants of hERG Blocker and Activator Binding. *Journal of Chemical Information and Modelling*, 60, 192−203.

[37] **Luo, F., Gu, J., Chen, L. and Xu, X.** (2014). Molecular docking and molecular dynamics studies on the structure–activity relationship of fluoroquinolone for the HERG channel. *Molecular BioSystems*, 10, 2863-2869.

[38] **Berman, H. M., Westbrook, J., Gilliland, G., Bhat, T. N., Weissig, H., Shindyalov, I. N. and Bourne, P. E.** (2000). The protein data bank, *Nucleic Acids Research*, 28 (1), 235-242.

[39] **Sastry, G. M., Adzhigirey, M., Day, T., Annabhimoju, R. and Sherman, W.** (2013). Protein and ligand preparation: parameters, protocols, and influence on virtual screening enrichments, *Journal of Computer-Aided Molecular Design*, 27 (3), 221-234.

[40] **Shelley, J. C., Cholleti, A., Frye, L. L., Greenwood, J. R., Timlin, M. R. and Uchimaya, M.** (2007). Epik: a software program for pK(a) prediction and protonation state generation for drug-like molecules, *Journal of Computer-Aided Molecular Design*, 21 (12), 681-691.

[41] URL <https://www.chemdiv.com/catalog/focused-and-targeted-libraries/ppi-tripeptide-mimetics-library/>, date retrieved 02.01.2024.

[42] **Kozakov, D., Hall, D. R., Xia, B., Porter, K. A., Padhorny, D., Yueh, C., Beglov, D. and Vajda, S.** (2017). The ClusPro web server for protein-protein docking, *Nature Protocols*, 12 (2), 255-278.

[43] **Kozakov, D., Beglov, D., Bohnuud, T., Mottarella, S. E., Xia, B., Hall, D. R. and Vajda, S.** (2013). How good is automated protein docking? *Proteins: Structure, Function, and Bioinformatics*, 81 (12), 2159-2166.

[44] **Kozakov, D., Brenke, R., Comeau, S. R. and Vajda, S.** (2006). PIPER: an FFT-based protein docking program with pairwise potentials, *Proteins: Structure, Function, and Bioinformatics*, 65 (2), 392-406.

[45] **Comeau, S. R., Gatchell, D. W., Vajda, S. and Camacho, C. J.** (2004). ClusPro: an automated docking and discrimination method for the prediction of protein complexes, *Bioinformatics*, 20 (1), 45-50.

[46] **Comeau, S. R., Gatchell, D. W., Vajda, S. and Camacho, C. J.** (2004). ClusPro: a fully automated algorithm for proteineprotein docking, *Nucleic Acids Research, 32 (suppl 2)*, W96-W99.

[47] **Huys, I., Xu, C., Wang, C., Vacher, H., Martin-Eauclaire, M., Chi, C. and Tytgat, J.** (2004). BmTx3, a scorpion toxin with two putative functional faces separately active on A-type K and HERG currents, *Biochemical Journal*, 378, 745-752.

[48] **Lomize, M. A., Lomize, A. L., Pogozheva, I. D. and Mosberg, H. I.** (2006). OPM: orientations of proteins in membranes database, *Bioinformatics*, 22 (5), 623-625.

[49] **Berendsen, H.J., van der Spoel, D. and van Drunen, R.** (1995). GROMACS: a message-passing parallel molecular dynamics implementation, *Computer Physics Communications*, 91 (1-3), 43-56.

[50] **Abraham, M. J., Murtola, T., Schulz, R., Pall, S., Smith, J. C., Hess, B. and Lindahl, E.** (2015). GROMACS: High performance molecular simulations through multi-level parallelism from laptops to supercomputers, *SoftwareX*, 1, 19-25.

[51] **Best, R.B., Zhu, X., Shim, J., Lopes, P., Mittal, J., Feig, M. Jr, A. D. M.** (2012). Optimization of the additive CHARMM all-atom protein force field targeting improved sampling of the backbone f, j and side-chain c(1) and c(2) dihedral angles, *Journal of Chemical Theory and Computation*, 8 (9), 3257-3273.

[52] **Jo, S., Kim, T., Iyer, V. G. and Im, W.** (2008). CHARMM-GUI: a web-based graphical user interface for CHARMM, *Journal of Computational Chemistry*, 29 (11), 1859-1865.

[53] **Jorgensen, W. L., Chandrasekhar, J., Madura, J. D., Impey, R. D. and Klein, M. L.** (1983). Comparison of simple potential functions for simulating liquid water, *The Journal of Chemical Physics*, 79, 926-935.

[54] **Darden, T., York, D. and Pedersen, L.** (1993). Particle mesh Ewald: an Nlog(N) method for Ewald sums in large systems, *The Journal of Chemical Physics*, 98, 10089-10092.

[55] **Hess, B., Bekker, H., Berendsen, H. J. and Fraaije, J. G. E. M.** (1997). LINCS: a linear constraint solver for Molecular simulations, *Journal of Computational Chemistry*, 18 (12), 1463-1472.

[56] **Pall, S., Hess, B.** (2013). A flexible algorithm for calculating pair interactions on SIMD architectures, *Computer Physics Communications*, 184, 2641-2650.

[57] **Cheng, A. and Merz, K.M.** (1996). Application of the Nose-Hoover chain algorithm to the study of protein dynamics, *The Journal of Physical Chemistry*, 100 (5), 1927-1937.

[58] **Berendsen, H. J. C., Postma, J. P. M., van Gunsteren, W. F., DiNola, A. and Haak, J. R.** (1984). Molecular dynamics with coupling to an external bath, *The Journal of Chemical Physics*, 81, 3684-3690.

[59] **Parrinello, M. and Rahman, A.** (1981). Polymorphic transitions in single crystals: a new molecular dynamics method, *Journal of Applied Physics*, 52, 7182-7190.

[60] **Miller III, B. R., McGee, T. D., Swails, J. M., Homeyer, N., Gohlke, H. and Roitberg, A. E.** (2012). MMPBSA. py: an efficient program for end-state free energy calculations, *Journal of Chemical Theory and Computation*, 8 (9), 3314-3321.

[61] **Kumari, R., Kumar, R., Lynn, A.** (2014). g_mmpbsa-A GROMACS tool for Highthroughput MM-PBSA calculations, *Journal of Chemical Information and Modelling*, 54 (7), 1951-1962.

[62] **Kortemme, T., Kim, D. E. and Baker, D.** (2004). Computational alanine scanning of proteinprotein interfaces, *Science's STKE*, (219), l2.

[63] **Beltran-Vidal, J., Carcamo-Noriega, E., Pastor, N., Zamudio-Zuniga, F., Guerrero-Vargas, J. A., Castano, S., Possani, L. D. and Restano-Cassulini, R.** (2011). Colombian Scorpion Centruroides margaritatus: Purification and Characterization of a Gamma Potassium Toxin with Full-Block Activity on the hERG1 Channel, *Toxins (Basel)*, 13(6), 407.

[64] **Colak Gunay, B., Yurtsever, M., Durdagi, S.** (2020). Elucidation of interaction mechanism of hERG1 potassium channel with scorpion toxins BeKm-1 and BmTx3b, *Journal of Molecular Graphics and Modelling*, 96, 107504.

[65] **Tubert-Drohman, I., Sherman, W., Repasky, M. and Beuming T.** (2013). Improved Docking of Polypeptides with Glide, *Journal of Chemical Information and Modelling,*, 53, 7, 1689–1699.

[66] **Friesner, R. A., Banks, J. L., Murphy, R. B., Halgren, T. A., Klicic, J. J., Mainz, D. T., … and Shenkin, P. S.** (2004). Glide: A New Approach for Rapid, Accurate Docking and Scoring. 1. Method and Assessment of Docking Accuracy, *Journal of Medicinal Chemistry*, 47, 7, 1739–1749.

[67] **Halgren, T. A., Murphy, R. B., Friesner, R. A., Beard, H. S., Frye, L. L., Pollard, W. T. and Banks, J. L.** (2004). Glide: A New Approach for Rapid, Accurate Docking and Scoring. 2. Enrichment Factors in Database Screening, *Journal of Medicinal Chemistry*, 47, 7, 1750–1759.

[68] **Lomize, A. L., Pogozheva, I. D., Lomize, M. A. and Mosberg, H. I.** (2009). Positioning of proteins in membranes: A computational approach, *Protein Science*, 15(6), 1318-1333.

[69] **Evans, D.J. and Holian, B.L.** (1985). The Nose–Hoover thermostat, *The Journal of Chemical Physics*, 83, 4069–4074.

[70] **Martyna, G. J., Tobias, D. J. and Klein, M. L.** (1994). Constant pressure molecular dynamics algorithms, *The Journal of Chemical Physics*, 101, 4177–4189.

[71] **Bowers, K. J., Chow, D. E., Xu, H., Dror, R. O., Eastwood, M. P., Gregersen, B. A., … and Shaw, D. E.** (2006). Scalable Algorithms for Molecular Dynamics Simulations on Commodity Clusters, Proceedings of the ACM/IEEE Conference on Supercomputing (SC06), Tampa, Florida.

[72] **Kamiya, K., Niwa, R., Mitcheson, J. S. and Sanguinetti, M. C.** (2006). Molecular determinants of HERG channel block, *Molecular Pharmacology*, 69 (5), 1709-1716.

[73] **Hmed, B., Serria, H. T. and Mounir, Z. K.** (2013). Scorpion peptides: potential use for new drug development, *Journal of Toxicology*, 958797.

[74] **Li, L., Li, C., Zhang, Z. and Alexov, E.** (2013). On the dielectric "constant" of proteins: smooth dielectric function for macromolecular modeling and its implementation in DelPhi, *Journal of Chemical Theory and Computation*, 9 (4), 2126-2136.

APPENDICES

APPENDIX A: Detailed Figures and Tables for Chapter 3

APPENDIX A : Detailed Figures and Tables for Chapter 3

(a) Apo Form

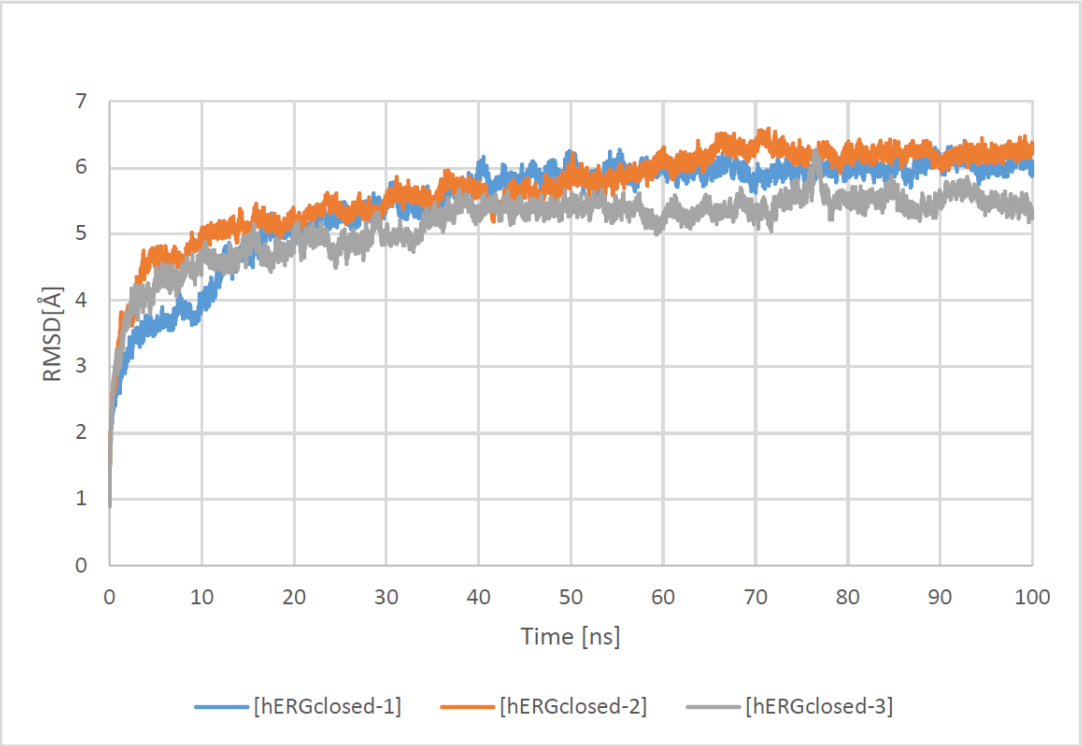

(b) [hERGclosed/bekm1-1]-complex

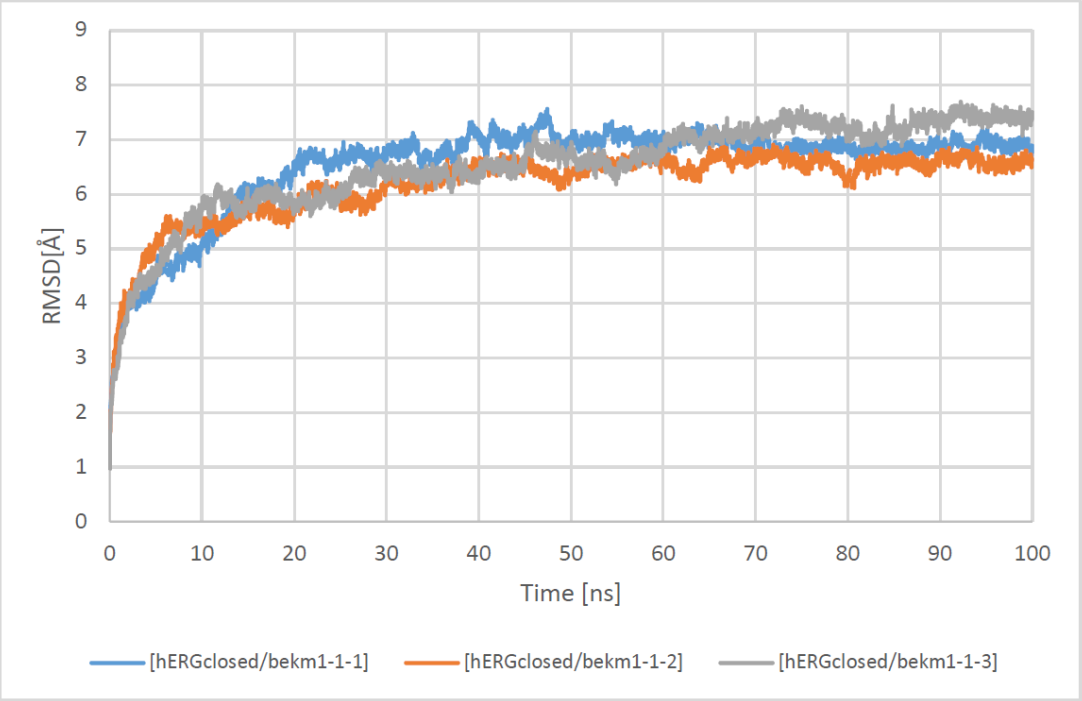

Figure A.1 : The RMSD graphs of **(a)** apo and **(b)** to **(m)** holo form of hERG1 closed state.

(c) [hERGclosed/bekm1-1] –hERG1

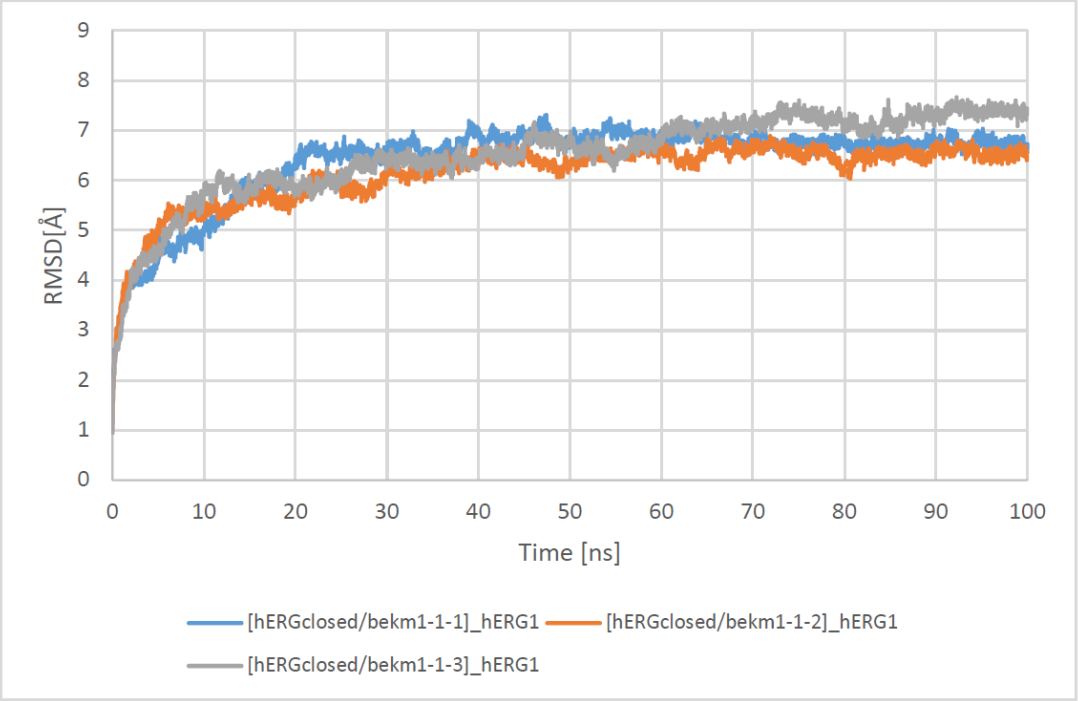

(d) [hERGclosed/bekm1-1] –toxin

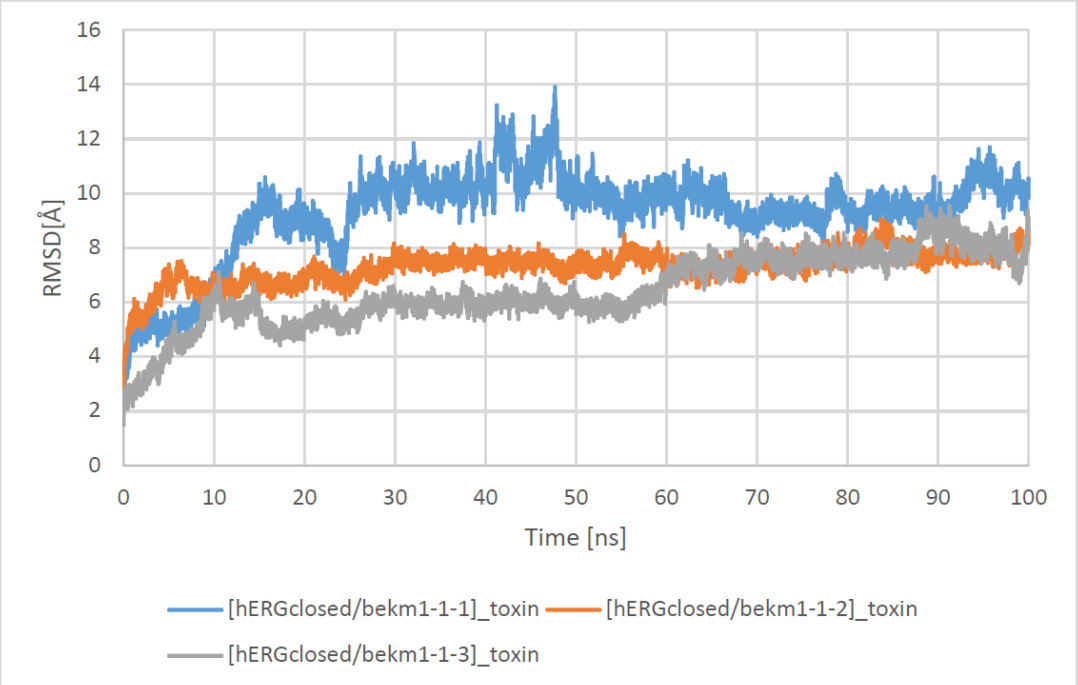

Figure A.1 (continued) : The RMSD graphs of **(a)** apo and **(b)** to **(m)** holo form of hERG1 closed state.

(e) [hERGclosed/bekm1-2]-complex

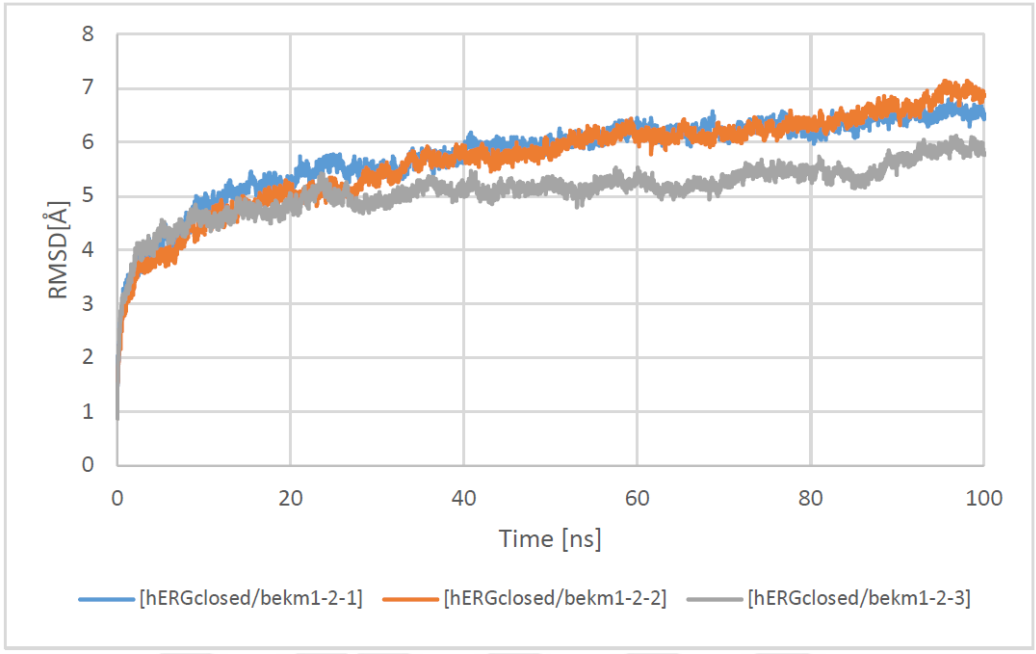

(f) [hERGclosed/bekm1-2]-hERG1

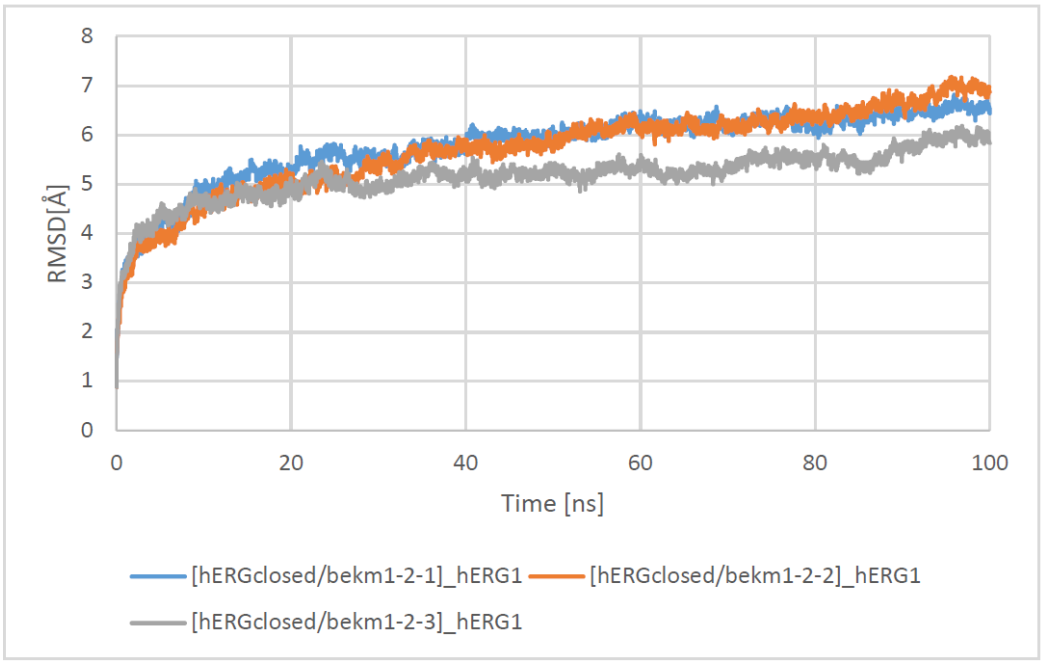

Figure A.1 (continued) : The RMSD graphs of **(a)** apo and **(b)** to **(m)** holo form of hERG1 closed state.

(g) [hERGclosed/bekm1-2]-toxin

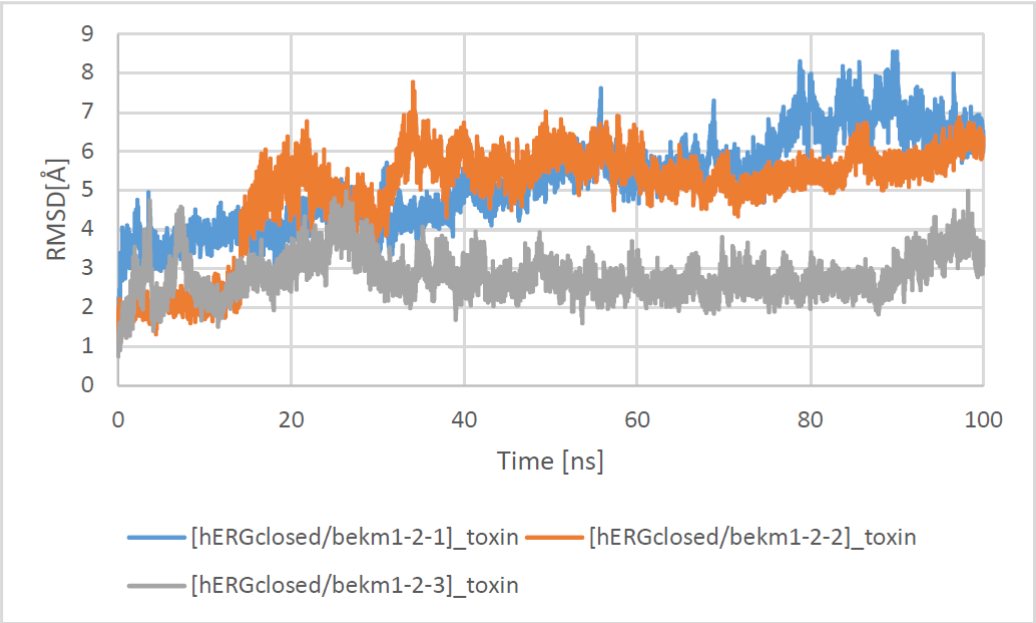

(h) [hERGclosed/bmtx3b-1-1]-complex

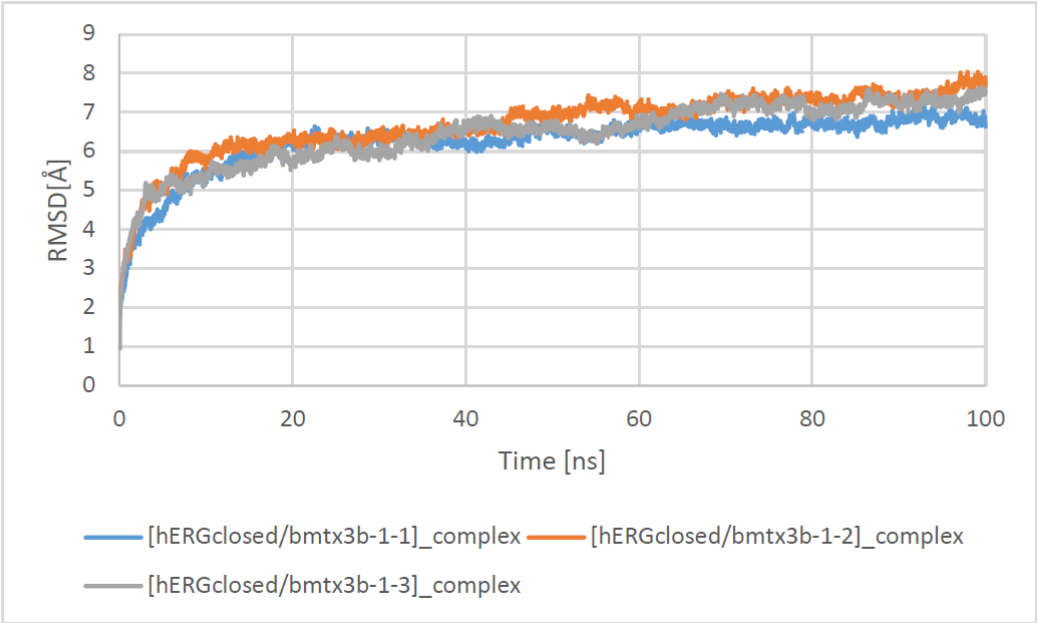

Figure A.1 (continued) : The RMSD graphs of **(a)** apo and **(b)** to **(m)** holo form of hERG1 closed state.

(i) [hERGclosed/bmtx3b-1-1]-hERG1

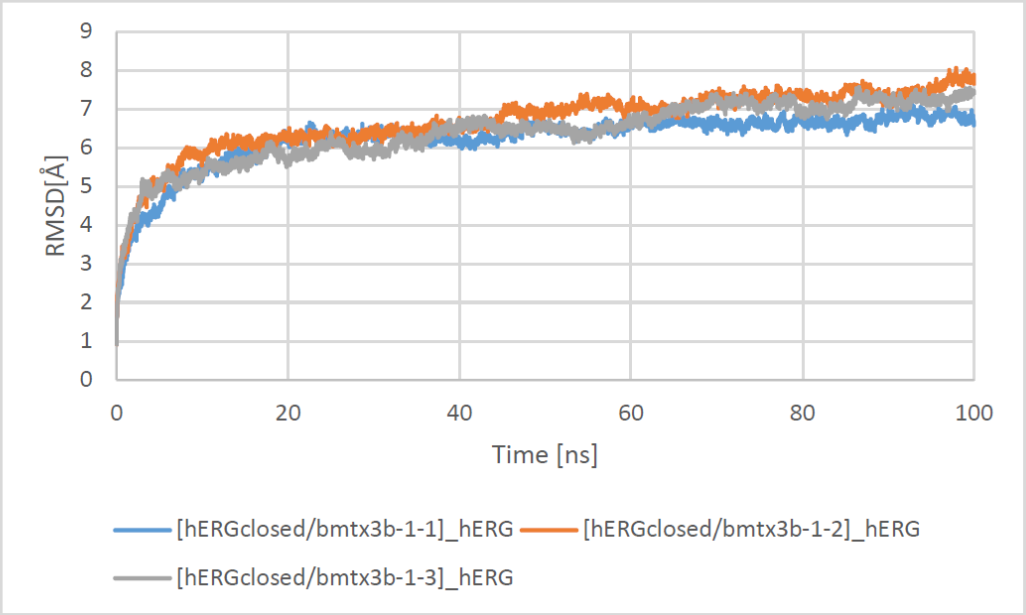

(j) [hERGclosed/bmtx3b-1-1]-toxin

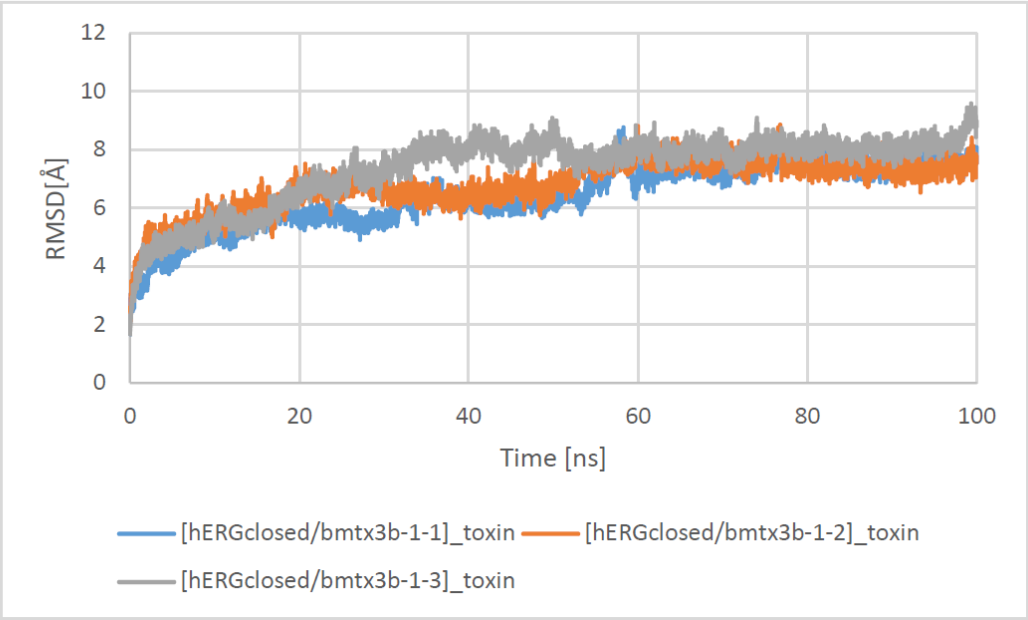

Figure A.1 (continued) : The RMSD graphs of **(a)** apo and **(b)** to **(m)** holo form of hERG1 closed state.

(k) [hERGclosed/bmtx3b-2-1]-complex

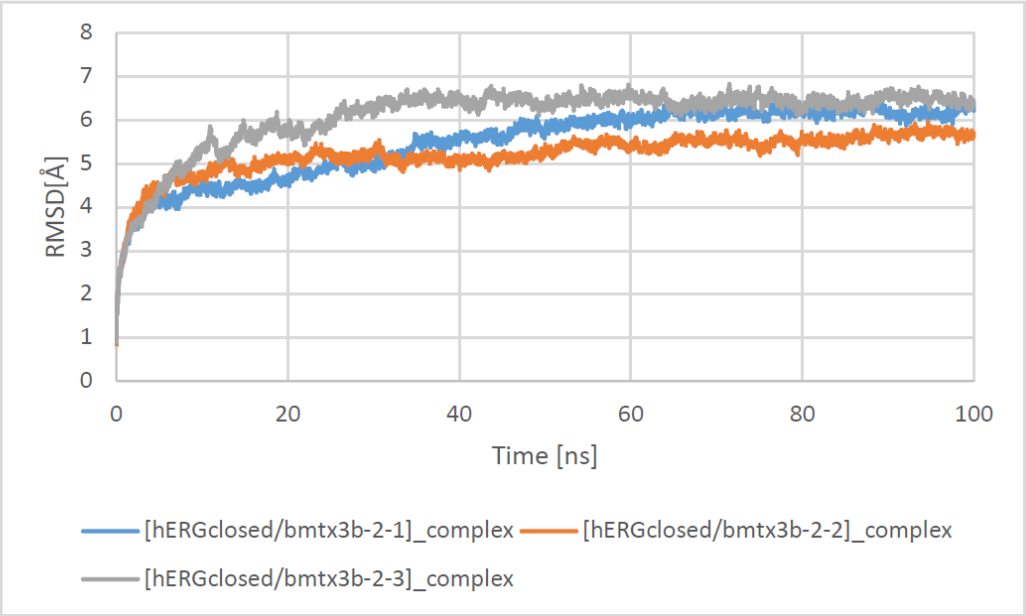

(l) [hERGclosed/bmtx3b-2-2]-hERG1

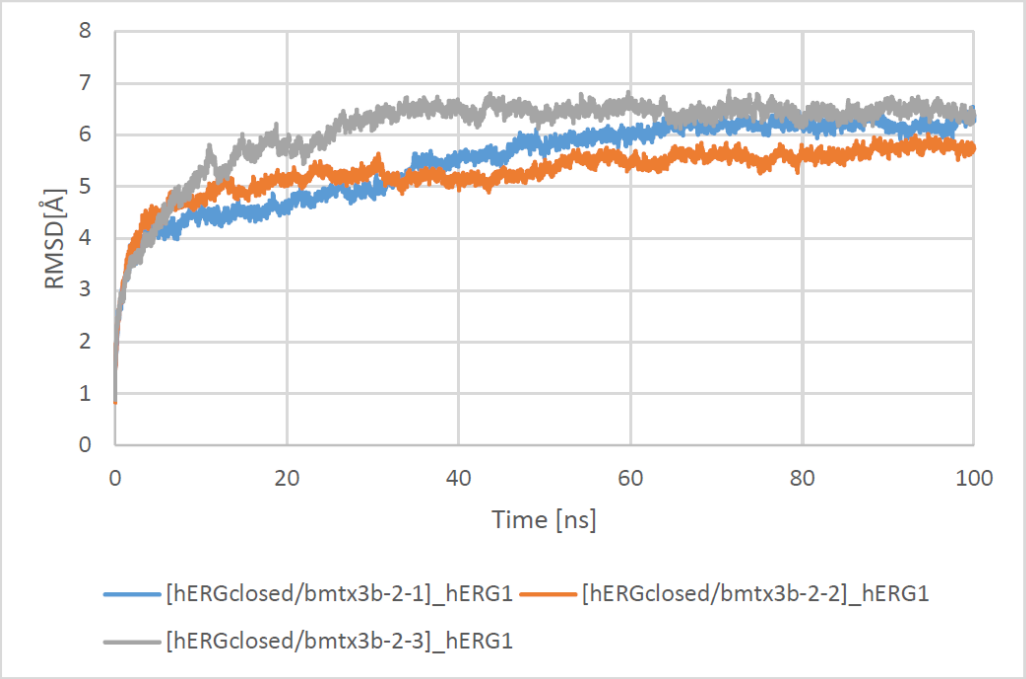

Figure A.1 (continued) : The RMSD graphs of **(a)** apo and **(b)** to **(m)** holo form of hERG1 closed state.

(m) [hERGclosed/bmtx3b-2-3]-toxin

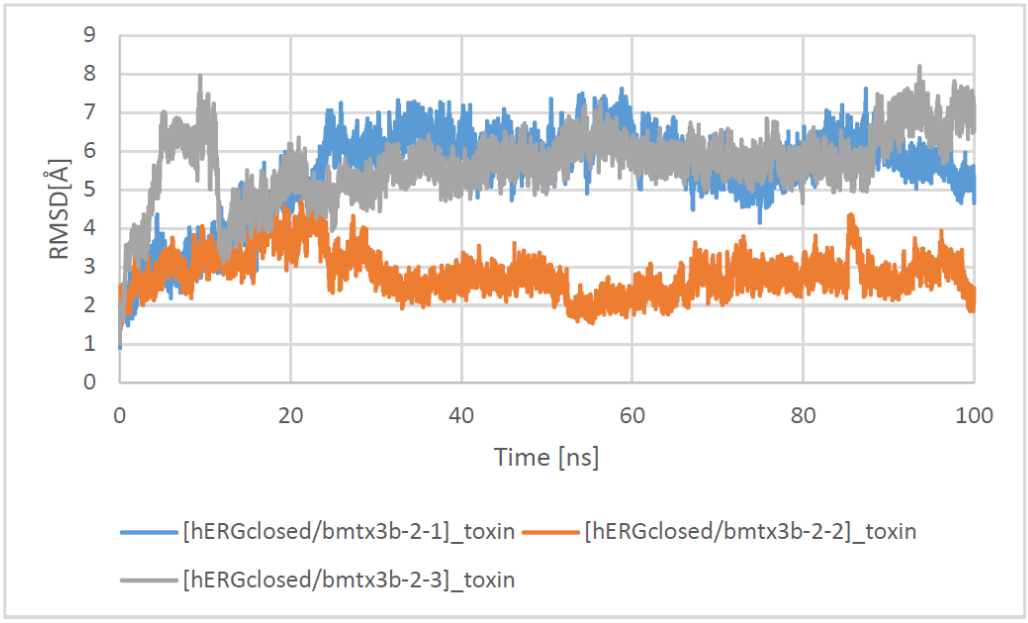

Figure A.1 (continued) : The RMSD graphs of **(a)** apo and **(b)** to **(m)** holo form of hERG1 closed state.

(a) Apo Form - [hERGclosed-1]

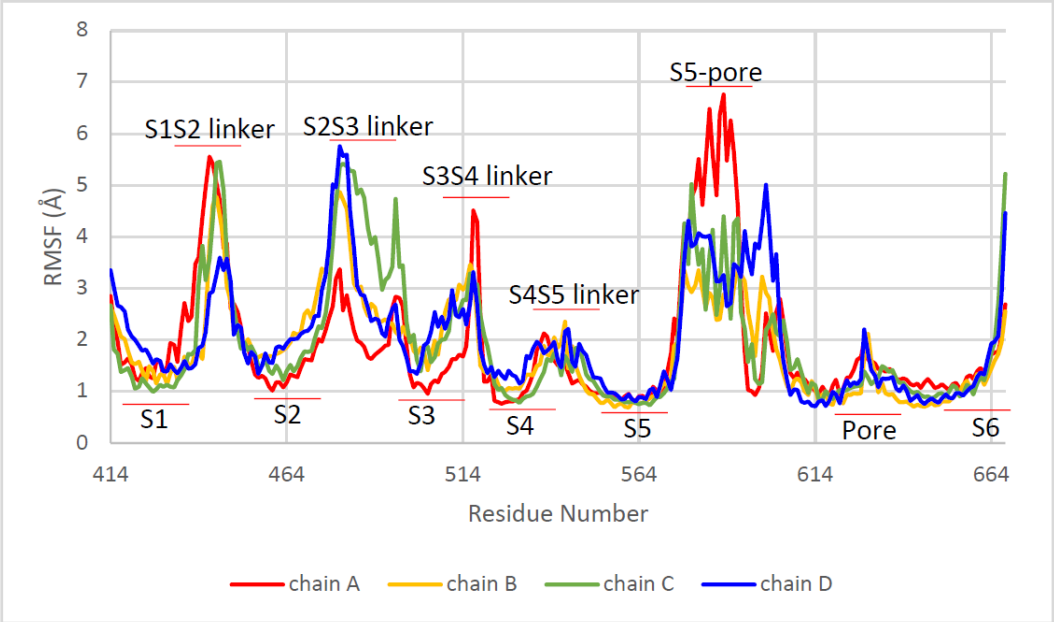

(b) Apo Form - [hERGclosed-2]

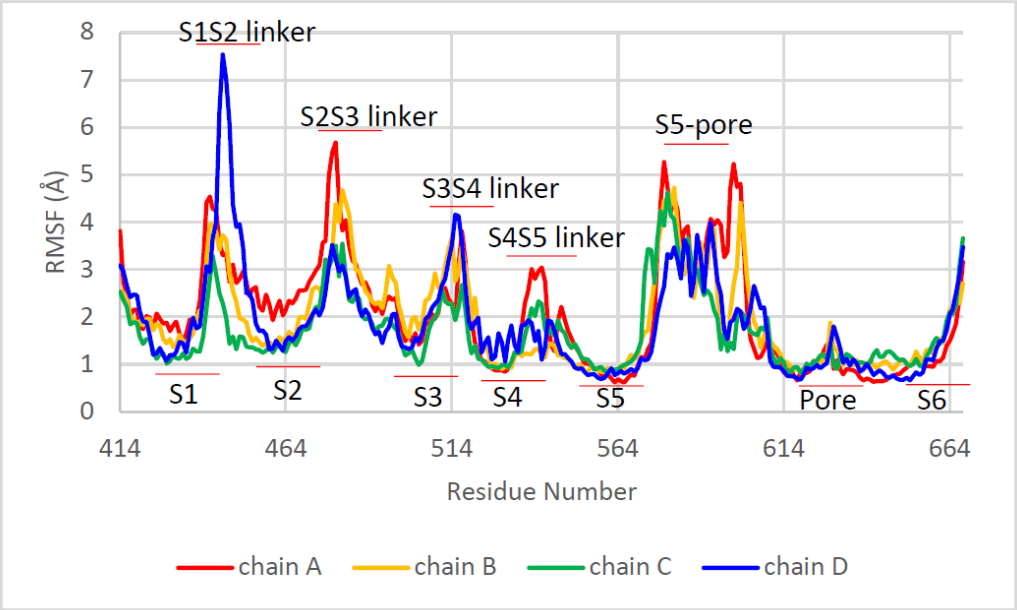

Figure A.2 : The RMSF graphs of **a** to **c)** apo and **d** to **o)** holo form of hERG1 closed state.

(c) Apo Form - [hERGclosed-3]

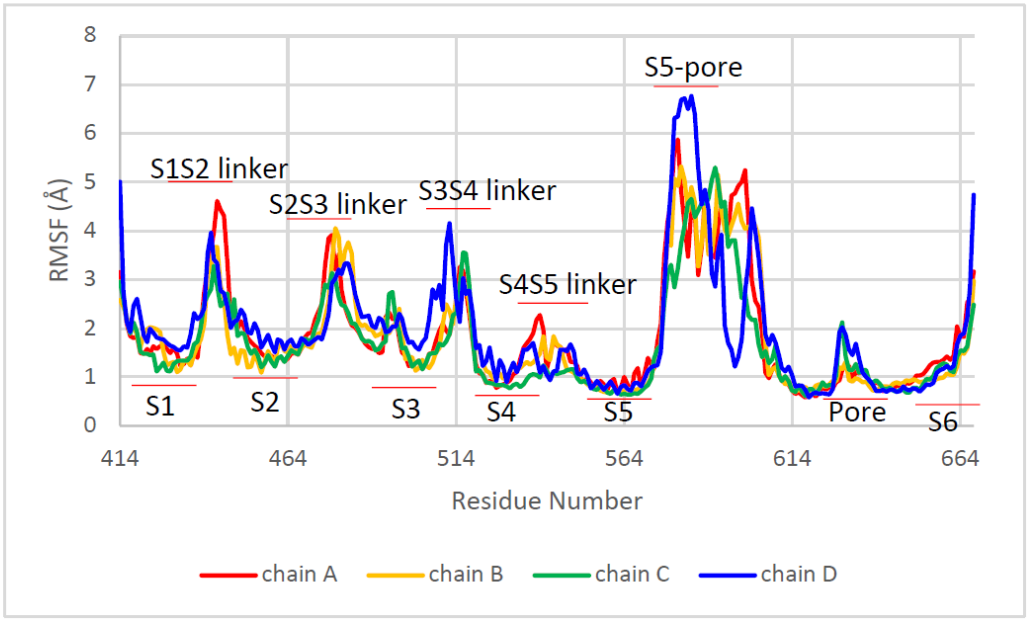

(d) Holo Form - [hERGclosed/bekm1-1] -1

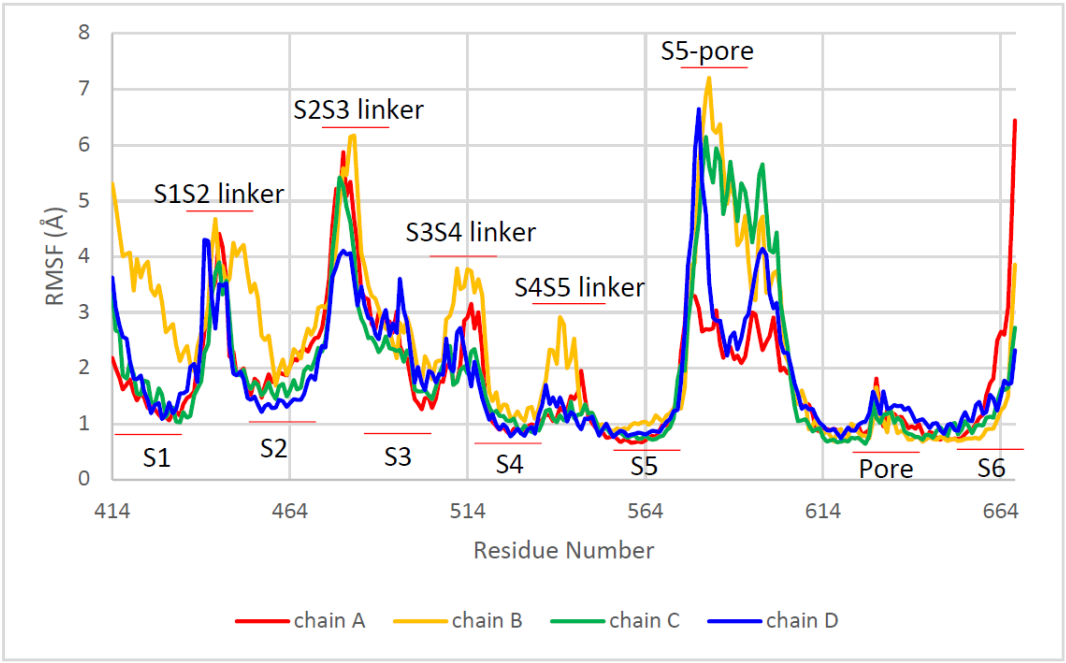

Figure A.2 (continued) : The RMSF graphs of **a** to **c)** apo and **d** to **o)** holo form of hERG1 closed state.

(e) Holo Form - [hERGclosed/bekm1-1] -2

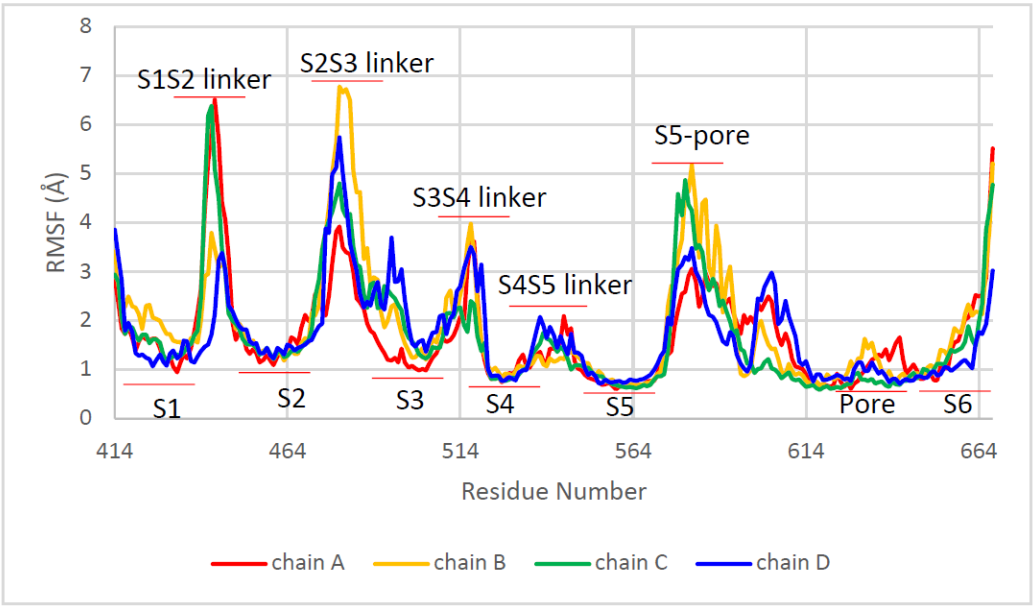

(f) Holo Form - [hERGclosed/bekm1-1] -3

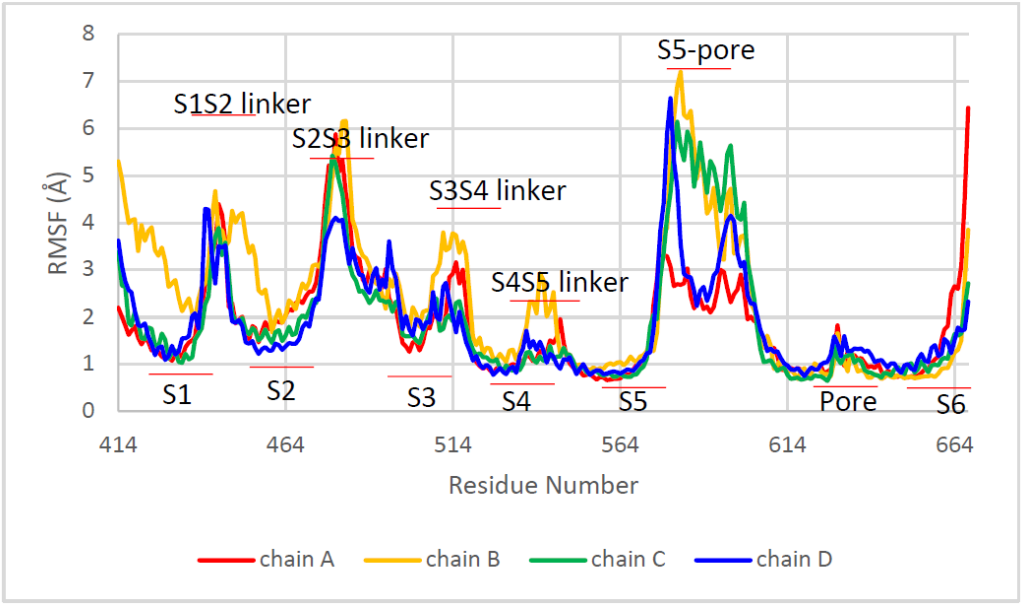

Figure A.2 (continued) : The RMSF graphs of **a** to **c)** apo and **d** to **o)** holo form of hERG1 closed state.

(g) Holo Form - [hERGclosed/bekm1-2] -1

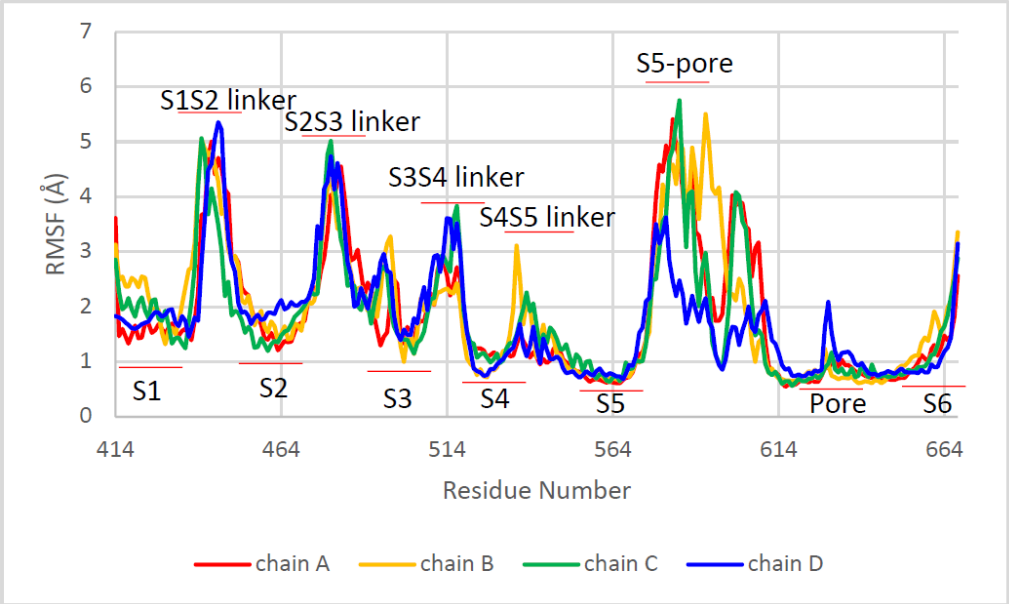

(h) Holo Form - [hERGclosed/bekm1-2] -2

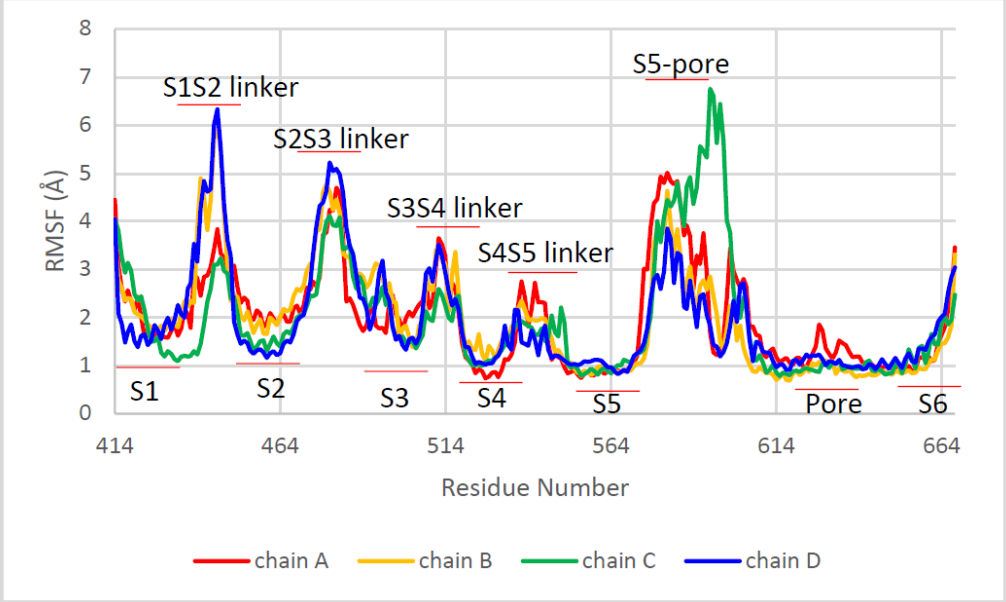

Figure A.2 (continued) : The RMSF graphs of **a** to **c)** apo and **d** to **o)** holo form of hERG1 closed state.

(i) Holo Form - [hERGclosed/bekm1-2] -3

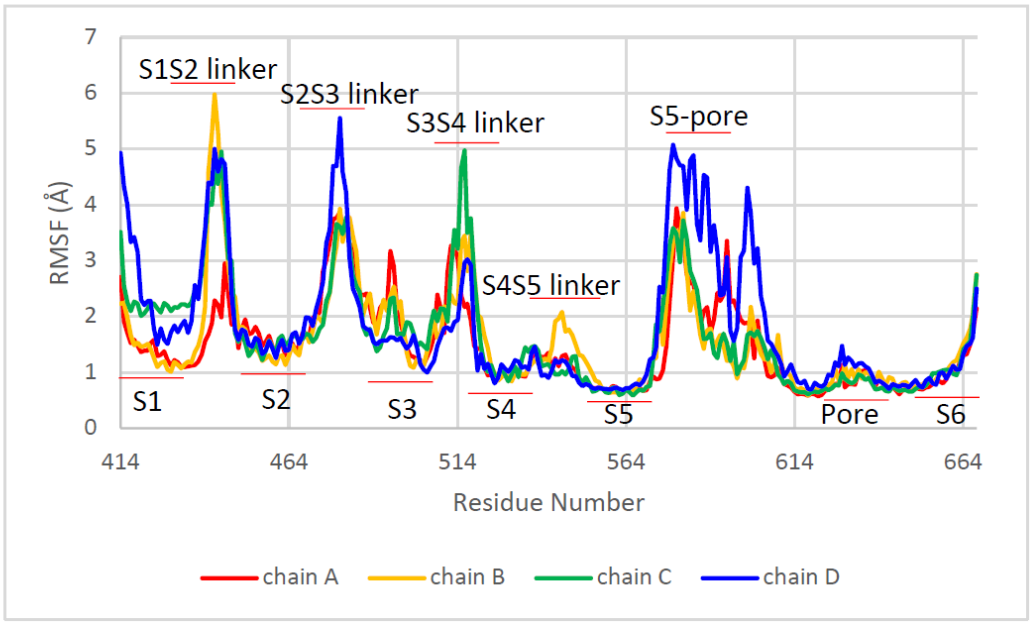

(j) Holo Form - [hERGclosed/bmtx3b-1]-1

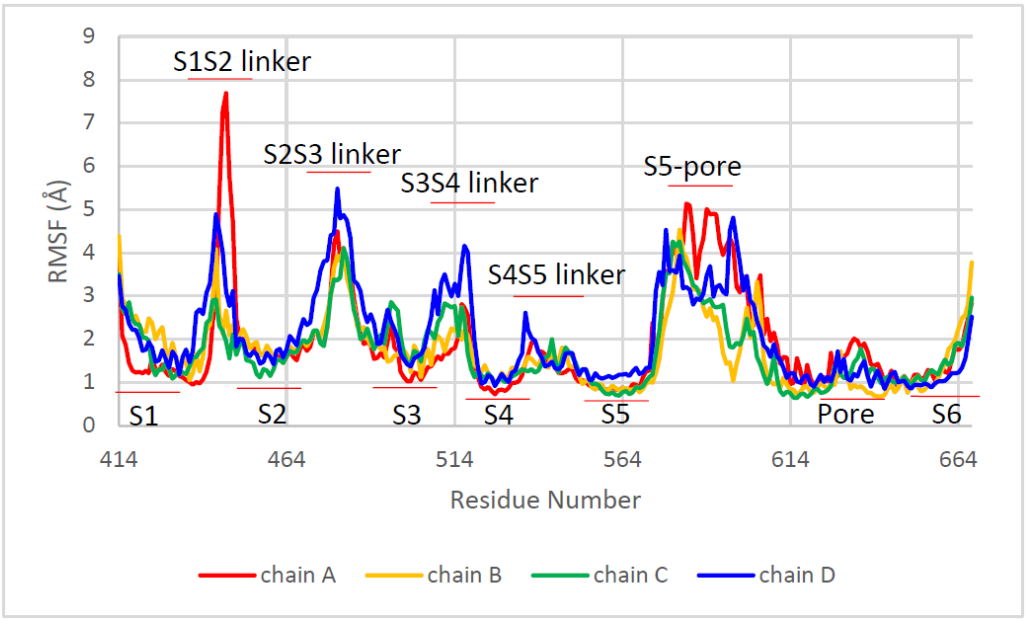

Figure A.2 (continued) : The RMSF graphs of **a** to **c)** apo and **d** to **o)** holo form of hERG1 closed state.

(k) Holo Form - [hERGclosed/bmtx3b-1]-2

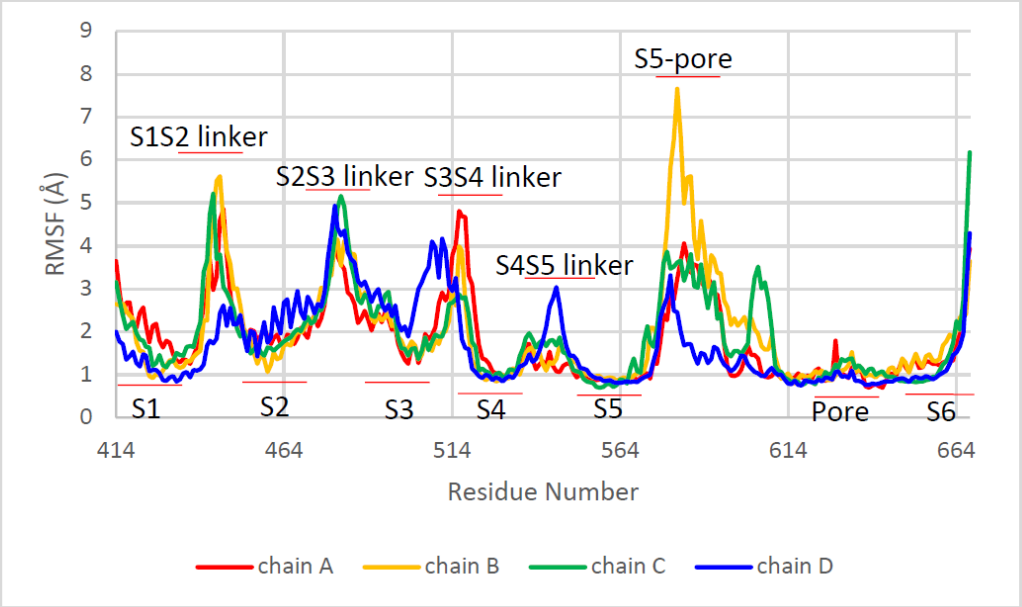

(l) Holo Form - [hERGclosed/bmtx3b-1]-3

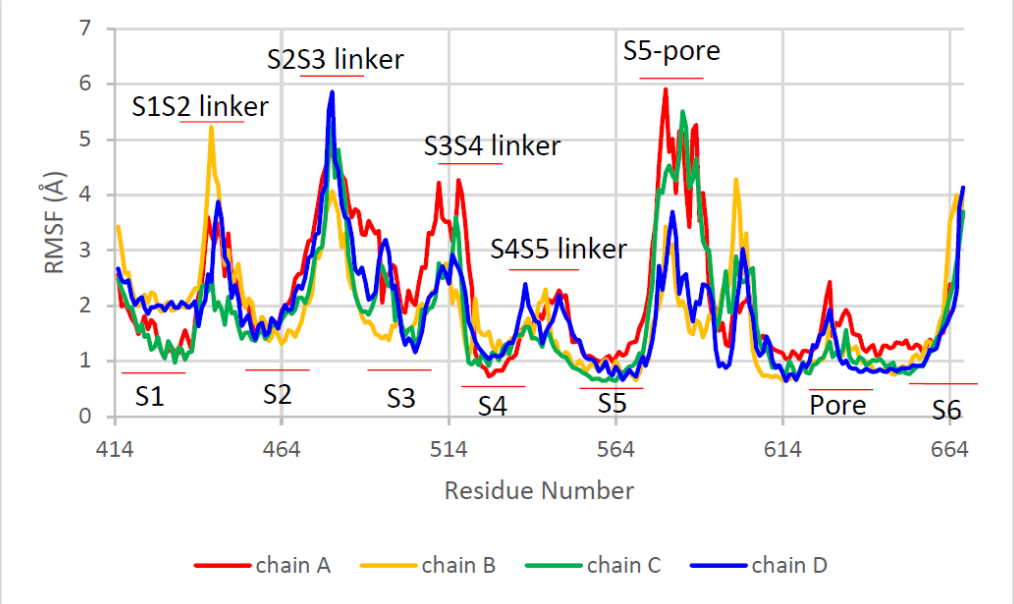

Figure A.2 (continued) : The RMSF graphs of **a** to **c)** apo and **d** to **o)** holo form of hERG1 closed state.

(m) Holo Form - [hERGclosed/bmtx3b-2]-1

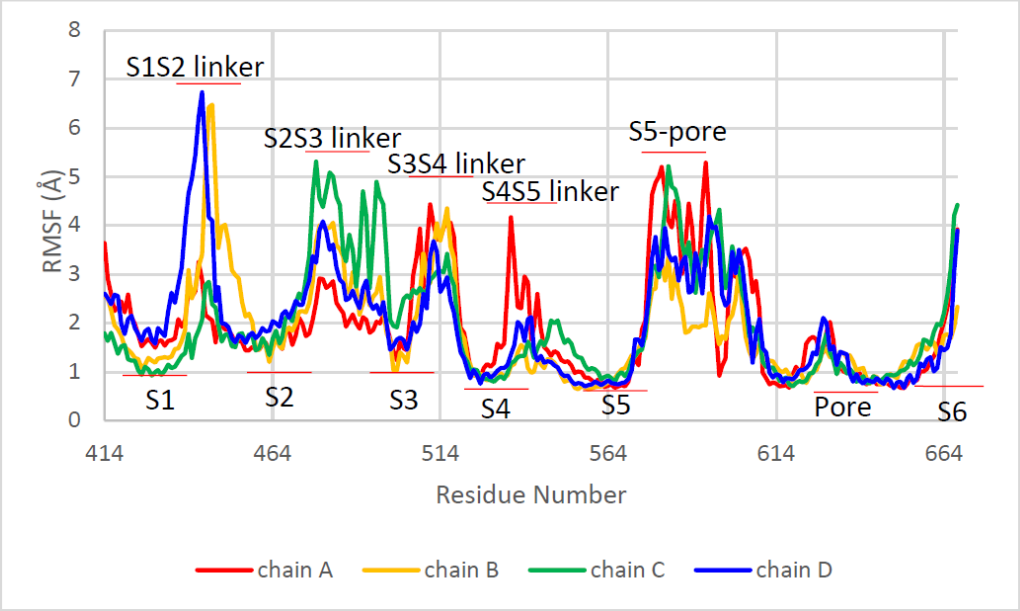

(n) Holo Form - [hERGclosed/bmtx3b-2]-2

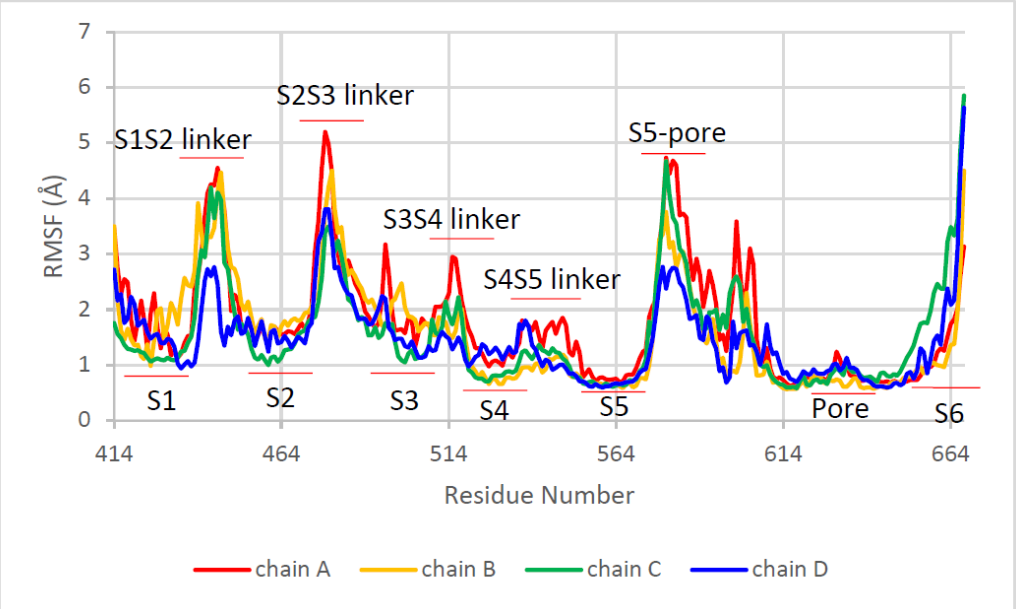

Figure A.2 (continued) : The RMSF graphs of **a** to **c)** apo and **d** to **o)** holo form of hERG1 closed state.

(o) Holo Form - [hERGclosed/bmtx3b-2]-3

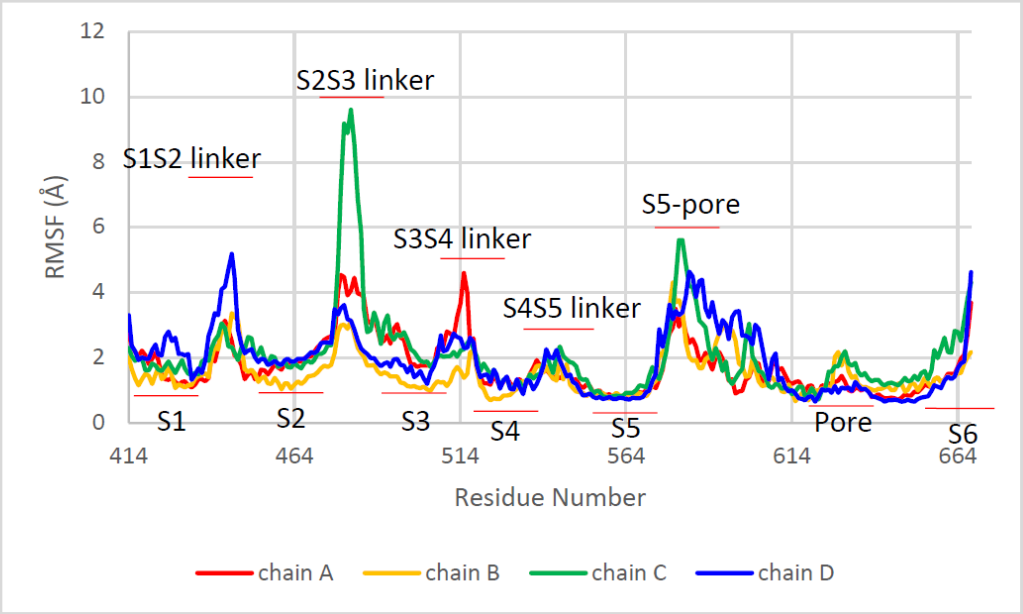

Figure A.2 (continued) : The RMSF graphs of **a** to **c)** apo and **d** to **o)** holo form of hERG1 closed state.

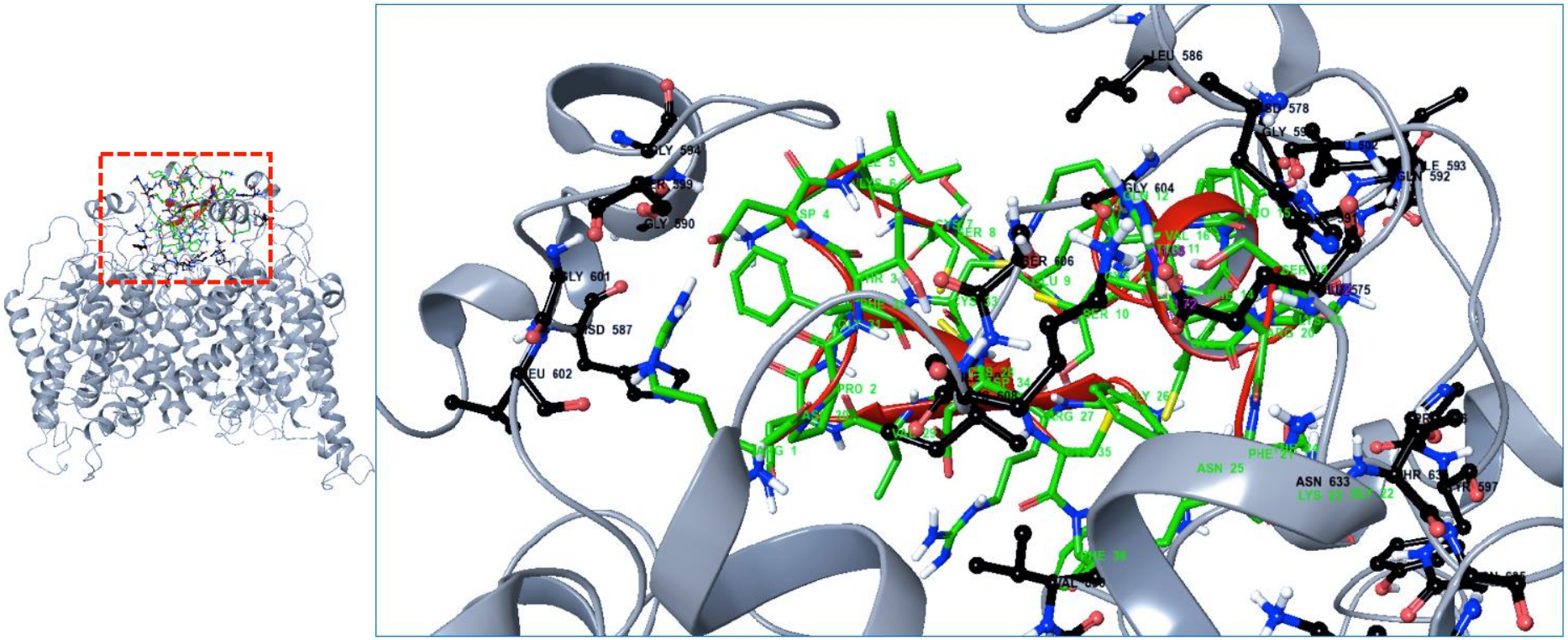

Figure A.3 : (i) 3D channel-BeKm1 toxin interactions map; and (ii) their corresponding 2D interactions.

ii)

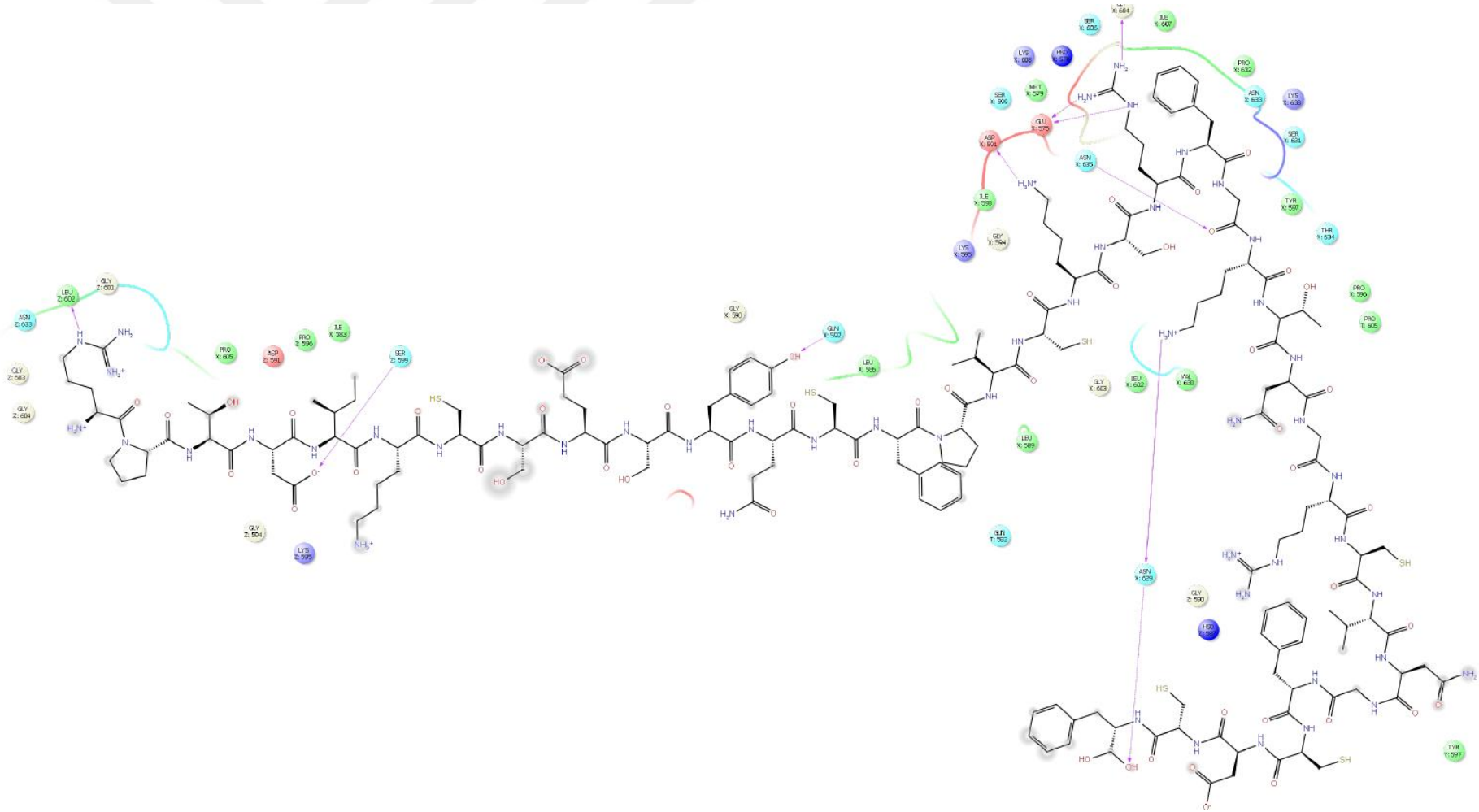

Figure A.3 (continued) : (i) 3D channel-BeKm1 toxin interactions map; and (ii) their corresponding 2D interactions.

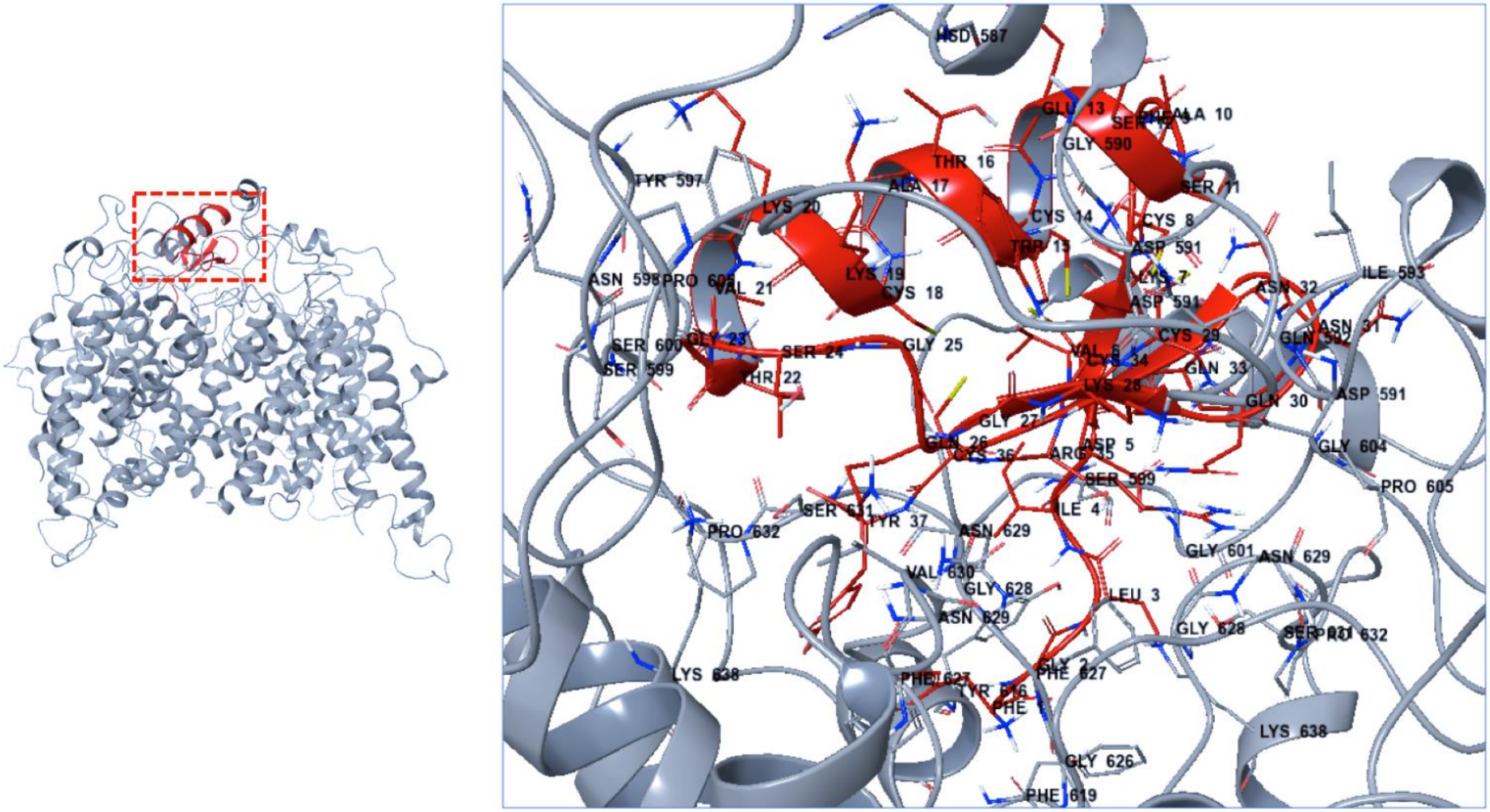

Figure A.4 : (i) 3D channel- BmTx31 toxin interactions map; and (ii) their corresponding 2D interactions.

ii)

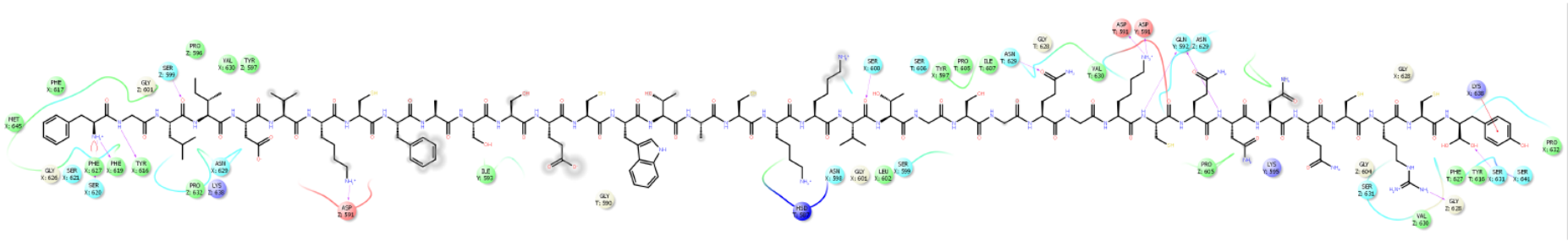

Figure A.4 (continued) : (i) 3D channel- BmTx31 toxin interactions map; and (ii) their corresponding 2D interactions.

[hERGclosed/bekm1-1]-1																				
	van der Waal energy				Electrostattic energy				Polar solvation energy				SASA energy				Binding energy			
pdie2	-129,785	+/-	1,507	kcal/mol	-433,606	+/-	3,9603	kcal/mol	301,346	+/-	4,921	kcal/mol	-15,959	+/-	0,147	kcal/mol	-278,094	+/-	1,509	kcal/mol
pdie4	-129,844	+/-	1,495	kcal/mol	-216,708	+/-	2,0505	kcal/mol	258,121	+/-	4,294	kcal/mol	-15,958	+/-	0,141	kcal/mol	-104,421	+/-	2,170	kcal/mol
pdie6	-129,693	+/-	1,466	kcal/mol	-144,456	+/-	1,3593	kcal/mol	229,156	+/-	3,754	kcal/mol	-15,962	+/-	0,143	kcal/mol	-61,165	+/-	2,472	kcal/mol
pdie8	-129,748	+/-	1,469	kcal/mol	-108,383	+/-	0,9828	kcal/mol	207,672	+/-	3,406	kcal/mol	-15,955	+/-	0,146	kcal/mol	-46,355	+/-	2,596	kcal/mol
[hERGclosed/bekm1-1]-2																				
	van der Waal energy				Electrostattic energy				Polar solvation energy				SASA energy				Binding energy			
pdie2	-159,543	+/-	1,055	kcal/mol	-420,875	+/-	2,1665	kcal/mol	321,843	+/-	2,656	kcal/mol	-19,084	+/-	0,106	kcal/mol	-277,629	+/-	1,574	kcal/mol
pdie4	-159,520	+/-	1,078	kcal/mol	-210,420	+/-	1,1349	kcal/mol	271,981	+/-	2,083	kcal/mol	-19,085	+/-	0,108	kcal/mol	-117,171	+/-	1,267	kcal/mol
pdie6	-159,562	+/-	1,068	kcal/mol	-140,290	+/-	0,7299	kcal/mol	238,669	+/-	1,864	kcal/mol	-19,089	+/-	0,108	kcal/mol	-80,332	+/-	1,192	kcal/mol
pdie8	-159,594	+/-	1,066	kcal/mol	-105,189	+/-	0,5411	kcal/mol	214,487	+/-	1,669	kcal/mol	-19,086	+/-	0,107	kcal/mol	-69,384	+/-	1,158	kcal/mol
[hERGclosed/bekm1-1]-3																				
	van der Waal energy				Electrostattic energy				Polar solvation energy				SASA energy				Binding energy			
pdie2	-132,62273	+/-	1,793	kcal/mol	-436,872	+/-	4,2871	kcal/mol	330,837	+/-	6,052	kcal/mol	-17,752	+/-	0,169	kcal/mol	-256,398	+/-	1,992	kcal/mol
pdie4	-132,66483	+/-	1,83	kcal/mol	-218,399	+/-	2,055	kcal/mol	283,681	+/-	4,978	kcal/mol	-17,749	+/-	0,165	kcal/mol	-85,076	+/-	2,499	kcal/mol
pdie6	-132,63086	+/-	1,867	kcal/mol	-145,626	+/-	1,4017	kcal/mol	251,503	+/-	4,375	kcal/mol	-17,755	+/-	0,175	kcal/mol	-44,467	+/-	2,589	kcal/mol
pdie8	-132,62273	+/-	1,785	kcal/mol	-109,160	+/-	1,0395	kcal/mol	227,552	+/-	3,859	kcal/mol	-17,746	+/-	0,170	kcal/mol	-32,010	+/-	2,550	kcal/mol
[hERGclosed/bekm1-2]-1																				
	van der Waal energy				Electrostattic energy				Polar solvation energy				SASA energy				Binding energy			
pdie2	-69,642823	+/-	0,92	kcal/mol	-375,800	+/-	3,1435	kcal/mol	222,420	+/-	4,111	kcal/mol	-10,094	+/-	0,111	kcal/mol	-233,013	+/-	2,619	kcal/mol
pdie4	-69,621531	+/-	0,917	kcal/mol	-187,852	+/-	1,5629	kcal/mol	194,132	+/-	3,645	kcal/mol	-10,094	+/-	0,108	kcal/mol	-73,387	+/-	2,798	kcal/mol
pdie6	-69,620574	+/-	0,886	kcal/mol	-125,222	+/-	1,0507	kcal/mol	174,428	+/-	3,378	kcal/mol	-10,099	+/-	0,112	kcal/mol	-30,691	+/-	2,822	kcal/mol
pdie8	-69,624402	+/-	0,901	kcal/mol	-93,916	+/-	0,7945	kcal/mol	159,450	+/-	3,256	kcal/mol	-10,098	+/-	0,111	kcal/mol	-14,248	+/-	2,862	kcal/mol
[hERGclosed/bekm1-2]-2																				
	van der Waal energy				Electrostattic energy				Polar solvation energy				SASA energy				Binding energy			
pdie2	-71,449522	+/-	1,419	kcal/mol	-387,774	+/-	4,3608	kcal/mol	219,774	+/-	5,420	kcal/mol	-9,967	+/-	0,189	kcal/mol	-249,640	+/-	3,200	kcal/mol
pdie4	-71,495933	+/-	1,4	kcal/mol	-193,995	+/-	2,2742	kcal/mol	198,208	+/-	4,567	kcal/mol	-9,948	+/-	0,183	kcal/mol	-77,178	+/-	3,149	kcal/mol

Figure A.5 : Free Binding Energy Results with different dielectric constants (pdie:2,4,6,8) for hERG-BeKm-1 and hERG-BmTx3B complexes.

pdie6	-71,436124	+/-	1,444	kcal/mol	-129,246	+/-	1,5435	kcal/mol	181,347	+/-	4,133	kcal/mol	-9,961	+/-	0,184	kcal/mol	-29,270	+/-	3,146	kcal/mol
pdie8	-71,448325	+/-	1,37	kcal/mol	-96,946	+/-	1,1404	kcal/mol	168,176	+/-	3,722	kcal/mol	-9,954	+/-	0,189	kcal/mol	-10,368	+/-	2,983	kcal/mol
[hERGclosed/bekm1-2]-3																				
	van der Waal energy				Electrostattic energy				Polar solvation energy				SASA energy				Binding energy			
pdie2	-73,363876	+/-	0,996	kcal/mol	-448,286	+/-	2,9617	kcal/mol	297,580	+/-	4,350	kcal/mol	-11,520	+/-	0,123	kcal/mol	-235,601	+/-	2,957	kcal/mol
pdie4	-73,345694	+/-	0,99	kcal/mol	-224,149	+/-	1,4847	kcal/mol	258,448	+/-	3,864	kcal/mol	-11,518	+/-	0,122	kcal/mol	-50,444	+/-	3,008	kcal/mol
pdie6	-73,364593	+/-	0,955	kcal/mol	-149,392	+/-	1,0301	kcal/mol	231,332	+/-	3,592	kcal/mol	-11,517	+/-	0,123	kcal/mol	-2,758	+/-	2,940	kcal/mol
pdie8	-73,379665	+/-	0,985	kcal/mol	-112,067	+/-	0,7356	kcal/mol	210,746	+/-	3,345	kcal/mol	-11,518	+/-	0,123	kcal/mol	13,778	+/-	2,784	kcal/mol
[hERGclosed/bmtx3b-1]-1																				
	van der Waal energy				Electrostattic energy				Polar solvation energy				SASA energy				Binding energy			
pdie2	-153,36675	+/-	1,191	kJ/mol	-496,321	+/-	4,0754	kcal/mol	410,219	+/-	4,972	kcal/mol	-19,804	+/-	0,109	kcal/mol	-258,992	+/-	1,662	kcal/mol
pdie4	-153,35694	+/-	1,235	kJ/mol	-248,150	+/-	2,088	kcal/mol	337,772	+/-	4,340	kcal/mol	-19,805	+/-	0,104	kcal/mol	-83,480	+/-	2,649	kcal/mol
pdie6	-153,39378	+/-	1,222	kJ/mol	-165,417	+/-	1,361	kcal/mol	292,752	+/-	3,825	kcal/mol	-19,801	+/-	0,105	kcal/mol	-45,982	+/-	2,844	kcal/mol
pdie8	-153,41172	+/-	1,228	kJ/mol	-124,075	+/-	1,0624	kcal/mol	260,636	+/-	3,508	kcal/mol	-19,805	+/-	0,104	kcal/mol	-36,607	+/-	2,894	kcal/mol
[hERGclosed/bmtx3b-1]-2																				
	van der Waal energy				Electrostattic energy				Polar solvation energy				SASA energy				Binding energy			
pdie2	-126,38397	+/-	1,668	kcal/mol	-449,639	+/-	3,3864	kcal/mol	336,015	+/-	5,439	kcal/mol	-15,283	+/-	0,156	kcal/mol	-255,433	+/-	2,463	kcal/mol
pdie4	-126,44378	+/-	1,626	kcal/mol	-224,778	+/-	1,7285	kcal/mol	281,513	+/-	4,708	kcal/mol	-15,285	+/-	0,154	kcal/mol	-85,180	+/-	3,033	kcal/mol
pdie6	-126,42488	+/-	1,646	kcal/mol	-149,866	+/-	1,1179	kcal/mol	246,590	+/-	4,386	kcal/mol	-15,280	+/-	0,153	kcal/mol	-45,155	+/-	3,078	kcal/mol
pdie8	-126,42943	+/-	1,689	kcal/mol	-112,394	+/-	0,8242	kcal/mol	221,247	+/-	4,026	kcal/mol	-15,284	+/-	0,154	kcal/mol	-33,006	+/-	2,974	kcal/mol
[hERGclosed/bmtx3b-1]-3																				
	van der Waal energy				Electrostattic energy				Polar solvation energy				SASA energy				Binding energy			
pdie2	-123,70096	+/-	1,582	kcal/mol	-424,744	+/-	2,3584	kcal/mol	312,376	+/-	3,132	kcal/mol	-15,069	+/-	0,136	kcal/mol	-251,252	+/-	1,894	kcal/mol
pdie4	-123,72967	+/-	1,573	kcal/mol	-212,382	+/-	1,1909	kcal/mol	248,136	+/-	2,599	kcal/mol	-15,060	+/-	0,139	kcal/mol	-102,994	+/-	1,770	kcal/mol
pdie6	-123,68134	+/-	1,622	kcal/mol	-123,681	+/-	1,6218	kcal/mol	211,090	+/-	2,306	kcal/mol	-15,059	+/-	0,139	kcal/mol	-69,232	+/-	1,678	kcal/mol
pdie8	-123,75766	+/-	1,598	kcal/mol	-106,176	+/-	0,5866	kcal/mol	186,050	+/-	2,140	kcal/mol	-15,058	+/-	0,137	kcal/mol	-58,818	+/-	1,706	kcal/mol
[hERGclosed/bmtx3b-2]-1																				
	van der Waal energy				Electrostattic energy				Polar solvation energy				SASA energy				Binding energy			
pdie2	-92,056938	+/-	1,548	kcal/mol	-399,182	+/-	5,2184	kcal/mol	257,838	+/-	6,240	kcal/mol	-12,653	+/-	0,191	kcal/mol	-246,400	+/-	2,988	kcal/mol
pdie4	-92,010766	+/-	1,604	kcal/mol	-199,584	+/-	2,5849	kcal/mol	223,030	+/-	4,884	kcal/mol	-12,645	+/-	0,193	kcal/mol	-81,200	+/-	2,915	kcal/mol
pdie6	-92,038995	+/-	1,6	kcal/mol	-133,076	+/-	1,7512	kcal/mol	199,314	+/-	4,237	kcal/mol	-12,652	+/-	0,191	kcal/mol	-38,504	+/-	2,939	kcal/mol

Figure A.5 (continued) : Free Binding Energy Results with different dielectric constants (pdie:2,4,6,8) for hERG-BeKm-1 and hERG-BmTx3B complexes.

pdie8	-91,972727	+/-	1,569	kcal/mol	-99,836	+/-	1,2409	kcal/mol	181,197	+/-	3,608	kcal/mol	-12,641	+/-	0,187	kcal/mol	-23,284	+/-	2,886	kcal/mol

[hERGclosed/bmtx3b-2]-2																			
	van der Waal energy				Electrostattic energy				Polar solvation energy				SASA energy				Binding energy			
pdie2	-96,337081	+/-	1,015	kcal/mol	-454,896	+/-	2,6715	kcal/mol	340,268	+/-	3,952	kcal/mol	-12,895	+/-	0,112	kcal/mol	-223,725	+/-	2,962	kcal/mol
pdie4	-96,362919	+/-	1,016	kcal/mol	-227,369	+/-	1,3519	kcal/mol	286,103	+/-	3,384	kcal/mol	-12,894	+/-	0,111	kcal/mol	-50,466	+/-	2,857	kcal/mol
pdie6	-96,393301	+/-	1,026	kcal/mol	-151,619	+/-	0,8914	kcal/mol	252,620	+/-	3,099	kcal/mol	-12,893	+/-	0,111	kcal/mol	-8,215	+/-	2,745	kcal/mol
pdie8	-96,37799	+/-	1,011	kcal/mol	-113,698	+/-	0,672	kcal/mol	228,241	+/-	2,788	kcal/mol	-12,898	+/-	0,113	kcal/mol	5,326	+/-	2,623	kcal/mol
[hERGclosed/bmtx3b-2]-3																			
	van der Waal energy				Electrostattic energy				Polar solvation energy				SASA energy				Binding energy			
pdie2	-71,479426	+/-	1,265	kcal/mol	-401,767	+/-	2,9904	kcal/mol	249,331	+/-	4,716	kcal/mol	-10,726	+/-	0,148	kcal/mol	-234,595	+/-	3,360	kcal/mol
pdie4	-71,547847	+/-	1,3	kcal/mol	-200,860	+/-	1,5572	kcal/mol	215,111	+/-	4,198	kcal/mol	-10,731	+/-	0,150	kcal/mol	-67,970	+/-	3,606	kcal/mol
pdie6	-71,461005	+/-	1,286	kcal/mol	-133,886	+/-	1,0428	kcal/mol	190,994	+/-	3,829	kcal/mol	-10,724	+/-	0,150	kcal/mol	-25,242	+/-	3,560	kcal/mol
pdie8	-71,466268	+/-	1,279	kcal/mol	-100,438	+/-	0,7804	kcal/mol	172,830	+/-	3,493	kcal/mol	-10,726	+/-	0,150	kcal/mol	-9,931	+/-	3,442	kcal/mol

Figure A.5 (continued) : Free Binding Energy Results with different dielectric constants (pdie:2,4,6,8) for hERG-BeKm-1 and hERG-BmTx3B complexes.

CURRICULUM VITAE

Name Surname **:** Beril ÇOLAK GÜNAY

EDUCATION **:**

- **B.Sc.** **:** 2007, Istanbul Technical University, Faculty of Science and Letters, Department of Chemistry
- **M.Sc.** **:** 2009, Istanbul Technical University, Institut of Science and Technology, Chemistry Program

PUBLICATIONS, PRESENTATIONS ON THE THESIS:

- **Colak Gunay, B., Yurtsever, M., Durdagi, S.** (2020). Elucidation of interaction mechanism of hERG1 potassium channel with scorpion toxins BeKm-1 and BmTx3b, *Journal of Molecular Graphics and Modelling*, 96, 107504.
- **Colak Gunay, B., Yurtsever, M., Durdagi, S.** 'In Silico Screening of Protein-Protein Interactions of hERG1 Potassium Ion Channels with Scorpion Toxins', 4th International Bau Drug Design Congress, October, 2016, İstanbul, Turkey.
- **Colak Gunay, B., Yurtsever, M., Durdagi, S.** 'In Silico Screening of Anticancer Potentials of Toxins: Protein-Protein Interactions of hERG Potassium Ion Channels with Conotoxins', 11th Chemical Physics Congress, October, 2014, İstanbul, Turkey.